NUMERICAL SOLUTION OF SOME FLUID FLOW PROBLEMS BY BOUNDARY INTEGRAL EQUATION TECHNIQUES

by

Charles Cameron Macaskill

B.Sc.(Hons.) (Math.Sci.), University of Adelaide

Thesis submitted for the degree of Doctor of Philosophy in the University of Adelaide

Department of Applied Mathematics,

December, 1977

July 1978

TABLE OF CONTENTS

SUMMARY

The thesis details the use of the boundary integral equation technique, in solving some problems in oscillatory viscous flow at low Reynolds number. Similar techniques are used to solve some water-wave reflection problems.

In the first part of the thesis, low Reynolds number viscous flow through one or more gaps in an infinitely thin wall is considered. The flow is considered to be oscillatory and the fluid incompressible. It is also assumed that velocity amplitude fluctuations are small so that the Navier-Stokes equations may be linearized. Flow through an arbitrary number of infinitely long slits in a wall is considered - this is a two-dimensional problem. In the more general 3-dimensional case, only axisymmetric flow through a circular gap is treated, although the method may be extended, at least in principle, to arrays of irregularly shaped holes. Each of these problems is formulated as a singular integral equation that is then solved numerically.

Results for the viscous flow problems outlined above are presented in terms of the "blockage coefficient" or the "effective gap size". These two quantities measure the degree to which the fluid flow is restricted on passing through the gaps in the wall. The numerical computations show good agreement with previous work, where applicable, and with analytical solutions that may be obtained in some limiting cases.

In the second part of the thesis, two fairly generalized water-wave problems are considered. The first is the reflection of water-waves by a submerged shelf of some prescribed shape, while the second is the reflection of water-

waves by an infinitely thin, vertical barrier of given permeability. A special case of the second problem is the reflection of water-waves through one or more gaps in an otherwise permeable breakwater.

Both water-wave problems are formulated in the two-dimensional case only. The method of solution is essentially the same in both problems. It is assumed that the flow is non-viscous and irrotational and that fluid motions are small enough so that linearization is possible.

By applying Green's theorem, singular integral equations may be obtained with unknowns being the boundary values of the potential function and its normal derivative. These may be solved using a similar method to that used for the viscous flow problems.

Reflection and transmission coefficients are presented for the water-wave problems. A variety of bottom geometries and breakwater configurations is considered. Good agreement is shown with earlier work by other authors in the field.

SIGNED STATEMENT

I hereby declare that this thesis contains no material which has been accepted for the award of any other degree or diploma in any University, and, to the best of my knowledge, it contains no material previously published by any other person, except where due reference is made in the text of the thesis.

C. MACASKILL

ACKNOWLEDGEMENTS

I would like to thank my supervisor, Professor E. O. Tuck, for the many enlightening discussions we have had during the course of this work, and for the encouragement and help he has given me throughout. Thanks are also due to Mrs. Gail Burner for her excellent typing.

The research associated with this thesis was carried out from February 1974 to December 1977, during which time I was supported by a Commonwealth Postgraduate Award.

GENERAL INTRODUCTION

The boundary integral equation technique is becoming widely accepted as a tool for the fast and accurate solution of problems that might previously have been solved by finite difference methods, or more recently by such procedures as the finite element technique or the "Marker and Cell" method. The obvious advantage of the boundary integral technique is that the only quantities that have to be specifically determined in the numerical solution process are boundary values. Once these have been obtained, the basic unknowns at any interior point may be found by the use of an appropriate integral relation. Other methods, by contrast, involve finding values at these interior points as part of the solution procedure, usually involving an excessive amount of computer time and often introducing large truncation errors. This is especially true in the case of infinite domains.

In general, in using the integral method, one applies Green's theorem to express, for example, a velocity potential anywhere in some fluid domain in terms of the boundary values of this potential and its normal derivative. Thus once the boundary values are known, the potential may be determined throughout the fluid. By a suitable limiting process, we may reduce the integral relation thus obtained to a singular integral equation involving only boundary values. (In some cases, we require more than a single integral equation - but the same methods of solution may be used for the solution of two, three or more coupled integral equations.)

This integral equation will usually be a Fredholm equation of the first or second kind. Equations of the second kind are generally amenable to any reasonable method of numerical

solution - for example, iteration methods are quite often used. By contrast, equations of the first kind can cause trouble and there is no guarantee that a particular numerical method will be successful in dealing with equations of this sort. In the present thesis, both types of equation arise. It is found that an extremely straightforward method first proposed by Tuck (1969) gives good results with both types.

In this procedure we divide the boundary, or range of integration, into a number of segments. The unknown function is considered to be slowly varying on the boundary so that it may be approximated as having a constant value over each small segment. (At points on the boundary where this assumption breaks down, near corners for example, the method can be improved by making the boundary segments smaller and smaller as the singular point is approached. In fact, the boundary may be divided in such a way as to exactly cancel out the effect of such singularities.) Once we have discretized the problem in this way, we can approximate the integral equation as a matrix equation of order N, where N is the number of segments. This matrix equation may then be inverted to return the boundary values of the (unknown) function.

As has been mentioned above, the method requires that the problem be expressed in terms of an integral relation over the boundary. Thus linearized water-wave problems may immediately be approached using this method, as in general a velocity potential exists satisfying Laplace's equation and Green's theorem allows the required integral relation to be derived. Thus, in Chapters 3 and 4 of the thesis, we formulate two water problems. Using the method outlined above, results are obtained for a wide range of geometries.

Specifically, in Chapter 3 we consider water-wave reflection, in water of finite depth, due to a change in depth. Only a two-dimensional formulation is attempted, although similar methods could be used to solve the more general three-dimensional problem, admittedly with some computational difficulty. The problem is set up as a set of coupled integral equations, rather than a single equation, but it is found that the numerical method may be successfully used.

In Chapter 4, the problem of water-wave reflection by a thin barrier of arbitrary permeability is considered, again with the restriction that the flow be two-dimensional. Both finite depth and infinite depth problems are considered. This formulation includes the special case of transmission through one or more gaps in an otherwise impermeable breakwater. Results are presented for a wide range of barrier geometries and water depths.

In Chapters 1 and 2 we consider oscillatory viscous flow at low Reynolds number, through one or more gaps in an otherwise impermeable wall. In Chapter 1, we formulate the problem for a single slit (two-dimensional flow) and a single circular hole (axisymmetric flow). In Chapter 2, we extend the model to consider unsteady viscous flow through a screen. In these problems there is no longer a velocity potential as was the case when dealing with water-waves. We assume, however, that velocity amplitude fluctuations are small, so that the Navier-Stokes equations may be linearized. This implies that the pressure throughout the flow-field still satisfies Laplace's equation and accordingly it is found that suitable integral relations may be obtained by distributing point pressures, of

unknown strength, across the openings in the wall. This unknown strength distribution is actually proportional to the normal velocity through the gap.

Once again, the numerical method of Tuck (1969) may be used successfully. Two points should be made, however. First, the integral equations derived in the viscous flow problems are of the first kind so that there is no guarantee of existence or uniqueness of solution. The method used here does, however, give answers that agree well with other work in the field, in regions where other theories are applicable (e.g. de Mestre and Guiney (1971), Sedov (1965)). Analytical solutions may be obtained in some limiting cases, and these results also agree with the numerical work. Secondly, the integral equations obtained have double-pole singularities (in contrast with the water-wave problems, where the dominant singularity is logarithmic). This might be expected to cause problems. In fact, it is possible to deal with such singularities using the Hadamard interpretation (see Mangler (1951)), and it is shown in the Appendices that careful interpretation of the double-pole leads to exactly the same result as is obtained by applying the numerical technique without regard to the divergent character of the integral equation.

Finally, in the Appendices, some simple test equations are considered, and some measure is made of the rate of convergence of the numerical method.

CHAPTER 1

UNSTEADY LOW-REYNOLDS-NUMBER OSCILLATORY FLOW THROUGH TWO AND THREE-DIMENSIONAL GAPS

1.1 Introduction

In this chapter we consider oscillatory low-Reynolds-number flow through a single gap in an otherwise impermeable wall. This work follows from the work of Tuck (1975) on the so-called "effective size" of a small gap in both viscous and non-viscous flows. A possible application is to acoustics, where the effective size is related to the acoustic impedance of the barrier (see Chapter 2). In a more general sense, this work allows the inclusion of real-fluid effects, usually appreciable only in the vicinity of the gap, in problems such as channel flow through a (small) restricted opening, or water-wave flow through a porous barrier.

Usually such contributions are determined experimentally. de Mestre and Guiney (1971) have, however, considered the problem of axisymmetric flow through a small hole at low Reynolds number. In their treatment, the flow near the gap is assumed to be completely dominated by viscous effects, so that a Stokes-flow formulation is possible. This type of flow is considered to be applicable in some inner region near the gap. Outside this region the flow is treated as being due to an oscillatory point source, so that no effects due to finite width of the gap are included. Such an approach is a good first approximation. However, as no matching procedure is carried out, there is some doubt as to which of the two (separate) solutions is applicable at a particular point. The present formulation attempts a more uniform approach in that the (linear) inertial terms are included even in the

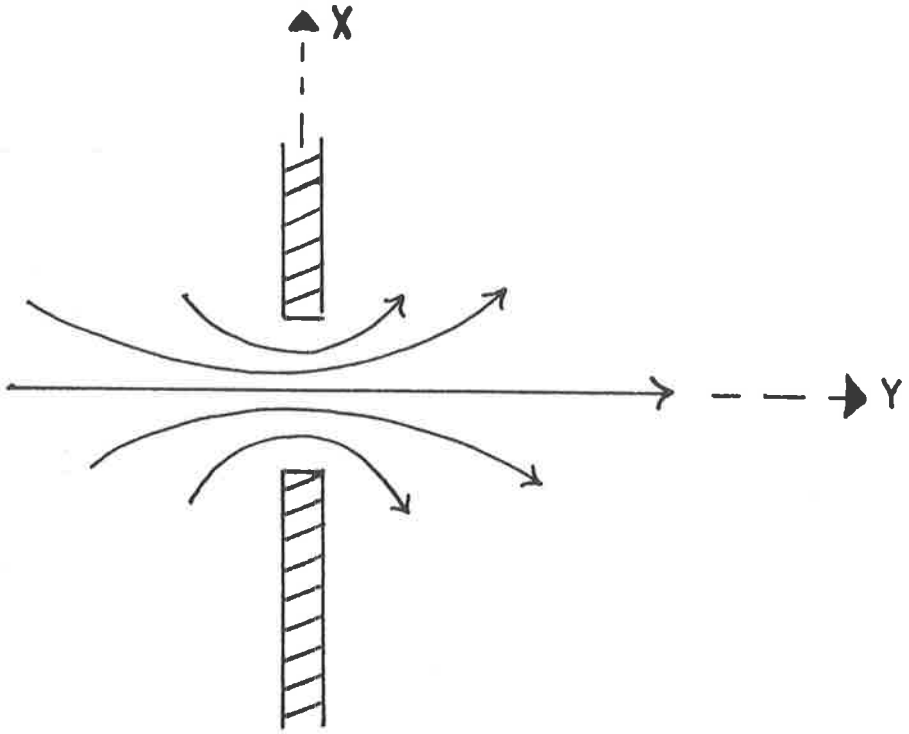

Figure 1 Sketch of two-dimensional flow through a gap in an infinite plane wall of zero thickness.

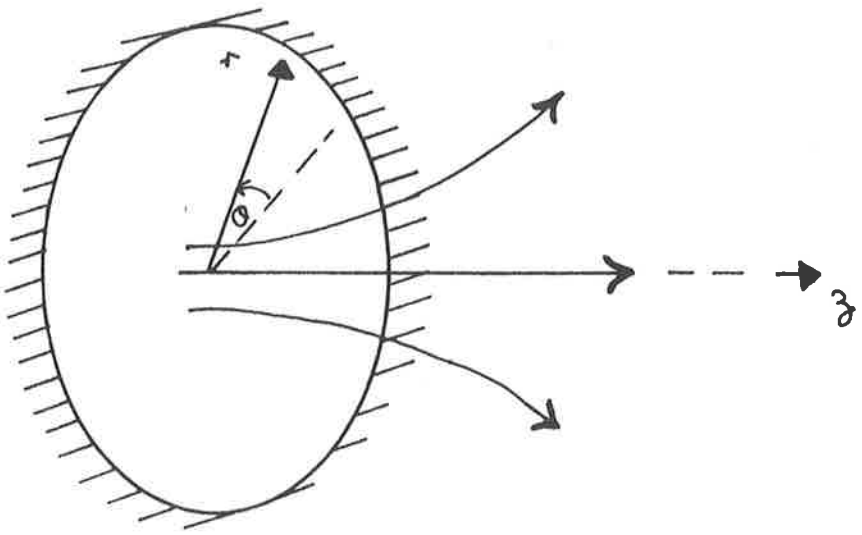

Figure 2 Axisymmetric flow through a circular gap in an infinite plane wall of zero thickness.

near vicinity of the gap while, conversely, the influence of the finite width of the gap is carried through to the far field. It must be noted, however, that this approach is limited to problems where velocity fluctuations are small enough so that non-linear terms in the Navier-Stokes equations may be neglected.

We assume that the flow is time-sinusoidal, of frequency σ, so that the normal velocity through the gap may be defined as $\mathcal{R}e(Ve^{i\sigma t})$. If a is a typical gap dimension and ν the kinematic viscosity, then we may define a true Reynolds number Va/ν which we take as small. This is equivalent to assuming that the velocity fluctuations are small, thus justifying linearization. Under this approximation, all quantities in the flow problem are proportional to V, and the only important non-dimensional parameter is the non-dimensional frequency

$$\beta = \sigma a^2/\nu \qquad (1.1.1)$$

which will be henceforth referred to as the Reynolds number.

As mentioned before, inertial terms are retained in the Navier-Stokes equations in this formulation. This means that if the influence of viscosity happens to be negligible even very close to the gap, the case of inviscid flow will be regained as $\beta \to \infty$.

In the following section, the problem of two-dimensional flow through a single slit will be considered. Later in the chapter axisymmetric flow through a circular gap is treated.

1.2 Mathematical Formulation (2-d hole)

We consider the flow situation shown in Figure 1 , with cartesian co-ordinates (x,y). The velocity vector

$\underset{\sim}{u}(x,y)e^{i\sigma t}$ is assumed to satisfy the linearized Navier-Stokes equation

$$i\sigma\underset{\sim}{u} = -\frac{1}{\rho}\underset{\sim}{\nabla}p + \nu\nabla^2\underset{\sim}{u} \tag{1.2.1}$$

where $p(x,y)e^{i\sigma t}$ is the pressure. Since we are also assuming a (locally) incompressible fluid, we can use a stream function $\psi(x,y)e^{i\sigma t}$ such that $\underset{\sim}{u} = (\psi_y, -\psi_x)$ and (1.2.1) then implies that

$$\nabla^4\psi = \alpha^2\nabla^2\psi \tag{1.2.2}$$

where $\alpha^2 = i\sigma/\nu$.

Using (1.2.1) and the incompressibility of the fluid, we have $\nabla^2 p=0$. The harmonic conjugate of the pressure, say $q(x,y)$, is then given by the solution of the Cauchy-Riemann equations

$$p_x = q_y, \quad p_y = -q_x \tag{1.2.3}$$

$q(x,y)$ is related to the vorticity ω by

$$q = -\mu(\omega + \alpha^2\psi) \tag{1.2.4}$$

where ω is defined as

$$\omega = -\nabla^2\psi \tag{1.2.5}$$

Here $\mu = \rho\nu$ is the dynamic viscosity.

Due to the influence of viscosity, vorticity ω is generated in the gap at $y=0$. This vorticity decays exponentially as $|y|\to\infty$. Because of this, at a large distance from the wall the flow becomes irrotational with $\omega=0$, $\underset{\sim}{\nabla}^2 u=0$. In this region the flow is described by a velocity potential proportional to $p(x,y)$,

$$\underset{\sim}{u} = \underset{\sim}{\nabla}\left(-\frac{1}{i\sigma\rho}\,p(x,y)\right), \quad |y| \to \infty \tag{1.2.6}$$

This velocity potential corresponds to that of a source-sink pair at $(x,y) = (0,0)$, given by

$$-\frac{1}{i\sigma\rho}\, p(x,y) \to \frac{1}{2\pi} \log (r/s)\ \text{sgn}\ y, \qquad |y| \to \infty \tag{1.2.7}$$

where s is an arbitrary constant, known as the effective gap size, and $r = \sqrt{x^2+y^2}$. This quantity s carries through to the outer flow field the effects due to viscosity, as well as the influence of the finite width of the gap. It should be noted that s may be complex-valued.

The irrotational flow (equation 1.2.7) at a great distance (relative to the gap width $2a$) from the slit, is the outer approximation to the inner flow through the slit. This must match with the inner approximation to the outer flow field for the particular problem being considered (e.g. acoustic streaming through a gap).

In the outer field there is an effective pressure jump across $y=0$, given by

$$\Delta p = \frac{\alpha^2 \mu}{\pi} \log s \tag{1.2.8}$$

so that (1.2.7) can be written

$$p(x,y) \to -\left(\frac{\alpha^2 \mu}{2\pi} \log r\right)\text{sgn}\ y \pm \frac{1}{2}\Delta p, \quad y \to \pm\infty \tag{1.2.9}$$

This means that for all gap configurations, in the outer flow field, the flow through the gap looks like that due to an oscillatory inviscid source-sink pair located at $(x,y) = (0,0)$. All information about the detailed flow in the neighbourhood of the gap is carried to the outer flow by the effective gap size. Alternatively, the pressure jump across $y=0$ may be thought of as conveying this information to the outer flow field.

Equation (1.2.9) provides a boundary condition at infinity for the problem, in terms of the pressure jump across the wall. This quantity still, however, remains to be determined.

The remaining boundary conditions are the no-slip condition $\underset{\sim}{u}=0$ on the wall

$$\psi_x(x,0) = \psi_y(x,0) = 0, \quad |x| > a \tag{1.2.10}$$

and the condition across the gap of normal streaming velocity, i.e.

$$\psi_y(x,0) = 0 \qquad |x| < a \tag{1.2.11}$$

and finally

$$\omega_y(x,0) = 0 \qquad |x| < a \tag{1.2.12}$$

which is equivalent to continuity of the pressure across the gap (by (1.2.3) and (1.2.5)).

1.3 Derivation of the Integral Equation (2-d hole)

We write

$$\psi(x,y) = \int_{-a}^{a} m(\xi)\, G(x,y,\xi)\, d\xi \tag{1.3.1}$$

where $m(\xi)$ is a source strength to be determined and is proportional to the velocity through the gap. $G(x,y,\xi)$ is any Green's function satisfying

$$\nabla^4\psi - \alpha^2\nabla^2\psi = \delta(x-\xi)\,\delta(y-\eta) \tag{1.3.2}$$

everywhere in the fluid. We choose $G(x,y,\xi) = G_0(x-\xi,y)$ where

$$G_0(x,y) = -2/\pi\alpha^2 \int_0^{\infty} (\lambda+\sqrt{\lambda^2+\alpha^2})(\lambda e^{-y\sqrt{\lambda^2+\alpha^2}} - \sqrt{\lambda^2+\alpha^2}\, e^{-\lambda y}) \sin \lambda x \, \frac{d\lambda}{\lambda} \tag{1.3.3}$$

(Tuck (1970)), which also satisfies the zero-velocity condition (1.2.10) everywhere on $y=0$ except at $x=0$. The pressure field corresponding to $\psi=G_0$ is $p=P_0$, where

$$P_0(x,y) = \frac{2}{\pi}\mu\left[\alpha^2 \log\sqrt{x^2+y^2} + \frac{x^2-y^2}{(x^2+y^2)^2} - \int_0^\infty \sqrt{\lambda^2+\alpha^2}\, e^{-\lambda y}\cos \lambda x\, dx\right] \tag{1.3.4}$$

and
$$P(x,\xi,y) = P_0(x-\xi,y) \tag{1.3.5}$$

As $r \to \infty$, $P(x,\xi,y) \to \frac{2\mu\alpha^2}{\pi}\log r$ (1.3.6)

The integral representation (1.3.1) for ψ implies a corresponding representation for the pressure,

$$p(x,y) = \int_{-a}^{a} m(\xi)\, P(x,y,\xi)\, d\xi + \frac{1}{2}\Delta p \tag{1.3.7}$$

where the arbitrary constant $\frac{1}{2}\Delta p$ is given by (1.2.8) and thus satisfies (1.2.7). In fact, as $r \to \infty$, we have from (1.3.6)

$$p(x,y) \to \frac{2\mu\alpha^2}{\pi}\int_{-a}^{a} m(\xi)d\xi.\ \log r + \frac{1}{2}\Delta p \tag{1.3.8}$$

and thus, using (1.2.9),

$$2\int_{-a}^{a} m(\xi)d\xi = -\frac{1}{2} \tag{1.3.9}$$

This normalization of the source strength m expresses continuity, since the quantity on the left is the net entering flux through the gap, and that on the right the net departing flux at $r = \infty$.

The pressure field representation (1.3.7) is valid only for $y > 0$. It may, however, be extended to $y < 0$ as an odd function of y. In general this would require a pressure jump across the gap $y=0$, $-a < x < a$, violating the requirement that pressure be continuous across the gap (see (1.2.12)).

This last condition allows us to obtain an integral equation to determine the unknown $m(\xi)$. We set $p(x,0) = 0$ across the gap, so that

$$\int_{-a}^{a} m(\xi)\ P(x,0,\xi)d\xi = -\frac{\mu\alpha^2}{2\pi} \log s \qquad (1.3.10)$$

The problem has thus reduced to solving (1.3.9) and (1.3.10) simultaneously for the unknown quantities $m(x)$ and s. Obviously, once $m(x)$ has been determined, the stream function for the entire flow field may be obtained from equation (1.3.1).

The problem can be further simplified if we adopt a non-dimensionalization as follows. We set

$$\xi = a\ \xi^*, \quad x = a\ x^* \qquad (1.3.11)$$

$$m(\xi) = -\frac{m^*(\xi^*)\ \log(s/a)}{2\pi a} \qquad (1.3.12)$$

and

$$P(x,0,\xi) = \mu\alpha^2\ P^*(x^*-\xi^*) \qquad (1.3.13)$$

For brevity, we omit the stars from now on.

The integral equation (1.3.10) then becomes

$$\int_{-1}^{1} m(\xi)\ P(x,\xi)d\xi = 1 \qquad (1.3.14)$$

or

$$\int_{0}^{1} m(\xi)(P(x,\xi) + P(x,-\xi))d\xi = 1, \qquad (1.3.15)$$

since $m(\xi)$ is an even function.

Finally, the normalization condition (1.3.9) becomes

$$-\int_{0}^{1} m(\xi)d\xi = -\pi/(4 \log s/a) \qquad (1.3.16)$$

or

$$\log s/a = \pi\left[4\int_{0}^{1} m(\xi)d\xi\right]^{-1} \qquad (1.3.17)$$

Once equation (1.3.15) has been solved for $m(\xi)$, (1.3.17) provides the effective gap size directly.

The normalized kernel can be written

$$P(x,\xi) = -Q'(x-\xi) - Q'(x+\xi) \tag{1.3.18}$$

At this stage Q must be determined by evaluating the indefinite integral of $P(x,\xi)$. The major problem here occurs in the evaluation of

$$Q_0(x,\xi) = \int^{\xi} \lim_{y\to 0} \frac{2}{\pi\alpha^2} \int_0^{\infty} \sqrt{\lambda^2+\alpha^2}\, e^{-\lambda y} \cos \lambda a(x-\xi)\, d\lambda d\xi \tag{1.3.19}$$

We may, however, rewrite the inner integral so that

$$Q_0(x,\xi) = \frac{2}{\pi\alpha^2} \int^{\xi} \left(\alpha^2 - \frac{1}{a^2}\frac{\partial^2}{\partial\xi^2}\right) \lim_{y\to 0} \int_0^{\infty} e^{-\lambda y} \frac{\cos \lambda a\,(x-\xi)}{\sqrt{\lambda^2+\alpha^2}}\, d\lambda d\xi \tag{1.3.20}$$

$$= \frac{2}{\pi} \int^{\xi} \left(1 - \frac{1}{i\beta}\frac{\partial^2}{\partial\xi^2}\right) K_0(\sqrt{i\beta}\,|x-\xi|) \tag{1.3.21}$$

where K_0 is a modified Bessel function.

Thus we may write

$$Q(x) = \frac{2}{\pi}\left(x \ln x - x - \frac{1}{i\beta x} + \frac{g(\sqrt{\beta x})}{\sqrt{i\beta}}\right) \tag{1.3.22}$$

where g is an odd function defined for $\theta > 0$ by

$$g(\theta) = K_0'(\sqrt{i\theta}) - \sqrt{i} \int_0^{\theta} K_0(\sqrt{it})\, dt \tag{1.3.23}$$

$g(\theta)$ may be written in terms of Kelvin functions (see Abramowitz and Stegun (1964), p.379) and their integrals, and may thus be evaluated numerically with little difficulty. $g(\theta)$ is calculated by using series representations for the Kelvin functions and for the integral of the modified Bessel function K_0.

The integral equation (1.3.14) is very singular. The kernel $P(x,\xi)$ has a double pole at $x=\xi$, of the form

$$P(x,\xi) \to \frac{4}{\pi i \beta (x-\xi)^2} , \quad \xi \to x \tag{1.3.24}$$

However, a direct integration of this kernel, as in (1.3.22), may be justified by use of the Hadamard interpretation. Mangler (1951) shows that correct answers are obtained in problems of this type by integrating straight through the singularity. For a more detailed discussion of this problem and the interpretation of double poles, reference should be made to the appendices.

1.4 Mathematical Formulation (3-d hole)

In this section the problem of flow through a circular hole is considered. Cylindrical polar coordinates r, z and θ are used. Due to the axisymmetry of the problem, there will be no functional dependence on θ (see Figure 2).

Under the same assumptions concerning velocity fluctuations and so on, that were used in the formulation for a two-dimensional slit, we still have the velocity vector $\underset{\sim}{u}(x,y)e^{i\omega t}$ satisfying (1.2.1).

It is, however, no longer possible to find a stream function satisfying (1.2.2). This problem may be overcome, however. If the components of $\underset{\sim}{u}$ in the r and z directions respectively are given by $u(r,z,t)$ and $v(r,z,t)$ then the continuity condition throughout the fluid is

$$\frac{1}{r}\frac{\partial}{\partial r}\left(\frac{r\partial u}{\partial r}\right) + \frac{\partial v}{\partial z} = 0 \tag{1.4.1}$$

This equation can be satisfied by the introduction of a stream function $\psi'(x,y,t)$ such that

$$u = \frac{1}{r}\frac{\partial \psi'}{\partial z} , \quad v = \frac{1}{r}\frac{\partial \psi'}{\partial r} \tag{1.4.2}$$

In terms of the stream function ψ' the Navier-Stokes equation (1.2.1) becomes

$$D^4\psi = \frac{1}{\nu}\frac{\partial}{\partial t}D^2\psi \tag{1.4.3}$$

where the operator D^2 is given by

$$D^2 = \frac{\partial^2}{\partial r^2} - \frac{1}{r}\frac{\partial}{\partial r} + \frac{\partial^2}{\partial z^2} \equiv \nabla^2 - \frac{2}{r}\frac{\partial}{\partial r} \tag{1.4.4}$$

If we now set $\psi' = \mathcal{R}e(\psi(r,z)e^{i\sigma t})$ (1.4.5)

then we obtain

$$D^4\psi = \alpha^2 D^2\psi \tag{1.4.6}$$

The vorticity can be shown to be given by

$$\omega = -\frac{1}{r}D^4\psi \tag{1.4.7}$$

which replaces (1.2.5) in the two-dimensional slit problem. Using (1.2.1) and the incompressibility of the fluid, we find that the pressure satisfies the equation

$$\underset{\sim}{\nabla}p = \mu(\nabla^2 - \alpha^2)\underset{\sim}{u} \tag{1.4.8}$$

On using the vector identity

$$\nabla\ u = \underset{\sim}{\nabla}(\underset{\sim}{\nabla}.\underset{\sim}{u}) - \underset{\sim}{\nabla} \times (\underset{\sim}{\nabla} \times \underset{\sim}{u}) \tag{1.4.9}$$

$$= -\underset{\sim}{\nabla} \times \underset{\sim}{u} \tag{1.4.10}$$

we obtain $\frac{\partial p}{\partial r} = -\frac{\mu}{r}\frac{\partial}{\partial z}(\alpha^2\psi + r\omega)$ (1.4.11)

and $\frac{\partial p}{\partial z} = \frac{\mu}{r}\frac{\partial}{\partial r}(\alpha^2\psi + r\omega)$ (1.4.12)

Equations (1.4.11) and (1.4.12) play a similar role to the Cauchy-Riemann equations (1.2.3) and equation (1.2.4) in the two-dimensional problem.

At a large distance $R = \sqrt{r^2 + z^2}$ from the wall, we

again have $\omega \to 0$ so that the velocity potential looks like a source-sink pair at $(r,z) = (0,0)$. It must be noted, however, that the flow is now three-dimensional, so that

$$-\frac{1}{i\sigma\rho}\, p(r,z) \to -\frac{1}{4\pi}\left(\frac{1}{R} - \frac{1}{s}\right) \operatorname{sgn} z, \quad z \to \pm\infty \tag{1.4.13}$$

where s is again the effective gap size.

Corresponding to (1.2.8), we write

$$\Delta p = -\frac{\alpha^2 \mu}{2\pi s} \tag{1.4.14}$$

so that (1.2.9) becomes

$$p(r,z) \to \frac{\alpha^2 \mu}{4\pi R} \operatorname{sgn} z \pm \frac{1}{2}\Delta p, \quad z \to \pm\infty \tag{1.4.15}$$

(1.4.15) is the boundary condition at infinity.

Boundary conditions on $z=0$ are also required in place of (1.2.10)-(1.2.12). Explicitly, these are

$$\psi_r(r,0) = \psi_z(r,0) = 0 \quad r > a \tag{1.4.16}$$

$$\psi_z(r,0) = 0 \quad r < a \tag{1.4.17}$$

and finally

$$\omega_z(r,0) = 0 \tag{1.4.18}$$

1.5 Derivation of the Integral Equation (3-d problem)

For a general hole in a plane wall, we can attempt a solution by distributing sources over the hole, i.e.

$$\psi(r,z,\theta) = \operatorname{sgn} z \iint_S m(q,\phi)\, G(r,q,\phi-\theta,z)\, dA \tag{1.5.1}$$

where $G(r,q,\phi,z)$ is the Green's function satisfying (1.4.6) everywhere except at $(r,z) = (0,0)$. This function is in fact the solution obtained by de Mestre and Guiney (1971). They used it to describe the stream function in the far-field for Stokes flow through an axisymmetric hole. It is given

by

$$G(r,q,\phi,z) = -\frac{\gamma}{\alpha^2}\int_0^\infty (\lambda + \sqrt{\lambda^2+\alpha^2})(\lambda e^{-\sqrt{\lambda^2+a^2}\ z} - \sqrt{\lambda^2+\alpha^2}\ e^{-\lambda z})\ J_1(\lambda\gamma)\,d\lambda \qquad (1.5.2)$$

with
$$\gamma = \sqrt{r^2+q^2-2rq\ \sin\phi} \qquad (1.5.3)$$

For a detailed derivation of equation (1.5.2), reference should be made to Guiney (1972).

The corresponding pressure distribution to $\psi=G$ can now be determined, using (1.4.11) and (1.4.12), as

$$P(r,q,\phi,z) = \alpha^2\mu\left(\frac{1}{\sqrt{\gamma^2+z^2}} - \frac{1}{\alpha^2(\gamma^2+z^2)^{3/2}} + \frac{3z^2}{\alpha^2(\gamma^2+z^2)^{5/2}} + \frac{1}{\alpha^2}\int_0^\infty \lambda\sqrt{\lambda^2+a^2}\ e^{-\lambda z}\ J_0(\lambda\gamma)\,d\lambda\right) \qquad (1.5.4)$$

As $R \to \infty$,
$$P(r,q,\phi,z) \to \frac{\alpha^2\mu}{R} \qquad (1.5.5)$$

We are particularly interested in the problem of axisymmetric flow through a circular gap. In this particular case we may ignore θ dependence. Henceforth this will be done. It should be noted, however, that the method will still work for non-axisymmetric flow through irregularly shaped holes. In such problems, however, the kernels of the integral equations can become extremely complicated, due to the additional parameter involved.

We may now write down an integral representation for the pressure, corresponding to equation (1.3.7) in the two-dimensional formulation, i.e.

$$p(r,z) = \int_0^a q\int_0^{2\pi} m(q,\phi)\ P(r,q,\phi,z)\ d\phi dq + \frac{1}{2}\Delta p \qquad (1.5.6)$$

where again the arbitrary constant Δp is given by (1.4.14). We now take the limit of (1.5.6) as $R \to \infty$ and find

$$p(r,z) \to \frac{\alpha^2 \mu}{R} \int_0^a q \int_0^{2\pi} m(q,\phi)\, d\phi\, dq + \frac{1}{2}\Delta p \qquad (1.5.7)$$

Using (1.4.13) we have

$$\frac{1}{8\pi^2} = \int_0^q qm(q)\, dq \qquad (1.5.8)$$

on noting that $m(q,\phi) = m(q)$ due to the axisymmetry of the problem.

Using similar reasoning to that detailed in section 3 we set $p(r,0) = 0$ across the gap, so that

$$\int_0^a qm(q) \int_0^{2\pi} P(r,q,\phi,0)\, d\phi\, dq = \frac{\alpha^2 \mu}{4\pi s} \qquad (1.5.9)$$

or

$$\int_0^a m(q)\, P_1(r,q)\, dq = \frac{\alpha^2 \mu}{4\pi s} \qquad (1.5.10)$$

where

$$P_1(r,q) = q \int_0^{2\pi} P(r,q,\phi,0)\, d\phi \qquad (1.5.11)$$

Once again we are faced with the problem of solving the equations (1.5.8) and (1.5.9) simultaneously to determine the unknowns $m(r)$ and s. In this case, however, we have some added difficulty in that the integral of the pressure Green's function must be obtained. The non-dimensionalization $r = ar^*$, $q = aq^*$, $P_1 = P_1^* \alpha^2 \mu / 4\pi s$ gives (we immediately omit the stars)

$$\int_0^1 m(q)\, P_1(r,q)\, dq = 1 \qquad (1.5.12)$$

and

$$\frac{s}{a} = 2\pi \int_0^1 qm(q)\, dq \qquad (1.5.13)$$

Although a formal analytic integration of the kernel

function $P_1(r,q)$ cannot be carried out, due to the complicated nature of the functions involved, a great deal of simplification may be made. This allows relatively fast and accurate computation of the kernel function.

In taking the limit as $z \to 0$ the third term in (1.5.4) vanishes. We consider the remaining terms one by one. After suitable substitutions, the first may be written as

$$I_1 = q \int_0^{2\pi} \frac{1}{(q+r)\sqrt{1-(4qr/(q+r)^2)\sin^2((\phi-\pi)/2)}}\, d\phi \qquad (1.5.14)$$

$$= \frac{2q}{q+r} \int_{-\pi/2}^{\pi/2} \frac{1}{\sqrt{1-\ell \sin^2 \nu}}\, d\nu \qquad (1.5.15)$$

where $\ell = 4rq/(r+q)^2$.

Finally we may recognise I_1 as

$$I_1 = \frac{4q}{q+r} K(\ell) \qquad (1.5.16)$$

where $K(\ell)$ is the complete elliptic integral of the first kind (see Abramowitz and Stegun (1964), p.590).

In a similar way, the second term in (1.5.4) is given by

$$I_2 = -\frac{2q}{(q+r)^3 \alpha^2 a^2} \int_{-\pi/2}^{\pi/2} \frac{d\nu}{(1-\ell \sin^2 \nu)^{3/2}} \qquad (1.5.17)$$

$$= -\frac{4q}{(q+r)^3 i\beta} \frac{1}{1-\ell} E(\ell) \qquad (1.5.18)$$

where $E(\ell)$ is the complete elliptic integral of the second kind. Equation (1.5.18) may be obtained from equation (1.5.17) with the use of relations (17.2.14) and (17.2.24) in Abramowitz and Stegun.

Finally the integral term in (1.5.4) must be considered. We have

$$I_3 = q \int_0^{2\pi} \lim_{z\to 0} \int_0^{\infty} \lambda\sqrt{\lambda^2+\alpha^2}\; e^{-\lambda z}\; J_0(\lambda\gamma)\, d\lambda\, d\phi \qquad (1.5.19)$$

$$= q \int_0^{2\pi} \lim_{z\to 0} \left(\alpha^2 + \frac{\partial^2}{\partial z^2}\right)\left(\int_0^{\infty} \frac{\lambda e^{-\lambda z} J_0(\lambda\gamma)\, d\lambda}{\sqrt{\lambda^2+\alpha^2}}\right) d\phi \qquad (1.5.20)$$

on interchanging the order of differentiation and integration. The inner integral is a standard Laplace transform so that we have

$$I_3 = q \int_0^{2\pi} \lim_{z\to 0} \left(\alpha^2 + \frac{\partial^2}{\partial z^2}\right) \frac{e^{-\alpha\sqrt{\gamma^2+z^2}}}{\sqrt{\gamma^2+z^2}}\, d\phi \qquad (1.5.21)$$

Finally, after some manipulation,

$$I_3 = \frac{4q}{q+r}\left[\int_0^1 \frac{e^{-\sqrt{i\beta}(q+r)\sqrt{1-\ell x^2}}}{\sqrt{1-\ell x^2}\;\sqrt{1-x^2}}\, dx - \frac{1}{\sqrt{i\beta}(q+r)^2}\int_0^1 \frac{e^{-\sqrt{i\beta}(q+r)\sqrt{1-\ell x^2}}}{(1-\ell x^2)\sqrt{1-x^2}}\, dx \right.$$
$$\left. - \frac{1}{i\beta}\int_0^1 \frac{e^{-\sqrt{i\beta}(q+r)\sqrt{1-\ell x^2}}}{(1-\ell x^2)^{3/2}\sqrt{1-x^2}}\, dx\right] \qquad (1.5.22)$$

Numerical evaluation of the integrals I_1 and I_2 is straightforward since accurate polynomial expansions exist for computing them (again, see Abramowitz and Stegun, Chap. 17). The integrals in (1.5.22) are unfortunately not so straightforward. As can be seen, the principal difficulty in evaluating these integrals occurs as $\ell \to 1$ when they become very singular. One method is just to ignore this problem and accept the computing time penalty for $\ell \to 1$. This would be a reasonable approach, except for the fact that $\ell \to 1$ corresponds to $q \to r$. This means that in our final matrix inversion, the elements with $\ell \to 1$ will be on or near the diagonal of the matrix. Since small variations in the on-diagonal elements can cause large errors in the final output, we must find a better way to evaluate I_3. To this end

we rewrite (1.5.22) as

$$I_3 = 4q\left[\int_{\sqrt{1-\ell}}^{1} \frac{e^{-\sqrt{i\beta}(q+r)x}}{\sqrt{\ell-1+x^2}\sqrt{1-x^2}}\left(\frac{1}{i\beta(q+r)^3x^2} + \frac{1}{\sqrt{i\beta}(q+r)^2x} - \frac{1}{q+r}\right)dx\right] \tag{1.5.23}$$

The two square root singularities in (1.5.23) may be dealt with by proper choice of integration mesh points. To overcome the remaining difficulties (encountered near $x=0$) we note that

$$e^{-x}\left(\frac{1}{x^2} + \frac{1}{x} - 1\right) \to \frac{1}{x^2} - 1.5 \text{ as } x \to 0 \tag{1.5.24}$$

so that writing (1.5.23) as

$$I_3 = 4q\int_{\sqrt{1-\ell}}^{1} \frac{e^{-\sqrt{i\beta}(q+r)x}}{\sqrt{\ell-1+x^2}\sqrt{1-x^2}}\left(\frac{1}{i\beta(q+r)^3x^2} + \frac{1}{\sqrt{i\beta}(q+r)^2x} - \frac{1}{q+r}\right)dx$$

$$- 4q\int_{\sqrt{1-\ell}}^{1} \frac{dx}{\sqrt{\ell-1+x^2}\sqrt{1-x^2}}\left(\frac{1}{i\beta(q+r)^3x^2} - \frac{1.5}{(q+r)}\right) + I_4 \tag{1.5.25}$$

allows the integral to be readily evaluated since the singularity near $x=0$ has been removed. I_4 may be recognised as

$$I_4 = -\frac{4q}{(q+r)^3 i\beta}\frac{1}{1-\ell}E(\ell) + \frac{6q}{q+r}K(\ell) \tag{1.5.26}$$

where $E(\ell)$ and $K(\ell)$ are easily evaluated as described earlier. Finally we have

$$P_1(r,q) = I_1 + I_2 + I_3 \tag{1.5.27}$$

so that we may now evaluate the pressure Green's function in a straightforward way.

At this stage we may examine the behaviour of the kernel

function as $r \to q$. It can be shown that the kernel behaves like

$$P_1(r,q) \to -5 \log |r-q| - \frac{4}{i\beta(r-q)^2} \quad \text{as} \quad r \to q \tag{1.5.28}$$

1.6 Asymptotic Results

In the case of a two-dimensional slit, some progress may be made in the solution of the integral equation (1.3.10), without recourse to numerical methods, in the special cases $\beta \to 0$ and $\beta \to \infty$. Due to the complicated nature of the kernel function, no such results have yet been obtained for the circular hole problem.

As $\beta \to \infty$, (1.3.10) reduces to

$$\frac{2}{\pi} \mu\alpha^2 \int_{-a}^{a} m(\xi) \log |x-\xi| d\xi = - \frac{\mu\alpha^2}{2\pi} \log s \tag{1.6.1}$$

or in non-dimensional variables (see 1.3)

$$\int_{-1}^{1} m(\xi) \log |x-\xi| d\xi = - \frac{1}{4} \log s/a \tag{1.6.2}$$

Differentiating this integral with respect to x gives

$$\int_{-1}^{1} \frac{m(\xi)}{x-\xi} = 0 \tag{1.6.3}$$

which has the solution $m(x) = D/\sqrt{1-x^2}$ where D is some constant. Note that this is a singular limit since the no-slip condition at $x = \pm 1$ (1.2.10) is no longer satisfied.

Using the normalization condition on the velocity through the gap (1.3.9) we find that $D = -\frac{1}{4}\pi$ so that

$$\log s/a = 1/\pi \int_{-1}^{1} \frac{\log|x-\xi|}{\sqrt{1-\xi^2}} d\xi \tag{1.6.4}$$

$$= - \log 2$$

Thus $s/a = 0.5$, which is in agreement with the results of inviscid theory that are applicable for the limit $\beta \to \infty$ (see Tuck (1975)).

When β is small, we find that

$$P(x,\xi) = \frac{4\mu}{\pi(x-\xi)^2} + \frac{3\mu\alpha^2 \log|x-\xi|}{\pi} + \frac{1}{\pi}\mu\alpha^2\left(\log\frac{\alpha}{2} + \gamma - \frac{1}{2}\right) \tag{1.6.5}$$

It is necessary to take all these terms for the limiting behaviour of the kernel because of the separate influences of the real and imaginary parts of the kernel function. An accurate solution (as $\beta \to 0$) for the imaginary part of $\log s/a$ may be obtained by merely considering the double-pole part of the expansion. The real part of $\log s/a$, however, is not obtained so easily. This, of course, is by far the most important quantity, since it determines the magnitude of the effective gap size, whereas the imaginary part merely determines the phase.

In non-dimensional form, (1.3.10) then becomes

$$\int_{-1}^{1} m(\xi)\left[0.75\log|x-\xi| + \frac{1}{\alpha^2 a^2 (x-\xi)^2}\right]d\xi = -\frac{1}{8}\log\frac{s}{a} + \frac{1}{16}[\log \alpha a - .416] \tag{1.6.6}$$

This may be rewritten as

$$\frac{1}{\pi}\int_{-1}^{1} m(\xi)\left[k^2\log|x-\xi| - \frac{d^2}{dx^2}\log|x-\xi|\right]d\xi = F \tag{1.6.7}$$

where $k = \sqrt{0.75\alpha a}$ and

$$F = -\frac{k^2}{6\pi}\log\left(\sqrt[4]{\frac{s/a}{i\beta}}\right) + 0.0347\,k^2 \tag{1.6.8}$$

For the present we let $F=-1$ and rewrite (1.6.7) as a linear

differential equation

$$\frac{d^2y}{dx^2} - k^2 y = 1 \qquad (1.6.9)$$

with $$y = \frac{1}{\pi}\int_{-1}^{1} m(\xi)\log|x-\xi|\,d\xi \qquad (1.6.10)$$

on interchanging the order of integration and differentiation.

Equation (1.6.9) implies

$$y = -\frac{1}{k^2} + A\cosh kx \qquad (1.6.11)$$

where A is some constant. We thus have, using (1.6.10)

$$\frac{1}{\pi}\int_{-1}^{1} m(\xi)\log|x-\xi|\,d\xi = -\frac{1}{k^2} + A\cosh kx \qquad (1.6.12)$$

Differentiating this expression with respect to x gives

$$\frac{1}{\pi}\int_{-1}^{1} \frac{m(\xi)\,d\xi}{x-\xi} = A\,k\sinh kx \qquad (1.6.13)$$

which may be recognised as a finite Hilbert transform. On using a standard inversion formula, we have

$$m(x) = -\frac{1}{\pi}\sqrt{1-x^2}\;\; A\,k\int_{-1}^{1} \frac{d\xi\,\sinh k\xi}{(\xi-x)\sqrt{1-\xi^2}} \qquad (1.6.14)$$

Here terms singular at $x = \pm 1$ have been omitted since at low frequency we require that the no-slip condition at the edge of the gap (1.2.10) should be satisfied. Unfortunately, the integral in (1.6.14) cannot be easily computed. To obtain a solution for low frequency we therefore return to equation (1.6.12). We assume we may write

$$m(x) = m_1(x)k^{-2} + m_2(x) + m_3(x)k^2 + m_4(x)k^4 + \ldots \qquad (1.6.15)$$

and $$A = a_1 k^{-2} + a_2 + a_3 k^2 + a_4 k^4 + \ldots \qquad (1.6.16)$$

The function $\cosh kx$ may be written as

$$\cosh kx = 1 + \frac{k^2x^2}{2!} + \frac{k^4x^4}{4!} + \frac{k^6x^6}{6!} + \ldots \qquad (1.6.17)$$

Inserting (1.6.15) - (1.6.17) in (1.6.12) gives

$$\begin{aligned} 1/k^2\,Lm_1 + Lm_2 + k^2\,Lm_3 + k^4\,Lm_4 + \ldots \\ = -1/k^2 + a_1/k^2 + (a_2 + a_1x^2/2!) \\ + k^2(a_3 + a_2x^2/2! + a_1x^2/4!) \\ + k^4(a_4 + a_3x^2/2! + a_2x^4/4! + a_1x^6/6!) \\ + \ldots \end{aligned} \qquad (1.6.18)$$

where the operator L is defined by

$$Lm = \frac{1}{\pi}\int_{-1}^{1} m(\xi)\,\log|x-\xi|\,d\xi \qquad (1.6.19)$$

Grouping together terms of like order in k we write

$$Lm_1 = (a_1 - 1) \qquad (1.6.20)$$

$$Lm_2 = (a_2 + a_1x^2/2!) \qquad (1.6.21)$$

$$Lm_3 = (a_3 + a_2x^2/2! + a_1x^4/4!) \qquad (1.6.22)$$

and so on.

We may now solve these equations in a recursive fashion. Differentiating (1.6.20) gives

$$\frac{1}{\pi}\int_{-1}^{1} \frac{m_1(\xi)}{x-\xi}\,d\xi = 0 \qquad (1.6.23)$$

which has the solution

$$m_1(x) = \frac{C}{\sqrt{1 - x^2}} \qquad (1.6.24)$$

Since m_1, m_2 etc. must all satisfy the edge condition (1.2.10), C must be zero and hence $m_1(x)$ must be zero everywhere. Thus $a_1 = 1$. (This may easily be verified.) Using this value for a_1 we may now solve equation (1.6.21) in the same

way. We have

$$\frac{1}{\pi} \int_{-1}^{1} \frac{m_2(\xi)}{x-\xi} d\xi = x \qquad (1.6.25)$$

so that $$m_2(x) = \sqrt{1 - x^2} \qquad (1.6.26)$$

Substituting (1.6.26) back into (1.6.21) gives

$$Lm_2 = \frac{1}{\pi} \int_{-1}^{1} \sqrt{1 - x^2} \log |x-\xi| d\xi \qquad (1.6.27)$$

$$= 0.5x^2 - 0.25 - 0.5 \log 2 \qquad (1.6.28)$$

so that $a_2 = -0.25 - 0.5 \log 2$ (1.6.29)

Proceeding in this manner we find

$$m_3(x) = 1/3!\ x^2\sqrt{1 - x^2} - (1/6 + 0.5 \log 2)\sqrt{1 - x^2} \qquad (1.6.30)$$

and

$$a_3 = -1/24 \log 2 + (1/6 + 0.5 \log 2)(1/4 + 0.5 \log 2) \qquad (1.6.31)$$

Collecting the above results we may write

$$m(x) = \sqrt{1 - x^2} + (1/3!\ x^2\sqrt{1 - x^2} - (1/6 + 0.5 \log 2)\sqrt{1 - x^2})$$

$$k^2 + 0(k^4)$$

$$= f(x) \qquad (1.6.32)$$

Thus the solution to the original equation (1.6.7) is

$$m(x) = Ff(x) \qquad (1.6.33)$$

The normalization condition for the velocity through the gap now allows us to determine the effective gap size s/a. We have

$$F \int_{-1}^{1} f(\xi) d\xi = -0.25 \qquad (1.6.34)$$

which implies

$$\log s/a = [0.25 \log i\beta + 4/i\beta - 1.058 - 1.5 \log 2] \qquad (1.6.35)$$

Equation (1.6.35) is a very simple result, and as will be shown later (in section 1.8) it gives very good results for values of β up to about 4.

1.7 Numerical Analysis

We have to solve the integral equations (1.3.15) and (1.5.12). In both cases we assume the unknown source strength $m(\xi)$ is proportional to the velocity across the gap and is a slowly-varying function of ξ, except at the edge of the gap $\xi=1$. We therefore divide the gap $0 < \xi < 1$ into a set of N segments $\xi_j < \xi < \xi_{j+1}$, on each of which we approximate $m(\xi) = \text{constant} = m_j$. Thus (1.3.15) becomes

$$\sum_{j=1}^{N} m_j \int_{\xi_j}^{\xi_{j+1}} P(x,\xi)\,d\xi = 1 \qquad 0 < x < 1 \tag{1.7.1}$$

We satisfy (1.7.1) at a set of N points $x = x_i$, so that

$$\sum_{j=1}^{N} A_{ij}\, m_j = 1 \qquad i = 1,2,\ldots,N \tag{1.7.2}$$

where

$$A_{ij} = \int_{\xi_j}^{\xi_{j+1}} P(x_i,\xi)\,d\xi \tag{1.7.3}$$

$$= \left[Q(x_i - \xi) - Q(x_i + \xi) \right]_{\xi_j}^{\xi_{j+1}} \tag{1.7.4}$$

The problem is therefore solved, upon solution by standard methods of the matrix-vector equation

$$A\,\underset{\sim}{m} = \underset{\sim}{1} \tag{1.7.5}$$

where

$$A = [A_{ij}] \tag{1.7.6}$$

$$\underset{\sim}{m} = [m_j] \tag{1.7.7}$$

and all elements of the vector $\underset{\sim}{1}$ are of unit value. We

choose as collocation points

$$\xi_j = \sin \frac{\pi}{2}\left(\frac{j-1}{N}\right) \qquad j = 1,2,\ldots,N+1 \tag{1.7.8}$$

and

$$x_i = \sin \frac{\pi}{2}\left(\frac{i-\frac{1}{2}}{N}\right) \qquad i = 1,\ldots,N \tag{1.7.9}$$

This non-uniform spacing accommodates the expected square-root singularity in the normal velocity as $\xi \to 1$, since the interval size tends to zero correspondingly.

The above procedure must be modified slightly in the case of the three-dimensional problem. Since it does not appear to be possible to determine the indefinite integral of the kernel function we may write down an expression like (1.7.3) but cannot continue through to one like (1.7.4). We have, with $r_j m_j$ taken as the unknown, (see end of this chapter),

$$\sum_{j=1}^{N} B_{ij}\, m_j r_j = 1 \qquad i = 1,\ldots,N \tag{1.7.10}$$

where

$$r_j B_{ij} = \int_{q_j}^{q_{j+1}} P_1(r_i, q)\, dq \tag{1.7.11}$$

and the points q_j, $j=1,\ldots,N+1$, r_i, $i=1,\ldots N$ are given by formulae like (1.7.8) and (1.7.9) respectively. Evaluation of B_{ij} by numerical integration techniques is possible but is also inaccurate and time-consuming due to the singularity as $q \to r_i$. This difficulty may be overcome by a process of "subtracting out the singularity" from the integral. Using (1.5.26)

$$r_j B_{ij} = \int_{q_j}^{q_{j+1}} \left[P_1(r_i, q) + 5 \log|r_i - q| + \frac{4}{i\beta (r_i - q)^2} \right] dq$$

$$- \left[5(q - r_i)\log|r_i - q| - 5q - \frac{4}{i\beta (q - r_i)} \right]_{q_j}^{q_{j+1}} \tag{1.7.12}$$

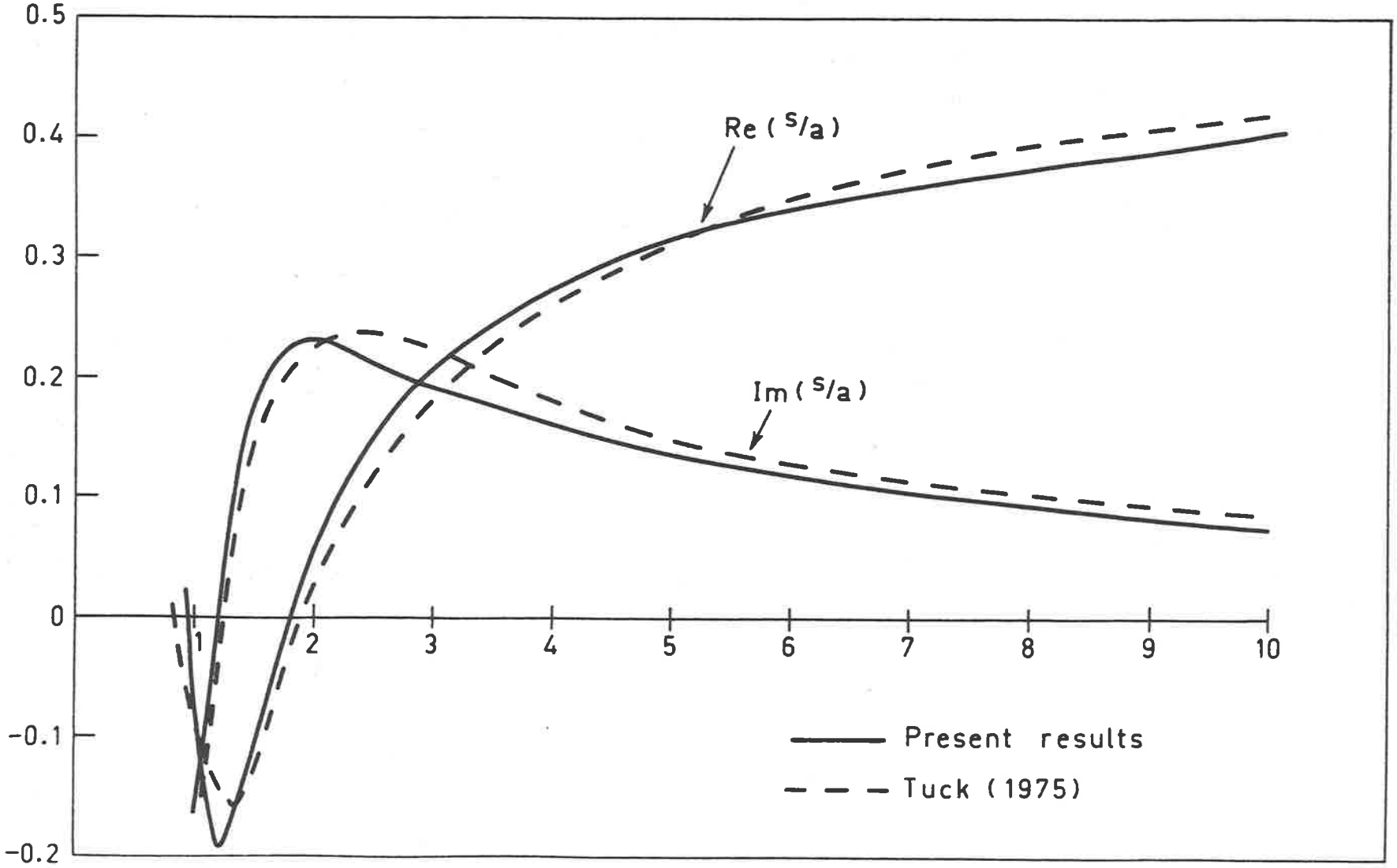

Figure 3 Real and imaginary parts for the effective size, s/a of a single two-dimensional gap, compared with the results of Tuck (1975).

The integral in (1.7.12) is now well-behaved as $q \to r_i$ and may be evaluated by standard numerical integration techniques (e.g. Simpson's rule). Again it should be noted that we have used the Hadamard interpretation of the double pole in integrating straight through the singularity (see Appendices). In fact, there is every chance that if we did not remove the singularity in this way, we would not be interpreting the double-pole singularity in the correct manner and so would not be able to obtain meaningful results at all.

1.8 Results

The preceding numerical procedures for both the two and three-dimensional problems were coded in Fortran on the Adelaide University CDC 6400 computer. The programme was run with various different numbers of mesh points and it was found that a 20-point mesh gave satisfactory accuracy for the two-dimensional problem. The circular hole numerical procedure was not so quickly convergent due to the fact that a large amount of numerical integration was entailed. Despite this fact, good results were obtained for this problem with a 40-point mesh. We consider the two-dimensional results first.

In Figure 3 the effective gap size s/a is compared with earlier results obtained in a quite different manner by Tuck (1975). Tuck states that his results are somewhat suspect for low-Reynolds number ($\beta < 1$). As can be seen, however, reasonable agreement is shown between the two sets of results. It is not shown on the figure, but both the real and imaginary parts of s/a oscillate in sign more and more quickly as $\beta \to 0$. This is due to the fact that Im log s/a becomes very large as $\beta \to 0$. Because of this it may appear

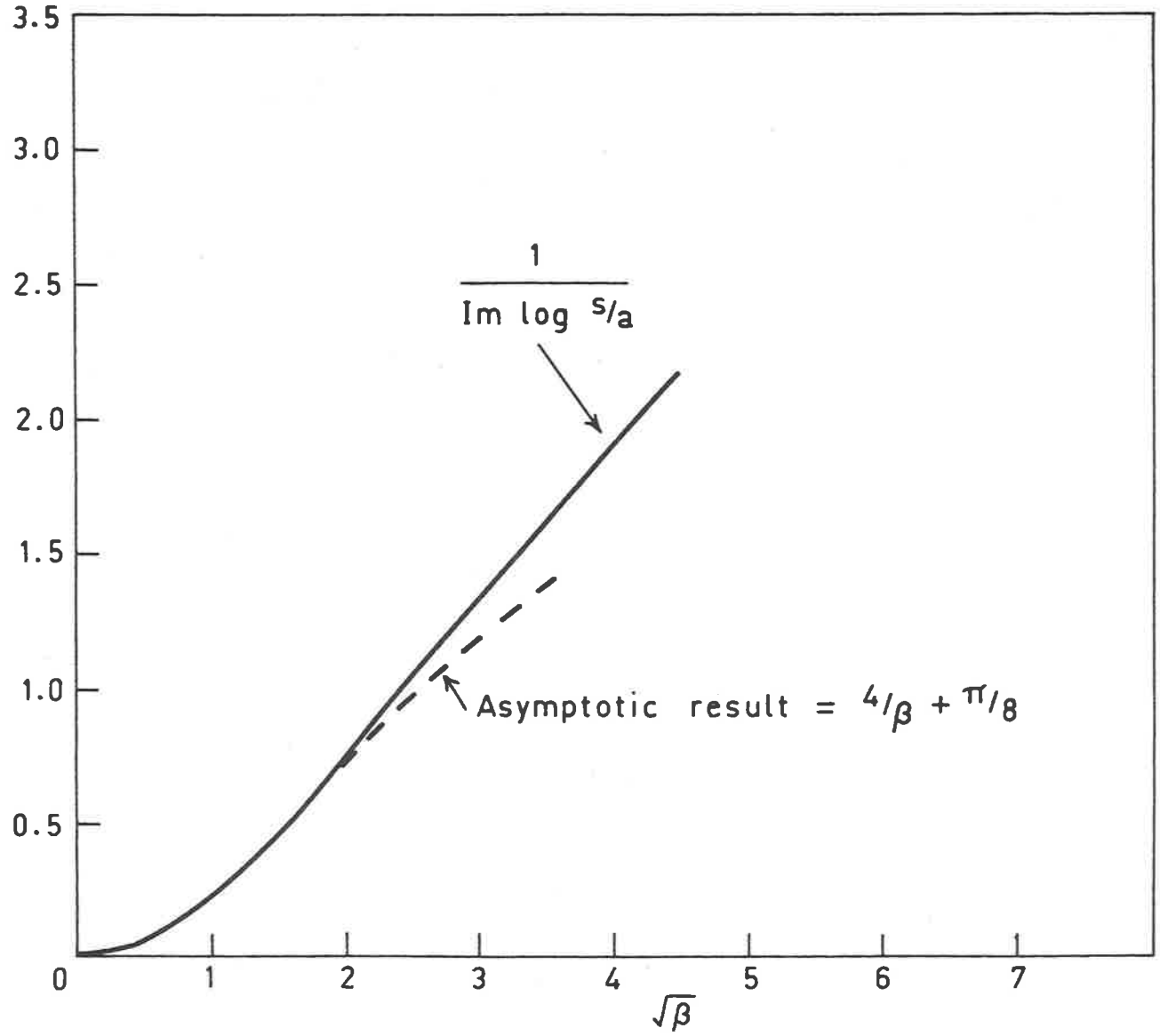

Figure 4 Comparison of analytic method and numerical method for single slit, at small Reynolds number. The imaginary part of s/a is shown.

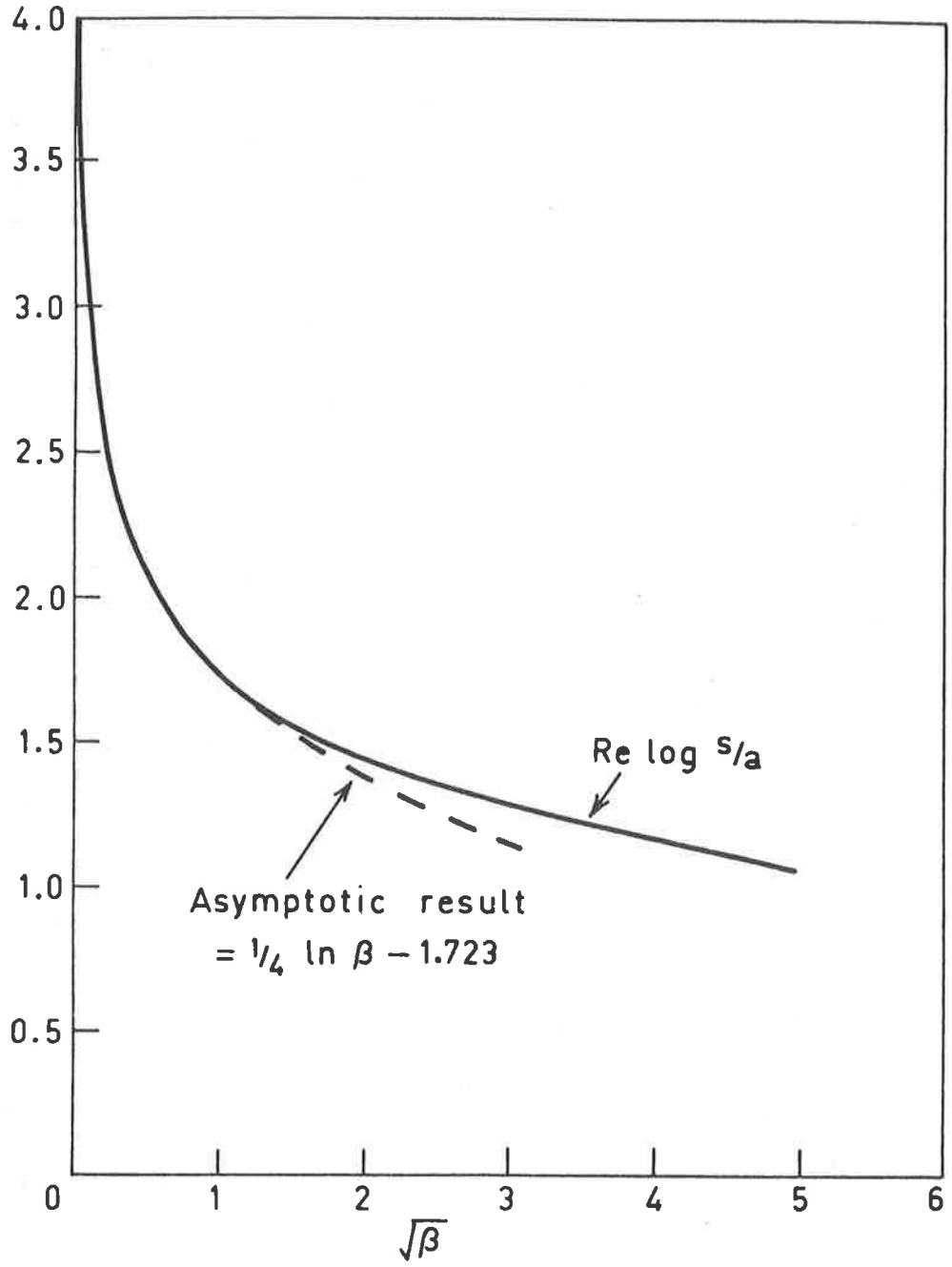

Figure 5 Comparison of analytic method and numerical method for single slit at low Reynolds number. The real part of s/a is shown.

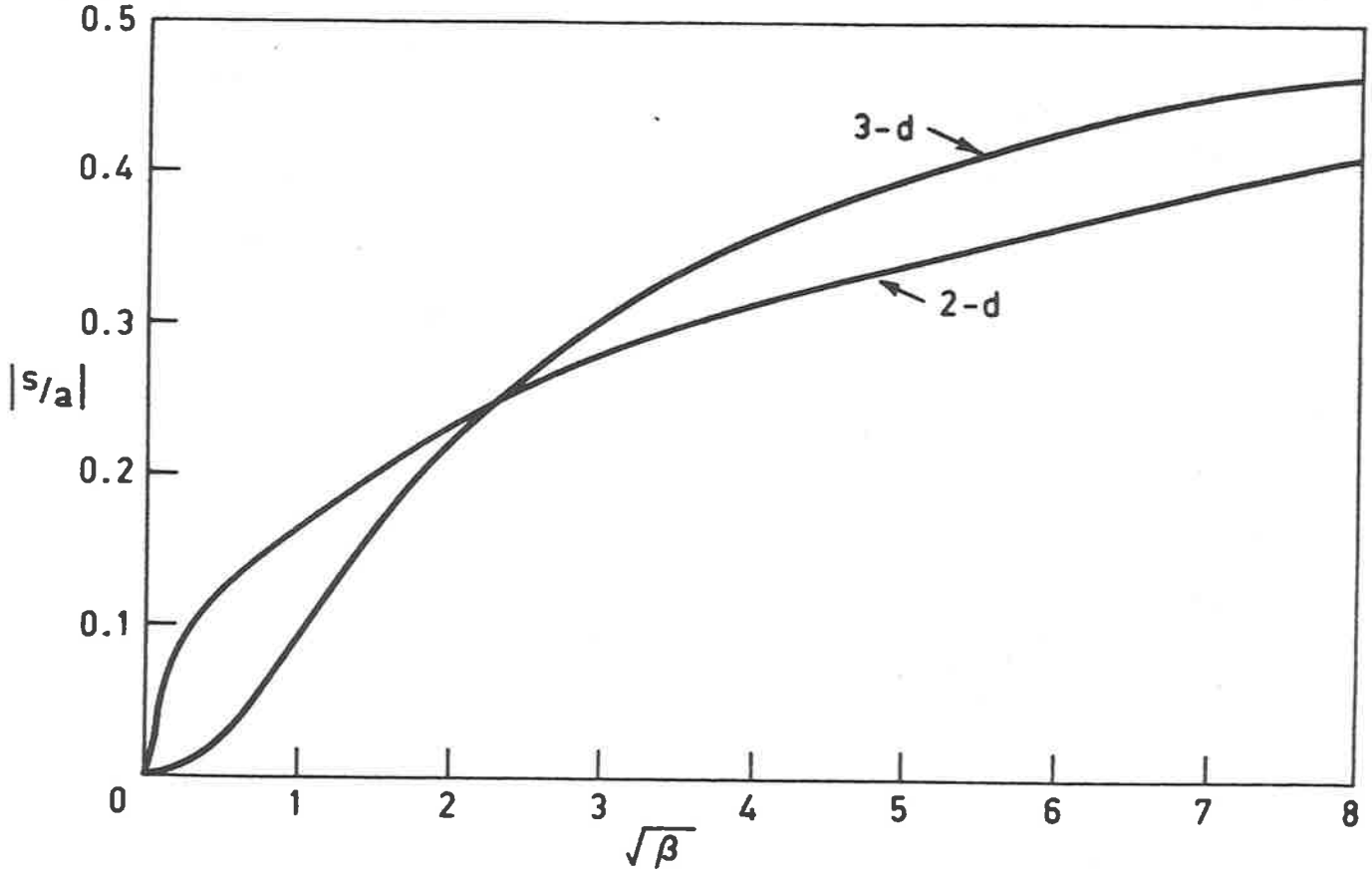

Figure 6 Graphical comparison of the effective gap size s/a of a circular hole, and of a single slit.

that accurate results are difficult to obtain as $\beta \to 0$. The present method is not, however, affected by this as its output is actually $\log s/a$, the real and imaginary parts of which are monotonic functions. Results for these two quantities are shown in Figures 4 and 5.

In Figure 4 we compare $[\mathrm{Im} \log s/a]^{-1}$ with the asymptotic approximation $(4\beta + \pi/8)^{-1}$ (see equation (1.6.35)). Excellent agreement is shown up to values of $\beta \simeq 4$ and, indeed, even at larger values of β the asymptotic results show the correct trend.

Similar good agreement between the asymptotic and numerical results is shown in Figure 5 where $\mathrm{Re} \log s/a$ is displayed.

Finally, in Figure 6 we display the magnitude of the effective gap size for both the two-dimensional slit and the circular hole. In each case the magnitude approaches the correct inviscid limits as $\beta \to \infty$, namely $s/a = 2/\pi$ for the hole and $s/a = 0.5$ for the slit. It should be noted, however, that in the case of a circular hole the inviscid limit is reached at a much lower value of β than for the slit. This indicates that local viscosity effects in the vicinity of the gap are more important in the two-dimensional problem.

As $\beta \to 0$ the approach to zero of the magnitude of s/a is much faster for the three-dimensional problem than it is for the two-dimensional one. It is not immediately obvious why this should be so. Since no asymptotic results are available for the circular hole, it is not possible to confirm the accuracy of the numerical method for small Reynolds number.

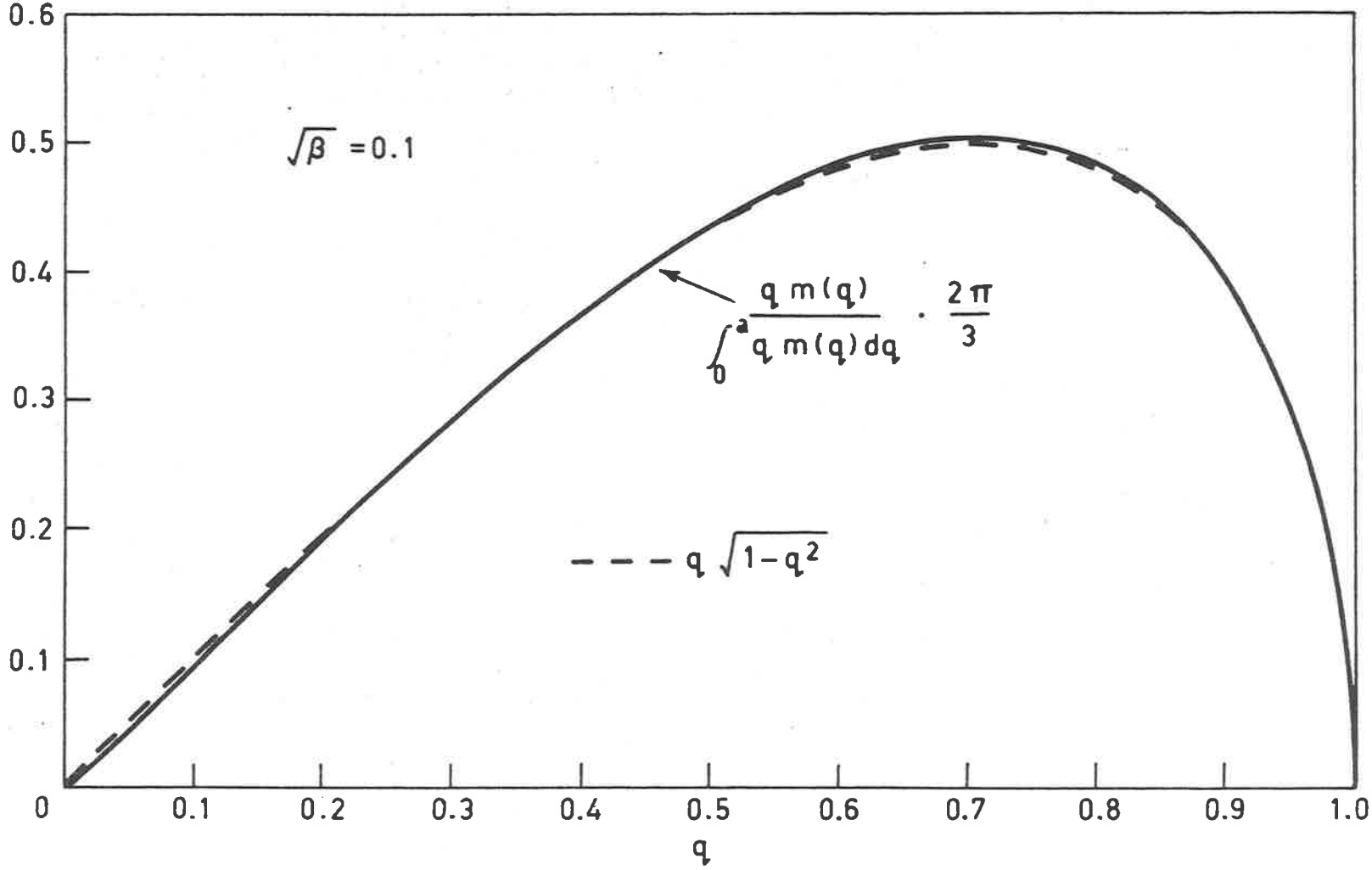

Figure 7 Normal fluid velocity across a circular hole at low Reynolds number. Comparison with de Mestre and Guiney (1971).

Fortunately, there are some analytic results available for axisymmetric flow at very small Reynolds number, due to de Mestre and Guiney (1971). In this limit as $\beta \to 0$ the notion of effective size has no real meaning (to all intents and purposes $|s/a| = 0.$) It is possible to compare the two methods, however, by considering the source strength across the gap. This, it may be recalled, is half the normal velocity through the gap. The normalized velocity at the gap is given by de Mestre and Guiney as

$$m(r) = -3\sqrt{1-r^2} \qquad (1.8.1)$$

where we have suppressed a sinusoidal time dependence.

In Figure 7 we compare $rm(r)$ as given by the numerical method, with the result (1.8.1) for $\beta = 0.1$. As can be seen, agreement is excellent right across the gap. This dispels any doubts that might remain as to the correctness at low-Reynolds number of the numerical method in the axisymmetric flow problems.

It is important to note, though, that the error in the numerical method is greatest near $r=0$. In fact, if we use the velocity $m(r)$ as our basic unknown and then solve as before, it is found that near $r=0$, the numerical solution is apparently wrong. This is caused by clumsy formulation of the problem. If we substitute the boundary condition (1.4.16) in the equation for the stream function (1.5.1), we can show that

$$2\int_0^a qm(q)\ \delta(q-r)\,dq = -rv(r) \qquad (1.8.2)$$

where $\delta(q-r)$ is a delta function. This implies that $m(r) = -v(r)/2$ for $r > 0$, as required. It also implies, however, that $m(r) = 0$ for $r \leqslant 0$. Thus the numerical method has to model a step function at $r=0$, if we use the

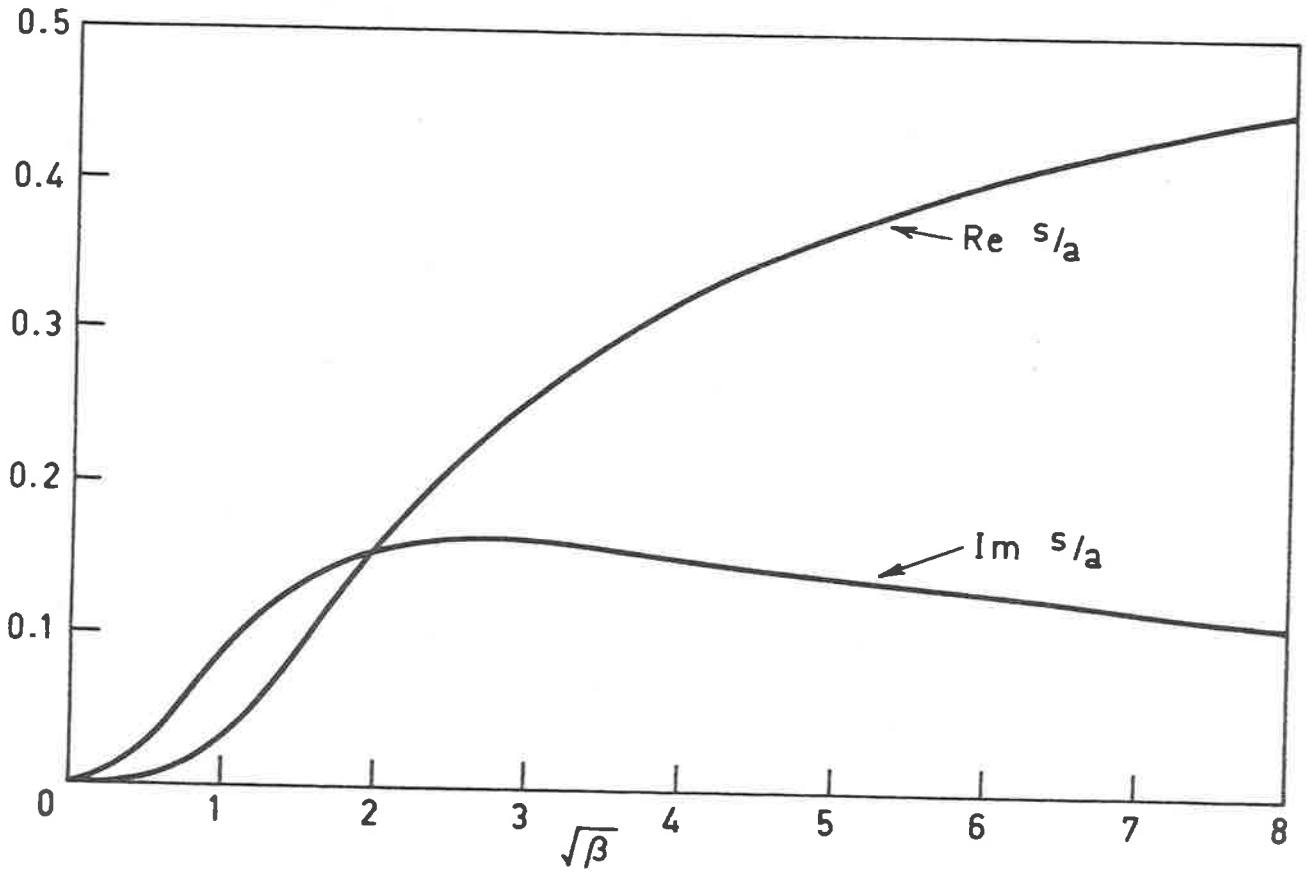

Figure 8 Real and imaginary parts of the effective gap size s/a of a circular hole.

source strength as our basic unknown. It does this reasonably successfully, but it seems better to use rm(r) as our unknown and thus avoid this difficulty. There is still a small problem, however, in that the first derivative of rm(r) is not continuous. This probably explains why the largest error occurs near r=0.

The last graph, Figure 8 shows the real and imaginary parts of the effective size for the circular gap. In contrast to the two-dimensional problem, there is no oscillation in the sign of these two quantities as $\beta \to 0$. At low-Reynolds number (<1) it may be noticed that the imaginary part of s/a dominates, indicating that there are almost no inertial effects for this range of β. This explains the good agreement demonstrated above with de Mestre and Guiney (1971), who ignore inertial effects completely in the near vicinity of the gap.

CHAPTER 2

UNSTEADY VISCOUS FLOW THROUGH A SCREEN

2.1 Introduction

This chapter is essentially an extension of the work presented in Chapter 1, where viscous flow through a single two-dimensional slit was described. Here we consider the situation where we have a regular array of slits of width $2a$ with centre separation $2b$. We use a similar method of solution to that described in Chapter 1.

The problem described here has direct application in the determination of the acoustic impedance of a thin permeable barrier. This impedance is a measure of the relationship between the pressure difference across the screen and the air velocity through the barrier. Thus, in a time-sinusoidal flow of radian frequency σ, we have

$$\Delta p = \Gamma . V \qquad (2.1.1)$$

where the pressure jump is $\mathcal{R}e(\Delta p e^{i\sigma t})$, the normal velocity is $\mathcal{R}e(Ve^{i\sigma t})$ and Γ is the acoustic impedance. To determine this impedance we need to know both the viscous dissipation, which determines the resistive part, and the inertia of the oscillating columns of air in the pores, which determines the reactive part. Usually these quantities are obtained experimentally, but here we may evaluate Γ theoretically using the ideas of Chapter 1.

We may still assume that viscous effects are important only in the near vicinity of the wall and that the velocity amplitude of the acoustic fluctuations is small enough so that linearization of the Navier-Stokes equations is permissible. To neglect compressibility near the pores we

need the additional assumption that the acoustic wavelength should be much larger than the pore dimensions. This is true in most practical applications. Since this formulation only determines an inner solution, i.e. one that is valid near the wall, one would need to match with an outer solution, where compressibility was included, to solve the complete acoustic problem. This will not, however, be considered here. Although we are primarily interested in the acoustic problem, the results presented here allow the determination of real fluid effects in problems such as channel flow through a screen or water-wave flow through a porous barrier.

As in Chapter 1, the only non-dimensional parameter in the local flow is the non-dimensional frequency β, defined in (1.1.1). The linearization of the Navier-Stokes equations implies that the true Reynolds number Va/ν is small, so that the velocity scale V is not dynamically significant. This was also the case for flow through a single slit. In Chapter 1, the obstruction to the flow was measured in terms of the "effective gap size". Here it is more suitable to use a non-dimensional blockage coefficient C. In the case where viscosity is unimportant, even in the neighbourhood of the pores (i.e. $\beta \to \infty$), this may be related to the impedance Γ by

$$\Gamma = -2i\sigma\rho aC \qquad (2.1.2)$$

In this limit, Γ is a purely imaginary quantity, while C is real and depends solely on the ratio of pore width to pore separation which we write as

$$\gamma = a/b \qquad (2.1.3)$$

As γ decreases from unity (i.e. no wall) to zero (i.e. no

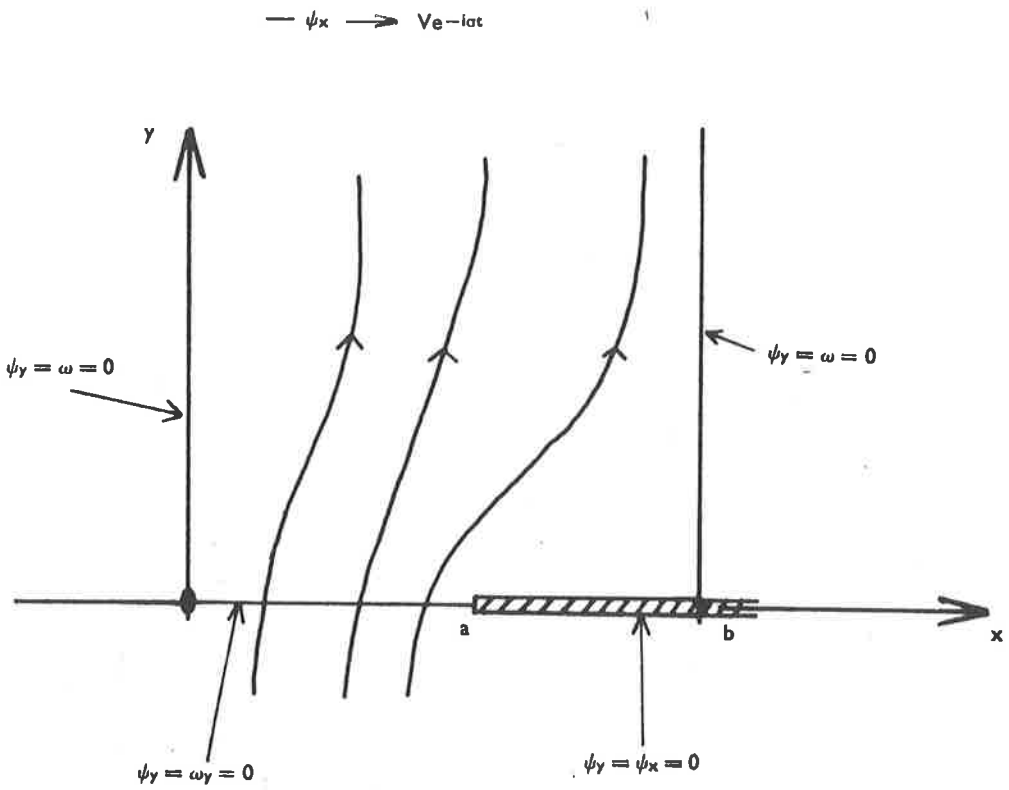

Figure 9 Schematic drawing of an elementary flow cell.

pores) the blockage coefficient C increases monotonically from zero to plus infinity.

In the more general problem considered here, Γ and C are now complex-valued and both depend on the additional parameter β. We present our output in terms of this non-dimensional complex-valued blockage coefficient.

If we introduce suitable planes of symmetry, we can confine attention to a flow cell as indicated in Figure 9. The bottom boundary of the cell $y=0$, $0 < x < b$ of the cell is divided into two portions. The section $0 < x < a$ represents half a slit while the remainder $a < x < b$ represents half a solid barrier. The side boundary $x=0$ is a plane of symmetry through the centre of a slit and that at $x=b$ is through the centre of a barrier. By superimposing image replicates of this cell we obtain the infinite array of slits as above.

Simple generalizations of this formulation are possible. Wall thickness can be readily included (admittedly with computational difficulty) while the problem where the slits are of varying width can be treated in a similar fashion.

2.2 Mathematical Formulation

Much of the following has appeared in Macaskill and Tuck (1977), but is reproduced here for completeness. To a large extent the method follows that for flow through a single slit (see Section 1.2).

Again, the Navier-Stokes equations take the form (1.2.1) with the stream function ψ satisfying (1.2.2). The pressure p is harmonic throughout the flow field and hence must satisfy the Cauchy-Riemann equations (1.2.3). Vorticity ω is generated at the wall $y=0$ and, as is the case with a single

slit, decays exponentially as $|y| \to \infty$. Thus we have the far-field boundary condition (1.2.6), relating the fluid velocity to the pressure in the outer region.

Since we now have flow through many gaps, the re-statement of the far-field condition (1.2.7) is no longer suitable. We suppose that the far-field velocity potential corresponds to a uniform oscillatory flow $u \to V_j$, so that

$$-\frac{1}{i\sigma\rho}\, p(x,y) \to V_y + \text{constant}, \quad |y| \to \infty \qquad (2.2.1)$$

This irrotational flow at a great distance (relative to the pore size) from the wall is the outer approximation to the inner flow through the pores. This must match with the inner approximation to the flow field being considered. V can thus be seen to be a velocity amplitude normal to the wall. The constant in (2.2.1) may be found by considering the pressure jump across the wall, in the same way that the effective gap size s was found in Chapter 1. Indeed, we may write in place of (1.2.9)

$$p(x,y) \to i\sigma\rho V_y \pm \tfrac{1}{2}\Delta p, \quad y \to \pm\infty \qquad (2.2.2),$$

or, using (2.1.1) and (2.1.2)

$$-\frac{1}{i\sigma\rho}\, p(x,y) \to V(y \pm aC), \quad y \to \pm\infty \qquad (2.2.3),$$

where we still have to find the blockage coefficient C as part of our solution.

The remaining boundary conditions are similar to those for the single slit (equations (1.2.10)-(1.2.12)). We must have

$$\psi_x(x,0) = \psi_y(x,0) = 0 \quad a < x < b \qquad (2.2.4)$$

the no-slip condition on the solid part of the boundary. The

pressure continuity condition (1.2.12) and the condition of normal streaming velocity through the gap (1.2.11) remain unchanged. Due to the change in the geometry of the problem, however, we must now specify extra conditions on the side boundaries $x=0,b$. These boundaries are stream surfaces, so that

$$\psi_y(0,y) = \psi_y(b,y) = 0, \quad y > 0 \tag{2.2.5}$$

The flow and hence the vorticity must be anti-symmetric about these surfaces, so that our final boundary condition is

$$\omega(0,y) = \omega(b,y) = 0 \tag{2.2.6}$$

2.3 Derivation of the Integral Equation

We write

$$\psi(x,y) = \int_0^a m(\xi)\, G(x,y,\xi)\, d\xi \tag{2.3.1}$$

where as in the single slit problem G is a Green's function satisfying (1.3.2) and $m(\xi)$ is a source strength to be determined. We can again use the function given in (1.3.3) as G. This satisfies the no-slip condition (2.2.4) but modifications must be made so that the additional side-boundary conditions (2.2.5) and (2.2.6) are satisfied. Thus we take

$$G(x,y,\xi) = \sum_{k=-\infty}^{\infty} [G_0(x - \xi + 2bk, y) + G_0(x + \xi + 2bk, y)] \tag{2.3.2}$$

where G_0 is defined in (1.3.3). This series can be shown to be convergent. For details, reference should be made to the appendix in Macaskill and Tuck (1977).

The pressure field P_0 corresponding to $\psi = G_0$ is given in (1.3.4). The pressure field $p = P$ which corresponds

to the modified Green's function G is

$$P(x,y,\xi) = \sum_{k=-\infty}^{\infty} [P_0(x - \xi + 2bk,y) + P_0(x + \xi + 2bk,y) + \bar{P}_k] \tag{2.3.3}$$

where $\bar{P}_k$ is a constant included to cancel the leading divergent term of (2.3.3) as $k \to \pm \infty$, namely

$$\bar{P}_k = -\frac{4}{\pi} \mu\alpha^2 \log 2b|k| \ , \ k \neq 0 \tag{2.3.4}$$

and P_0 is the function defined in (1.3.4).

$\bar{P}_0$ may be chosen arbitrarily. We take

$$\bar{P}_0 = \frac{4}{\pi} \mu\alpha^2 \log \frac{\pi}{b} + \frac{2\mu\alpha}{b} \tag{2.3.5}$$

If $\bar{P}_0$ satisfies (2.3.5) then $P(x,y,\xi)$ has the simple limiting form

$$P(x,y,\xi) \to \frac{2\mu\alpha^2}{b} y + 0(e^{-\pi y/b}), \ y \to \infty \tag{2.3.6}$$

(For details, again see the appendix in Macaskill and Tuck (1977)).

We can now write down an expression like (1.3.7) for the pressure through the flow field,

$$p(x,y) = \int_0^a m(\xi) \ P(x,y,\xi) d\xi + \tfrac{1}{2}\Delta p \tag{2.3.7}$$

where the arbitrary constant Δp is

$$\tfrac{1}{2}\Delta p = - i\sigma\rho aCV = - \mu\alpha^2 aCV \tag{2.3.8}$$

which satisfies (2.2.2) by virtue of the limiting behaviour of P given in (2.3.6). In fact, we may write

$$P(x,y) \to \frac{2\mu\alpha}{b} \int_0^a m(\xi) d\xi \ y + \tfrac{1}{2}\Delta p \tag{2.3.9}$$

corresponding to equation (1.3.8). Finally, on comparing (2.2.2) and (2.3.9), we may determine the normalization

condition on the source strength m,

$$-2\int_0^a m(\xi)\,d\xi = bV \tag{2.3.10}$$

As in Section 1.3 we may now obtain our final integral equation by setting $p(x,0) = 0$ across the gap, so that

$$\int_0^a m(\xi)\ P(x,0,\xi)\,d\xi = \mu\alpha^2 CV \quad 0 < x < a \tag{2.3.11}$$

Using a similar non-dimensionalization to that described in Chapter 1, with

$$m(\xi) = CVm^*(\xi^*) \tag{2.3.12}$$

equation (2.3.11) becomes

$$\int_0^1 m(\xi)\ P(x,\xi)\,d\xi = 1 \tag{2.3.13}$$

Using (2.3.10), we can express the blockage coefficient C directly in terms of the unknown source strength $m(\xi)$, i.e.

$$-2CVa\int_0^1 m(\xi)\ d\xi = bV \tag{2.3.14}$$

or

$$C = -\left[2\gamma\int_0^1 m(\xi)\,d\xi\right]^{-1} \tag{2.3.15}$$

Thus, once (2.3.13) is solved, the blockage coefficient is immediately available.

Once again we need $Q(x,\xi)$, the indefinite integral of P (see (1.3.18)). Now, however, the kernel function is more complicated, since it satisfies the additional boundary conditions (2.2.5) and (2.2.6). Therefore in determining $Q(x,\xi)$ we must first perform the summation in (2.3.3). We write

$$Q'(x) = \left(1 - \frac{1}{i\beta}\,\frac{\partial^2}{\partial x^2}\right)\left[-\frac{\gamma}{\sqrt{i\beta}} + \frac{2}{\pi}\log 2 \sin\left|\frac{\pi}{2}\gamma x\right| \right. \quad -$$

$$- \frac{2}{\pi} \sum_{k=-\infty}^{\infty} K_0 (\sqrt{i\beta}\ |x + 2k/\gamma|) \Bigg] \qquad (2.3.16)$$

The last term in the above equation follows directly from (1.3.21). In the appendix to Macaskill and Tuck it is shown that the leading terms give the contribution shown in (2.3.16) so long as the arbitrary constants $\bar{P}_k$ are chosen as in (2.3.4) and (2.3.5). $Q'(x)$ is an even function of the argument x and depends implicitly on the two parameters γ and β. At this stage we may determine the (odd) function Q as

$$Q(x) = - \gamma x (i\beta)^{-\frac{1}{2}} - (2/\pi^2 \gamma)\ f(\pi\gamma x) - (\gamma/i\beta)\ \cot(\pi\gamma x/2)$$

$$+ \frac{2}{\pi} (i\beta)^{-\frac{1}{2}} \sum_{k=-\infty}^{\infty} g(\beta^{\frac{1}{2}}(x + 2k/\gamma)) \qquad (2.3.17)$$

f and g are odd functions defined for $\theta > 0$. $g(\theta)$ is given in (1.3.23) while f is defined by

$$f(\theta) = - \int_0^{\theta} \log \sin \frac{t}{2}\, dt \qquad (2.3.18)$$

$f(\theta)$ is Clausen's integral (Abramowitz and Stegun (1964), p.1005). It may be evaluated numerically by direct trapezoidal integration after a preliminary integration by parts. This means that for numerical purposes we write

$$f(\theta) = - \theta \log \sin \frac{\theta}{2} + \int_0^{\theta} \frac{t}{2} \cot \frac{t}{2}\, dt \qquad (2.3.19)$$

where the integral is non-singular at $\theta = 0$.

We find that the kernel of the equation (2.3.13) has a double-pole singularity like that for the single-gap kernel (see (1.3.24)). Once again we may use the Hadamard interpretation to overcome this difficulty. The numerical method is

exactly the same as that described in Section 1.7, the only difference being that we use the kernel function (2.3.3) instead of the single-gap kernel when evaluating the matrix elements A_{ij} in equation (1.7.3).

2.4 Asymptotic Results

No general analytic results for the cases $\beta \to 0$ or $\beta \to \infty$ were obtained, in contrast to the single-gap problem. This was fundamentally due to the more complicated nature of the kernel in the many gap problem. It is possible, however, to compare the results obtained here with those obtained using the single-gap formulation when γ is small, i.e. when the gap width is small compared to the gap separation. In fact, for small γ it is possible to obtain an exact result for the limit $\beta \to \infty$.

When $\gamma \to 0$, the kernel $P(x,\xi)$ becomes

$$P(x,\xi) = P_1(x,\xi) + P_1(x,-\xi) + \frac{4}{\pi} \log \pi\gamma + \frac{2\gamma}{\sqrt{i\beta}} \qquad (2.4.1)$$

where

$$P_1(x,\xi) = \log |\xi-x| + \frac{1}{i\beta(\xi-x)^2} - \left(1 - \frac{1}{i\beta}\frac{\partial^2}{\partial\xi^2}\right) K_0(\sqrt{i\beta}|\xi-x|) \qquad (2.4.2)$$

In fact $P_1(x,\xi) + P_1(x,-\xi)$ may be recognised as the kernel for the integral equation describing viscous flow through a single gap (see eqn. (1.3.15)). For convenience, we rewrite (1.3.15) as

$$\int_0^1 m_1(\xi)(P_1(x,\xi) + P_1(x,-\xi))d\xi = 1 \qquad (2.4.3)$$

so that we may differentiate between the two different unknowns, $m(\xi)$ for the many gap problem and $m_1(\xi)$ for the single gap. Using (2.4.1) and (2.4.3) we may rewrite the

integral equation (2.3.13) as

$$\int_0^1 m(\xi)\,(P_1(x,\xi) + P_1(x,-\xi))\,d\xi + \frac{2}{\pi}\int_0^1 m(\xi)\left(\frac{\pi\gamma}{\sqrt{i\beta}} + 2\log \pi\gamma\right)d\xi = 1 \qquad (2.4.4)$$

when γ is small. Now we can use the normalization conditions on the two unknowns $m_1(\xi)$ and $m(\xi)$, (1.3.17) and (2.3.15) respectively, to give

$$\int_0^1 m(\xi)\,d\xi = -\frac{2\log(s/a)}{\gamma C\pi}\int_0^1 m_1(\xi)\,d\xi \qquad (2.4.5)$$

so that equation (2.4.4) implies, on using (1.3.15) and (2.4.5) to simplify the first integral, and (2.3.15) to reduce the second integral

$$-\frac{2\log(s/a)}{\gamma C\pi} - \frac{1}{\pi\gamma C}\left(\frac{\pi\gamma}{\sqrt{i\beta}} + 2\log \pi\gamma\right) = 1 \qquad (2.4.6)$$

or

$$\log s/a = -\left(\frac{\pi\gamma C}{2} + \frac{\pi\gamma}{2\sqrt{i\beta}} + \log \pi\gamma\right) \qquad (2.4.7)$$

This result allows a comparison between the numerical results obtained for the many gap problem and the single gap results presented in Chapter 1.

In the limit as $\beta \to \infty$, that is, as we approach inviscid flow, $s/a \to \frac{1}{2}$ (see Tuck (1975)) and we have, from (2.4.7)

$$C = -\frac{2}{\pi\gamma}\log\left(\frac{\pi\gamma}{2}\right) \qquad (2.4.8)$$

which is in agreement with an exact result of Sedov (1965) for inviscid channel flow through a small (centred) gap.

2.5 Results

The preceding numerical procedure was coded in Fortran on the Adelaide University CDC 6400 computer. The program was run with various different numbers of mesh points and it was found

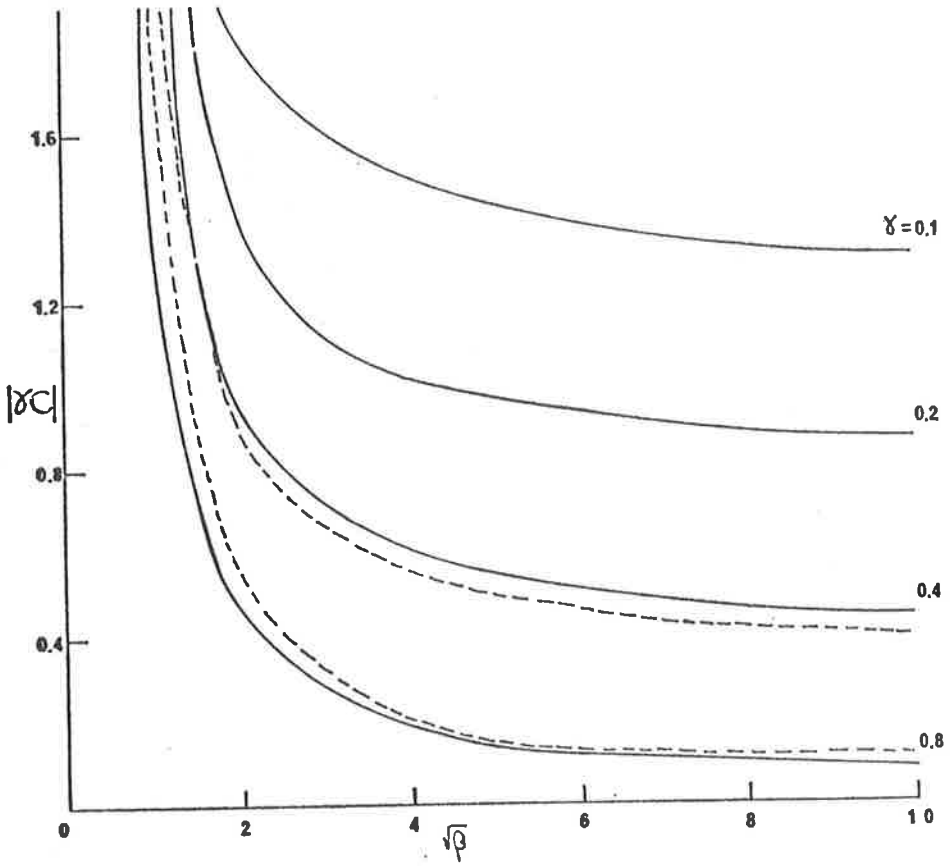

Figure 10 $|\gamma C|$ for a screen. The dashed lines are the approximation for small γ, using the single slit result; the two results coalesce for $\gamma = 0.1$ and 0.2.

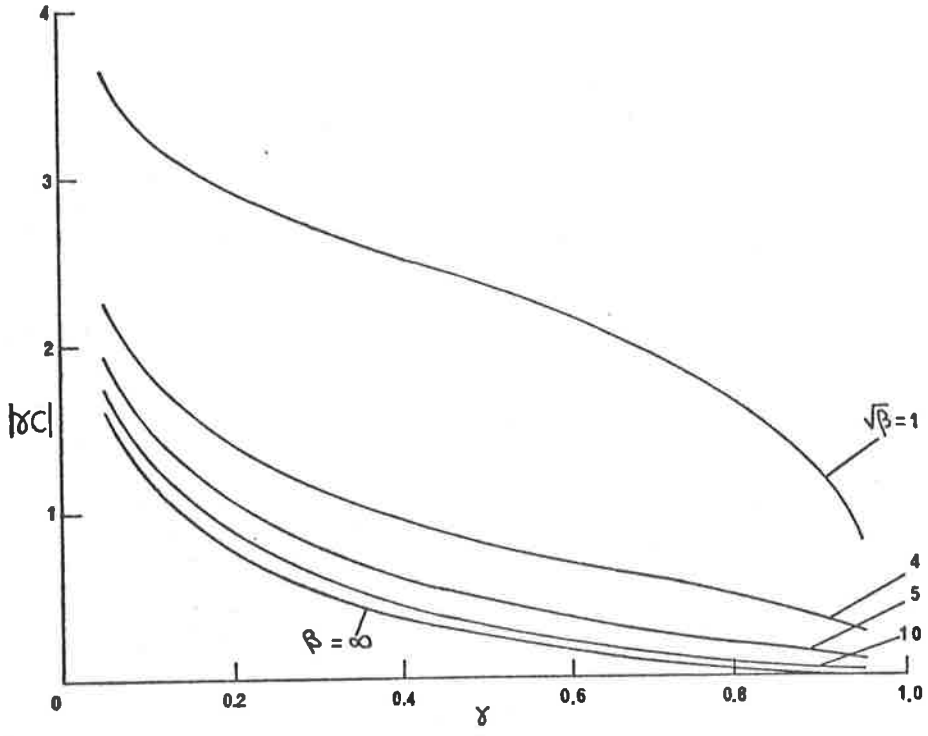

Figure 11 The variation of the magnitude of the scaled blockage coefficient $|\gamma C|$ with γ, for various Reynolds number β.

that a 40-point mesh gave satisfactory accuracy.

The blockage coefficient C was obtained for various values of the parameters β,γ. In Figure 10, the magnitude of C, suitably scaled, is plotted against $\sqrt{\beta}$, for values of γ ranging from 0.1 to 0.8. As might be expected, for fixed β, the blockage coefficient increases as γ decreases. That is, there is greater impedance when γ is small, since the flow is restricted as γ decreases. Indeed in the limit $\gamma \to 0$ we would expect no flow at all, and thus the blockage coefficient would be infinite. The results are consistent with this. At the other end of the scale as $\gamma \to 1$, the blockage coefficient should approach zero. This corresponds to a completely unrestricted flow. Again, the computed results tend to confirm this.

For fixed γ, we should expect the blockage coefficient to decrease as the non-dimensional Reynolds number β increases, due to the fact that increase in β corresponds to a decrease in viscosity. Lower viscosity implies less impedance to flow through the slits and in Figure 10 we can see the obstruction to the flow decreasing as β increases.

For both large and small β, the present results can be compared with work done elsewhere. Very large Reynolds number β corresponds to inviscid flow. In Figure 11 compare the result (2.4.8) for inviscid flow in a channel, with the present work. The magnitude of the blockage coefficient is plotted against γ for various values of β. It can be seen that for values of β greater than about one hundred, there is excellent agreement between the viscous and inviscid results over the whole range of γ. This means that inviscid theory may be safely applied to flow situations

where the Reynolds number is of the order of one hundred or more. For very small β, which corresponds to very viscous Stokes flow, there are no general results for arrays of slits.

For small γ, the flow situation can be compared with the problem for a single slit, using the asymptotic result (2.4.7)

$$\gamma C \to -(2/\pi) \log(\pi\gamma s/a) - \gamma(i\beta)^{-\frac{1}{2}} \qquad (2.5.1)$$

In Figure 10, the magnitude of the right-hand side of (2.5.1) is compared with $|\gamma C|$, using the results of Chapter 1 for $s(\beta)$. These results are shown dotted. For $\gamma = 0.1$ and $\gamma = 0.2$ the small-γ approximation is indistinguishable from the exact computations, and the accuracy remains within about 10% up to $\gamma \sim 0.4$, which is somewhat surprising, as this represents quite large holes. Even at $\gamma = 0.8$ the agreement appears good for the magnitude except for small β, but there is a much larger error in the phase.

CHAPTER 3

REFLECTION OF WATER WAVES BY A SUBMERGED SHELF

3.1 Introduction

In this chapter we present a method for determining the amount of reflection that takes place when a plane progressive water wave moves from one region of constant depth to another region of the same or different constant depth, separated by an intermediate region of given bottom topography. As in most previous work only the two-dimensional problem is considered, although extension to three-dimensions is possible.

It is assumed that wave amplitudes are small so that the problem may be linearized. The fluid is further assumed non-viscous and the flow irrotational, so that Laplace's equation holds throughout the fluid.

The simpler problem of reflection by a vertical step was considered by several authors, including Hilaly (1967), and Bartholomeusz (1958). However, few results have been obtained for the more general problem outlined above.

Evans (1972), using a Green's theorem approach, was able to reduce the problem to that of solving one singular integral equation. However, the kernel required in this formulation is extremely complicated and Evans gave no results. For general bottom topography this method appears limited in practical application. Fitzgerald (1976) has recently solved the problem numerically for certain types of bottom by an inverse method. The results he presents are rather restricted, however, and only those types of bottom which can be mapped uniformly by a specific analytic function to a bottom of fixed depth are considered.

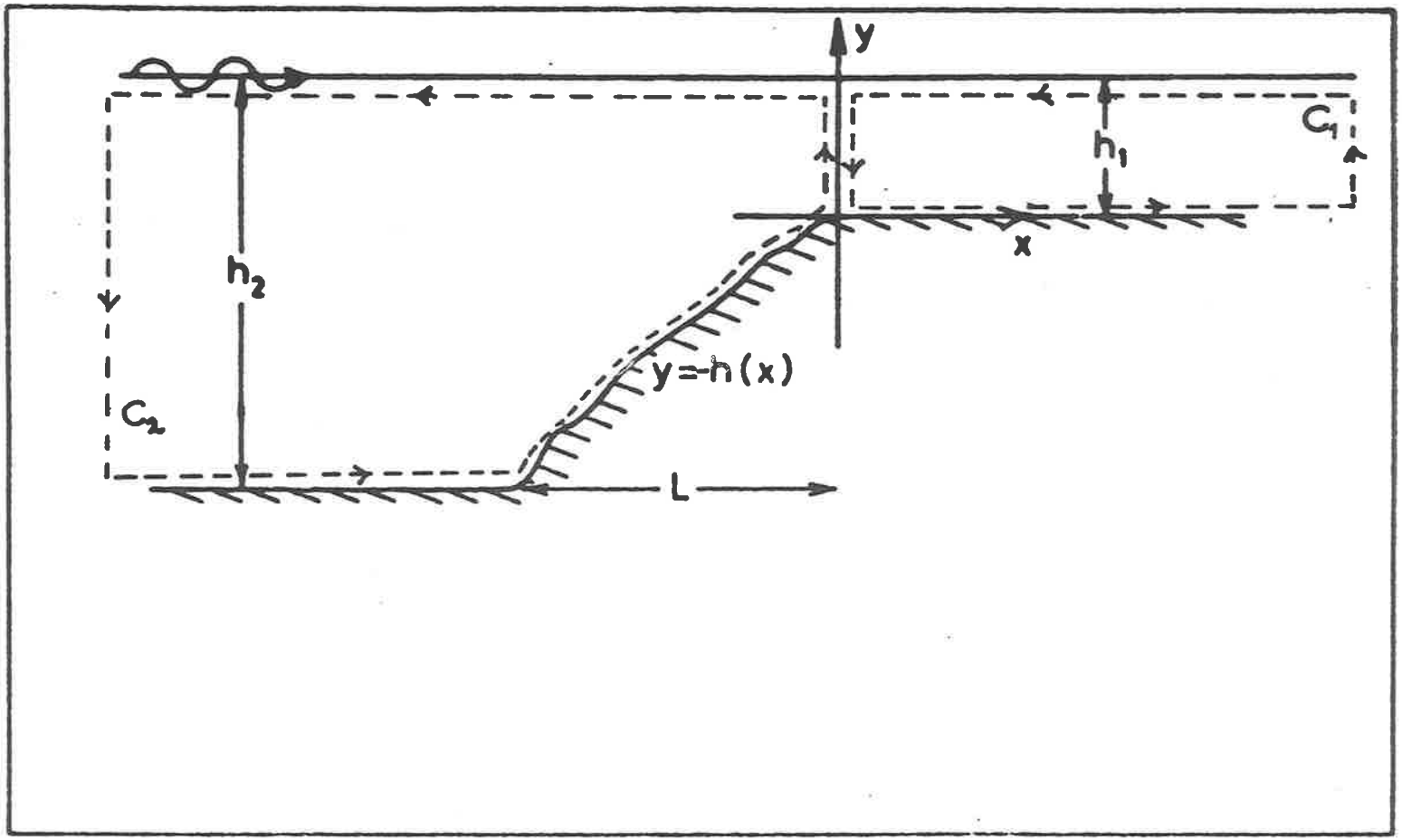

Figure 12 Sketch of bottom geometry.

Yeung (1975) by contrast, developed an integral equation which uses a distribution of simple sources. The drawback of this method, however, is that equations of large order must be inverted to obtain accurate results.

There is also some analytic work by Roseau (1976), but these results are only valid for a particular shelf profile.

Here we steer a mid-course between the two extremes advocated by Yeung and Evans. By using the finite depth Green's function (Wehausen & Laitone, 1960), the number of points at which the potential function and its derivatives must be evaluated is much less than in Yeung's method, yet the kernel functions for the integral equation do not become computationally unmanageable as in the method proposed by Evans.

3.2 Mathematical Formulation

Cartesian coordinates x and y are used. The region $(-L,0)$ of varying depth is given by $y = -h(x)$ where $h(x)$ is known (see Fig.12). For $x > 0$ we assume constant depth $y = -h_1$, and for $x < -L$ we have $y = -h_2$, where for definiteness we assume $h_2 \leq h_1$. An important parameter here is α, given by h_1/h_2.

We assume that the fluid motion may be described by the velocity potential $\Phi(x,y,t)$ such that

$$\Phi(x,y,t) = \mathcal{R}e[\phi(x,y)e^{-i\sigma t}] \qquad (3.2.1)$$

where σ is the wave frequency. The function ϕ satisfies Laplace's equation

$$\nabla^2\phi = 0 \qquad (3.2.2)$$

If we assume that all disturbances of the free surface are of small amplitude then the linearized free-surface

condition applies. This is given by

$$\frac{\partial \phi}{\partial y} - \nu\phi = 0, \quad y = 0 \tag{3.2.3}$$

where $\nu = \sigma^2/g$ and g is the acceleration due to gravity. We also have the condition that there should be no normal fluid velocity on the bottom, so that

$$\frac{\partial \phi}{\partial n} = 0 \quad \text{for} \quad \begin{array}{ll} y = -h_2, & -\infty \leqslant x \leqslant -L \\ y = -h(x), & -L \leqslant x \leqslant 0 \\ y = -h_1, & 0 < x < \infty \end{array} \tag{3.2.4}$$

We consider the reflection and transmission of a plane progressive wave, which for convenience is assumed to have unit amplitude. This implies

$$\phi(x,y) \to (e^{iK_2x} + \rho e^{-iK_2x}) \frac{\cosh K_2(y+h_2)}{\cosh K_2 h_2} \quad \text{as } x \to -\infty \tag{3.2.5}$$

and

$$\phi(x,y) \to \tau e^{iK_1x} \frac{\cosh K_1(y+h_1)}{\cosh K_1 h_1} \quad \text{as } x \to \infty \tag{3.2.6}$$

where ρ and τ are the complex-valued reflection and transmission coefficients, to be determined. K_1 and K_2 are the characteristic wave numbers for waves of frequency σ in water depths h_1, h_2 respectively, given by $K_j \tanh K_j h_j = \nu$, $j = 1,2$.

3.3 Formulation of the Integral Equation

Ideally, one might wish to formulate the problem in terms of a single integral equation involving only the velocity potential on $y = -h(x)$, as was done by Evans (1972). As has been mentioned before, however, this leads to an integral equation with an extremely complicated kernel, since the Green's function required must satisfy two separate radiation conditions for $x \to \pm\infty$, involving two different

wave numbers, as well as Laplace's equation (3.2.2) and the boundary conditions (3.2.3) and (3.2.4). The use of this kernel can be avoided, at the expense of producing more complicated integral equations, if the fluid region is considered to be artificially divided into two parts by the arc $-h_1 \leqslant y \leqslant 0$, $x = 0$. We find then that the problem may be formulated in terms of the two finite-depth Green's functions, appropriate for a source in constant water-depths h_1 and h_2 respectively.

We define the Green's function $G(x,y;\xi,\eta;h)$ which is a unit outgoing wave source at the point (ξ,y) in water of depth h. This function then satisfies

$$\nabla^2 G = \delta(x-\xi, y-\eta) \tag{3.3.1}$$

and the boundary condition

$$\frac{\partial G}{\partial y} - \nu G = 0, \quad y = 0 \tag{3.3.2}$$

and

$$\frac{\partial G}{\partial y} = 0, \quad y = -h. \tag{3.3.3}$$

Finally the function obeys the radiation condition,

$$G(x,y;\xi,\eta;h) \to -im(\eta)\cosh K(y+h)e^{iK|x-\xi|} \tag{3.3.4}$$

as $x \to \pm \infty$, where

$$m(\eta) = \frac{\cosh K(\eta+h)}{Kh + \sinh Kh \cosh Kh} \tag{3.3.5}$$

(see Wehausen and Laitone (1960) p.483)

By the use of Green's second identity we may now set up the problem as a set of coupled integral equations. In the region $\xi > 0$ we apply the identity on the closed circuit C_1 (see Fig. 12) to obtain

$$\phi(\xi,\eta) = \oint_{C_1} \phi(x,y) \frac{\partial G}{\partial n}(x,y;\xi,\eta;h_1) - \frac{\partial \phi}{\partial n}(x,y)\, G(x,y;\xi,\eta;h_1)\, d\ell \tag{3.3.6}$$

where (ξ,η) is a fixed point in the region $\xi > 0$ and $\partial/\partial n$ indicates the normal derivative with respect to the (x,y) coordinates of integration. Now the boundary conditions (3.2.3) and (3.2.4), together with (3.3.2) and (3.3.3), ensure that there is no contribution to the integral either from points on the free surface or on the bottom $y = -h_1$.

Since both G and ϕ behave like outgoing waves as $x \to \infty$, there is similarly no contribution to the integral from the arc $-h_1 < y < 0$, $x = \infty$. Equation (3.3.6) therefore reduces to

$$\phi(\xi,\eta) = \int_W G(0_+,y;\xi,\eta;h_1)\ \frac{\partial\phi}{\partial x}(0_+,y) - \phi(0_+,y)\ \frac{\partial G}{\partial x}(0_+,y;\xi,\eta;h_1)\,dy \tag{3.3.7}$$

where W is the arc $0 \geqslant y \geqslant -h_1$, $x = 0$.

For $\xi < 0$, Green's identity gives us (see Fig. 12)

$$\phi(\xi,\eta) = \oint_{C_2} \phi(x,y)\ \frac{\partial G}{\partial n}(x,y;\xi,\eta;h_2) - \frac{\partial\phi}{\partial n}(x,y)\ G(x,y;\xi,\eta;h_2)\,d\ell \tag{3.3.8}$$

In this case we again get no contribution from the free surface or the flat part of the bottom $-\infty < x < -L$. There is, however, a contribution from the arc $-h_2 < y < 0$, $x = -\infty$ since the Green's function represents a purely outgoing wave, whereas the potential function ϕ has an incident part and a reflected part. We find

$$\phi(\xi,\eta) = \phi_0(\xi,\eta) + \int_B \phi(x,y)\ \frac{\partial G}{\partial n}(x,y;\xi,\eta;h_2)\,d\ell$$

$$- \int_W \left(\frac{\partial\phi}{\partial x}(0_-,y)\ G(0_-,y,\xi,\eta;h_2) - \phi(0_-,y)\ \frac{\partial G}{\partial x}(0_-,y;\xi,\eta;h_2) \right) dy \tag{3.3.9}$$

where the arc B is the varying-depth portion of the bottom, given by $y = -h(x)$, $-L < x < 0$. ϕ_0 is the contribution

to the integral from the part of the contour $-h_2 < y < 0$, $x = -\infty$, and is given by

$$\phi_0(\xi,\eta) = \frac{\cosh K_2(\eta+h_2)}{\cosh K_2 h_2} e^{iK_2\xi} \tag{3.3.10}$$

The integral relations (3.3.8) and (3.3.9) are formulated in terms of the potential at any point in the fluid and the boundary values of the potential function and its normal derivative on the arcs B and W. To obtain integral equations that can be solved (numerically or otherwise), we need to adjust the equations so that only the boundary values of the potential and its normal derivative appear.

In equation (3.3.9) we allow the point (ξ,η) to approach the arc B. Since $\partial G/\partial n$ behaves like a delta function as $(\xi,\eta) \to (x,y)$ we obtain

$$\frac{1}{2}\phi(\xi,\eta) = \phi_0(\xi,\eta) + \int\!\!\!\!\!\!-_B \phi(x,y)\,\frac{\partial G}{\partial n}(x,y;\xi,\eta;h_2)\,d\ell$$

$$-\int_W \frac{\partial\phi}{\partial x}(0_-,y)\,G(0_-,y;\xi,\eta;h_2)\,dy + \int_W \phi(0_-,y)\,\frac{\partial G}{\partial x}(0_-,y;\xi,\eta;h_2)\,dy \tag{3.3.11}$$

for $(\xi,\eta) \in B$. The bar on the first integral indicates a Cauchy principal value.

If (ξ,η) approaches a point on W from the left in equation (3.3.9) we find

$$\frac{1}{2}\phi(0_-,\eta) = \phi_0(0_-,\eta) + \int_B \phi(x,y)\,\frac{\partial G}{\partial n}(x,y;0_-,\eta;h_2)\,d\ell$$

$$-\int_W \frac{\partial\phi}{\partial x}(0_-,y)\,G(0_-,y,0_-,\eta;h_2)\,dy \tag{3.3.12}$$

Finally we return to equation (3.3.7) and allow (ξ,η) to approach $(0_+,\eta)$ so that

$$\phi(0_+,\eta) = 2\int_W \frac{\partial\phi}{\partial x}(0_+,y)\,G(0_+,y;0_+,\eta;h_1)\,dy \tag{3.3.13}$$

Equations (3.3.11), (3.3.12) and (3.3.13) represent a set of coupled integral equations, involving only the boundary values of the potential function or its normal derivative. W, of course, is only an artificial boundary but that does not affect the validity of the argument. One last step remains before the set of integral equations can be solved. We must use the continuity of the potential function and its ξ-wise derivative across $\xi = 0$. We may write

$$\phi(0,\eta) = \phi(0_-,\eta) = \phi(0_+,\eta) \qquad (3.3.14)$$

and

$$\phi_\xi(0,\eta) = \phi_\xi(0_-,\eta) = \phi_\xi(0_+,\eta) \qquad (3.3.15)$$

On using the above equations, the set of integral equations (3.3.11)-(3.3.13) then involves only the function $\phi(\xi,\eta)$ for $(\xi,\eta) \in W$ or B, and the normal velocity across $\xi = 0$, $\phi_\xi(0,\eta)$ for $(0,\eta) \in W$. These equations may now be set up as a matrix equation upon suitable discretization and solved by direct inversion. For moderate values of the parameter νh it is possible that some sort of iterative process might also be successful, but the complicated nature of the kernel makes this appear a very difficult task.

Once we have solved the system of equations, we are in a position to find the complex-valued reflection and transmission coefficients, ρ and τ respectively. For the reflection coefficient, for example, we allow $\xi \to -\infty$ in (3.3.9) and equate the right hand side of this equation with the far-field behaviour of ϕ as given by equation (3.2.5). On using the asymptotic forms for G and $\partial G/\partial n$ we find

$$\rho = \frac{\cosh K_2 h_2}{K_2 h_2 + \tfrac{1}{2}\sinh K_2 h_2} \int_{-L}^{0} K_2 \phi(x,-h(x))(\cosh K_2(y+h_2)e^{iK_2x} + \sinh K_2(y+h_2)ie^{iK_2x})dx +$$

$$+\int_{-h_1}^{0} i\phi_x(0,y)\cosh K_2(y+h_2)\,dy - \frac{K_2}{K_2h_2 + \tfrac{1}{2}\sinh K_2h_2}\int_{-h_1}^{0}\phi(0,y)\cosh K_2(y+h_2)\,dy \qquad (3.3.16)$$

Note that all the integrals in (3.3.16) involve only the boundary values ϕ, ϕ_x which we assume known, once equations (3.3.11)-(3.3.13) have been solved. A similar expression may easily be found for the transmission coefficient τ.

3.4 Numerical Analysis

To solve the equations (3.3.11)-(3.3.13) numerically, we require some method of discretization. The assumption we make is that both ϕ and its derivative ϕ_x are slowly-varying on the arcs B and W. Therefore, the arc B is divided into N segments (x_j, x_{j+1}), $j = 1,\ldots,N$, such that $x_j < x < x_{j+1}$. In each segment the approximation $\phi(x,y) = \phi_j$ = constant is made. In the same way the arc W may be divided into M segments (y_j, y_{j+1}) with $\phi(0,y) = \phi_j$ and $\phi_x(0,y) = \phi_{xj}$ for $j = N+1,\ldots,M+N$. Note that generally we take $M = N$ but with certain problems it is advantageous to allow M to differ from N. For example, if the depth change is very gradual so that the arc B is much longer than the arc W, then it is necessary to make $N > M$ to ensure that our assumption of slowly varying potential function ϕ on B is consistent. Note that no assumptions have been made here about the choice of meshpoints x_j, y_j. In a general sense, an equally spaced mesh is probably the best choice if the ensuing program is to deal with a variety of problems. This was the procedure finally adopted in the present work. It would be preferable, however, to choose meshpoints that would take account of the singular behaviour

at the corner $(x,y) = (0,-h_1)$. (This was the method used in Chapter 1 where a Chebychev mesh was used to counteract a square-root singularity.) This procedure would almost certainly give improved convergence. It should be noted that the most singular behaviour occurs in the problem of a single step where the velocity near the corner behaves like $Ar^{-\frac{1}{3}}$, with A some constant and r the distance from the corner. Even in this problem, very satisfactory convergence was achieved with a uniform distribution of mesh points. Thus the benefits of using an uneven mesh, especially when the angle at the corner is close to π radians, may not be all that great.

The integral equations must be satisfied at the $N+M$ points

$$\xi_i = \frac{(x_i + x_{i+1})}{2} \qquad i = 1,\ldots,N \qquad (3.4.1)$$

$$\eta_1 = \frac{(y_i + y_{i+1})}{2} \qquad i = N+1,\ldots,N+M \qquad (3.4.2)$$

Thus equations (3.3.11)-(3.3.13) may be rewritten as

$$\frac{\phi_i}{2} = \phi_0(\xi_i,-h(\xi_i)) + \sum_{j=1}^{N} \phi_j \int_{x_j}^{x_{j+1}} \frac{\partial G}{\partial n}(x,-h(x);\xi_i,-h(\xi_i);h_2)\,dx$$

$$- \sum_{j=N+1}^{N+M} \phi_{xj} \int_{y_j}^{y_{j+1}} G(0,y;\xi_i,-h(\xi_i);h_2)\,dy$$

$$+ \sum_{j=N+1}^{N+M} \phi_j \int_{y_j}^{y_{j+1}} \frac{\partial G}{\partial x}(0,y;\xi_i,-h(\xi_i);h_2)\,dy \qquad (3.4.3)$$

$$i = 1,\ldots,N$$

$$\frac{\phi_i}{2} = \phi_0(0,\eta_i) + \sum_{j=1}^{N} \phi_j \int_{x_j}^{x_{j+1}} \frac{\partial G}{\partial n}(x,-h(x);0,\eta_i;h_2)\,dx$$

$$- \sum_{j=N+1}^{N+M} \phi_{xj} \int_{y_j}^{y_{j+1}} G(0,y;0,\eta_i;h_2)\,dy \qquad (3.4.4)$$

$$i = N+1,\ldots,N+M$$

and

$$\phi_i = 2 \sum_{j=N+1}^{N+M} \phi_{xj} \int_{y_j}^{y_{j+1}} G(0,y;0,\eta_i;h_1)\,dy \qquad (3.4.5)$$

$$i = N+1,\ldots,N+M.$$

We have used the notation $\partial G/\partial n$ to represent $-h'(x)\,\partial G/\partial x - \partial G/\partial y$.

We finally rewrite the above equations in simpler form. We have

$$\frac{\phi_i}{2} = \phi_{0i} + \sum_{j=1}^{N} \phi_j A_{ij} - \sum_{j=N+1}^{N+M} (\phi_{xj} B_{ij} - \phi_j C_{ij}) \qquad (3.4.6)$$

where $\phi_{0i} = \phi_0(\xi_i, -h(\xi_i))$ and i runs from 1 to N, with

$$\frac{\phi_i}{2} = \phi_{0i} + \sum_{j=1}^{N} \phi_j D_{ij} - \sum_{j=N+1}^{N+M} \phi_{xj} E_{ij} \qquad (3.4.7)$$

and finally

$$\phi_i = \sum_{j=N+1}^{N+M} \phi_{xj} F_{ij} \qquad (3.4.8)$$

In equations (3.4.7) and (3.4.8) $i = N+1,\ldots,N+M$ and $\phi_{0i} = \phi_0(0,\eta_i)$. The elements $A_{ij},\ldots,F_{ij}$ are all integrals that may be evaluated analytically. Methods for evaluating them will be derived in the next section. Specifically, they are given by

$$A_{ij} = \int_{x_j}^{x_{j+1}} \frac{\partial G}{\partial n}(x,-h(x);\xi_i,-h(\xi_i);h_2)\,dx \qquad (3.4.9),$$

$$B_{ij} = \int_{y_j}^{y_{j+1}} G(0,y;\xi_i,-h(\xi_i);h_2)\,dy \qquad (3.4.10),$$

$$C_{ij} = \int_{y_j}^{y_{j+1}} \frac{\partial G}{\partial x}(0,y;\xi_i,-h(\xi_i);h_2)\,dy \qquad (3.4.11),$$

$$D_{ij} = \int_{x_j}^{x_{j+1}} \frac{\partial G}{\partial n}(x,-h(x);0,\eta_i;h_2)\,dx \qquad (3.4.12),$$

$$E_{ij} = \int_{y_j}^{y_{j+1}} G(0,y;0,\eta_i;h_2)\,dy \qquad (3.4.13),$$

and $$F_{ij} = 2\int_{y_j}^{y_{j+1}} G(0,y;0,\eta_i;h_1)\,dy \qquad (3.4.14)$$

Having obtained the discretized equations (3.4.6)-(3.4.8) we are in a position to recast the problem in matrix form. We have

$$Z\underset{\sim}{\Phi} = \underset{\sim}{\Phi}_0 \qquad (4.3.15)$$

where $Z =$

$$\begin{array}{c} \\ N\{ \\ M\{ \\ M\{ \end{array} \begin{array}{c} \overbrace{}^{N} \\ \\ \\ \\ \end{array} \begin{array}{c} \overbrace{}^{M} \\ \\ \\ \\ \end{array} \begin{array}{c} \overbrace{}^{M} \\ \\ \\ \\ \end{array} \begin{bmatrix} \tfrac{1}{2} I_N - A & B & -C \\ \tfrac{1}{2} I - D & E & 0 \\ 0 & I_M - F & 0 \end{bmatrix} \qquad (3.4.16)$$

I_N represents an identity matrix of order N and the coefficients outside the matrix indicate the order of the submatrices. The vectors $\underset{\sim}{\Phi}$ and $\underset{\sim}{\Phi}_0$ are given by

$$\underset{\sim}{\Phi} = [\phi_1,\ldots,\phi_N,\phi_{x_{N+1}},\ldots,\phi_{x_{N+M}},\phi_{N+1},\ldots,\phi_{N+M}]^t \qquad (3.4.17)$$

and

$$\underset{\sim}{\Phi}_0 = [\phi_{0_1},\ldots,\phi_{0_{N+M}},0,\underbrace{\ldots,0}_{M \text{ terms}}]^t \qquad (3.4.18)$$

Solution of equation (3.4.16) by standard inversion procedures therefore solves the original problem. The only remaining difficulty is the evaluation of the matrix elements $A_{ij}, B_{ij}, \ldots, F_{ij}$.

3.5 Evaluation of the Green's Function

In determining $A_{ij},\ldots,F_{ij}$ we require an efficient method for evaluating the indefinite integrals of the finite depth Green's function and its normal derivative on $y = -h(x)$. This section details such a method. An alternative approach would be to determine a good method for finding the function itself, rather than its integral, and then using numerical integration to determine the matrix elements $A_{ij},\ldots,F_{ij}$. Although the present problem has been set up so as to avoid this numerical integration, in many other problems this cannot be done. Thus an efficient method for evaluating the Green's function itself is also of interest. For example, Sheridan (1975), describes a straightforward method for determining the Green's function. It is thought that the method described here is a distinct improvement, especially for small values of the x and ξ parameters.

Two forms of the Green's function are available. One is an integral representation

$$G(x,y;\xi,\eta;h) = \frac{1}{2\pi}\left[\log\left(\frac{\sqrt{(x-\xi)^2 + (y-\eta)^2}}{h}\right) + \log\left(\frac{\sqrt{(x-\xi)^2 + (y+\eta+2h)^2}}{h}\right)\right] - \frac{1}{\pi}\int_0^\infty \left(e^{-kh} G_B \cosh k(h+y) \cos k(x-\xi) - \frac{e^{-kh}}{k}\right)dk - i\, G_A \cos K(x-\xi) \cosh K(y+h) \qquad (3.5.1)$$

where
$$G_A = \frac{\nu+K}{K}\ \frac{e^{-Kh}\sinh Kh \cosh K(h+\eta)}{\nu h + \sinh^2 Kh} \qquad (3.5.2)$$

and
$$G_B = \frac{\nu+k}{k}\ \frac{e^{-kh}\cosh k(h+\eta)}{k\sinh kh - \nu\cosh kh} \qquad (3.5.3)$$

Alternatively, the function can be expressed in terms of the series expansion

$$G(x,y;\xi,\eta;h) = -\sum_{n=1}^{\infty} P_n \cos m_n(y+h) e^{-m_n|x-\xi|} - i\, G_A\, e^{+iK|x-\xi|}\cosh K(y+h) \qquad (3.5.4)$$

where G_A is given by equation (3.5.2) and

$$P_n = \frac{1}{m_n} \frac{m_n^2 + \nu^2}{hm_n^2 + h\nu^2 - \nu} \cos m_n(\eta+D) \qquad (3.5.5)$$

The m_n's, $n=1,\ldots,\infty$, are the real roots of the equation

$$-m_n \tan m_n h = \nu \qquad (3.5.6)$$

For a derivation of the above forms and other alternative formulations, reference should be made to either Wehausen and Laitone (1960) or Thorne (1953).

We must now decide which form of the Green's function to use in evaluating the kernels. The integral representation (3.5.1) can be conveniently and reasonably accurately calculated by numerical integration for small values of $X = x-\xi$. For large values of X, however, the integral has a rapidly oscillating kernel, which means that a large amount of computing time is necessary to obtain an accurate answer by, say, Simpson's method. Obviously some method for treating integrals of this type, such as Filon's method (Filon (1929)), could be used. It seems more reasonable, though, to use the series representation (3.5.4) for large X. It can be seen that this expression is self-truncating for large values of the X-argument and thus can be very rapidly and accurately calculated for these large values. For small

values of the argument, by contrast, it is found that the series representation is not a suitable one to use, since many terms in the series have to be used to obtain satisfactory accuracy.

In the light of the above statements, a reasonable approach to the problem appears to be to use the integral representation for all small values of X up to, say, $X = 0.5$ and then to change over to the series representation for all larger values of the argument. Indeed, this is quite an effective approach and in the original computer programme that was set up to solve the water-wave reflection problem, this method was used successfully. It was observed, however, that the calculation of the Green's function using (3.5.1) was still somewhat cumbersome and inefficient due to the complicated nature of the kernel and the fact that an infinite range of integration was involved. Evaluation of the series representation, by contrast, was extremely straightforward, the only difficulty being, as has been mentioned above, the extremely slow convergence for small values of the argument X. On investigating the reasons for this slow convergence, it was found that the problem could be overcome by a relatively simple re-organization of equation (3.5.4). We shall now consider this problem in more detail.

We rewrite (3.5.4) for convenience as

$$G(x,y;\xi,\eta;h) = -\sum_{m=1}^{\infty} Q_n(x,y;\xi,\eta;h) - i\, G_A \cosh K(y+h) e^{iK|x-\xi|} \tag{3.5.7}$$

where $$Q_n = P_n \cos m_n(y+h) e^{-m_n|x-\xi|} \tag{3.5.8}$$

For moderate values of the non-dimensional parameter νh, as

$n \to \infty$ it can be shown that

$$m_n \to \frac{n\pi}{h} \tag{3.5.9}$$

so that as $n \to \infty$,

$$Q_n \to \frac{1}{n\pi} \cos \frac{\pi n}{h}(y+h) \cos \frac{\pi n}{h}(\eta+h) \, e^{-n\pi/h|x-\xi|} = Q_n^* \tag{3.5.10}$$

We now consider the behaviour of

$$R(x,y;\xi,\eta;h) = \sum_{n=1}^{\infty} \frac{1}{n\pi} \cos \frac{\pi n}{h}(y+h) \cos \frac{\pi n}{h}(\eta+h) e^{-n\pi/h|x-\xi|} \tag{3.5.11}$$

This series is only slowly convergent for small $|x-\xi|$. Because of this the expansion (3.5.4) for G is also slowly convergent. It is possible, however, to evaluate $R(x,y;\xi,\eta;h)$ exactly. We write

$$R(x,y;\xi,\eta;h) = \frac{1}{2} \sum_{n=1}^{\infty} \frac{1}{n\pi} \left(\cos \frac{\pi n}{h}(y+\eta+2h) e^{-\pi n/h|x-\xi|} \right) + \frac{1}{2} \sum_{n=1}^{\infty} \frac{1}{n\pi} \left(\cos \frac{\pi n}{h}(y-\eta) e^{-\pi n/h|x-\xi|} \right) \tag{3.5.12}$$

$$= R_1(x,y;\xi,\eta;h) + R_2(x,y;\xi,\eta;h) \tag{3.5.13}$$

We consider only the second series R_2 (the first is almost the same). We put

$$Z = Y + iX \tag{3.5.14}$$

where $Y = \pi/h(y-\eta)$, $X = \pi/h|x-\xi|$

Then R_2 is given by

$$R_2(x,y;\xi,\eta;h) = \frac{1}{2}\pi \sum_{n=1}^{\infty} \left(\mathrm{Re} \frac{\cos nZ}{n} - \mathrm{Im} \frac{\sin nZ}{n} \right) \tag{3.5.15}$$

These two series may be summed immediately (see Abramowitz and Stegun, (1964)), so that

$$R_2(x,y;\xi,\eta;h) = -\frac{1}{2\pi}\left(\mathrm{Re}\log(2\sin\frac{Z}{2}) + \mathrm{Im}(\tfrac{1}{2}\pi - Z)\right) \qquad (3.5.16)$$

$$= -\frac{1}{2\pi}\log 2\sqrt{\sin^2\frac{Y}{2}\cosh^2\frac{X}{2} + \cos^2\frac{Y}{2}\sinh^2\frac{X}{2}} + \frac{X}{2\pi} \qquad (3.5.17)$$

Note that when $X=0$, this reduces to the simple form

$$R_2(x,y;x,\eta;h) = -\frac{1}{2\pi}\log 2\sin\left(\frac{\pi}{2h}|y-\eta|\right) \qquad (3.5.18)$$

Equation (3.5.12) may now be rewritten, using (3.5.17), as

$R(x,y;\xi,\eta;h) =$

$$-\frac{1}{2\pi}\log 2\sqrt{\sin^2\frac{(y-\eta)}{2h}\pi\cosh^2\frac{|x-\xi|}{2h}\pi + \cos^2\frac{(y-\eta)}{2h}\pi\sinh^2\frac{|x-\xi|}{2h}\pi}$$

$$-\frac{1}{2\pi}\log 2\sqrt{\sin^2\frac{(y+\eta+2h)}{2h}\pi\cosh^2\frac{|x-\xi|}{2h}\pi + \cos^2\frac{(y+\eta+2h)}{2h}\pi\sinh^2\frac{|x-\xi|}{2h}\pi}$$

$$+\frac{|x-\xi|}{h} \qquad (3.5.19)$$

Although (3.5.19) appears at first sight to be rather clumsy, in computational terms it is far superior to the representation (3.5.13) since no summation is required. Once an exact expression for R has been determined we are immediately in a position to reorganise the Green's function (3.5.7) so that it may be efficiently computed for small X. We write

$$G(x,y;\xi,\eta;h) = -iG_A\cosh K(y+h)e^{iK|x-\xi|}$$

$$-\sum_{n=1}^{\infty}(Q_n - Q_n^*) - R(x,y;\xi,\eta;h) \qquad (3.5.20)$$

Since as n becomes larger $Q_n \to Q_n^*$ the summation in (3.5.20) is highly convergent for any value of the argument X. Because of this, very few terms will give a good approximation. It should be remembered, however, that this method does not overcome the problem of slow convergence for large values of

Kh	Ky	Kη	No. of terms	New Method ℜe G.	Series ℜe G.
1	-0.35	-0.4	10	-.1851856	-.2568542
1	-0.35	-0.4	100	-.1850087	-.1840531
1	-0.35	-0.4	1000	-.1850087	-.1851612
1	-0.35	-0.4	10000	-.1850087	-.1850253
1	-0.35	-0.95	10	.1496019	.1497054
1	-0.35	-0.95	100	.1495876	.1480071
1	-0.35	-0.95	1000	.1495876	.1494285
1	-0.35	-0.95	10000	.1495876	.1495717
1	-0.96	-0.95	10	-.8230905	-.7548512
1	-0.96	-0.95	100	-.8230853	-.8334187
1	-0.96	-0.95	1000	-.8230851	-.8230820
1	-0.96	-0.95	10000	-.8230851	-.8230994
1	-0.05	-0.06	10	-.7050828	-.6056878
1	-0.05	-0.06	100	-.7068106	-.7170789
1	-0.05	-0.06	1000	-.7068104	-.7068079
1	-0.05	-0.06	10000	-.7068104	-.7068247
10	-5.	-6.	10	-.3892591	-.3856073
10	-5.	-6.	100	-.3935326	-.3949584
10	-5.	-6.	1000	-.3935325	-.3936899

Table 1. Table shows improvement in calculating Green's function for x=0 over numerical summation of the standard series.

the parameter νh, (i.e. for very short waves), since then the approximation (3.5.9) does not hold until n becomes large. This sort of problem is, of course, also present when the standard representations (3.5.1) and (3.5.7) are used. This is a separate problem in evaluating these Green's functions, and as yet no simple method has been found to overcome it.

At this stage, some comparison of (3.5.20) and (3.5.7) is in order. We consider $X=0$ (whose equation (3.5.20) shows the greatest improvement over (3.5.7)) and in table 1 show the results obtained with the two methods for various numbers of terms in the infinite series. As can be seen, (3.5.20) is markedly superior. The table also shows that the efficiency of either method degrades as the parameter νh increases.

Using equation (3.5.4), we may now determine the integrals $A_{ij},\ldots,F_{ij}$ as given by equations (3.4.9)-(3.4.14). Fundamentally, the two integrals we require are

$$I_1 = \int_{x_j}^{x_{j+1}} - \frac{dh}{dx}\frac{\partial G}{\partial x}(x,y;\xi,\eta;h) - \frac{\partial G}{\partial y}(x,y;\xi,\eta;h)\,dx \qquad (3.5.21)$$

where $y = -h(x)$, and

$$I_2 = \int_{y_j}^{y_{j+1}} G(x,y;\xi,\eta;h)\,dy \qquad (3.5.22)$$

where (ξ,η) may take any values. First we look at the evaluation of I_1. If we carry out a direct integration on equation (3.5.4) substituting for the values of R, Q_n^* and Q_n using (3.5.19), (3.5.10) and (3.5.8) respectively, we find

$$I_1 = \Big[\operatorname{sgn}(x-\xi) \Big(e^{iK|x-\xi|} G_A \sinh K(y+h) + \sum_{n=1}^{\infty} J_n - \frac{1}{2} - \sum_{j=1}^{2} \frac{1}{2\pi} \arctan N_j \Big) \Big]_{x_j}^{x_{j+1}} \qquad (3.5.23)$$

where $$J_n = e^{-m_n|x-\xi|} P_n \sin m_n(y+h) - \frac{1}{n\pi} e^{-n\pi/h|x-\xi|} \sin \frac{n\pi}{h}(y+h) \cos \frac{n\pi}{h}(\eta+h) \qquad (3.5.24)$$

$$N_j = \frac{\cos \frac{\pi}{2h} Y_j \sinh \frac{\pi}{2h} |x-\xi|}{\sin \frac{\pi}{2h} Y_j \cosh \frac{\pi}{2h} |x-\xi|} \qquad (3.5.25)$$

and $Y_1 = y-\eta$, $Y_2 = y+\eta+2h$.

Note that in working out the $\int G_n \, d\ell$ it is easier to return to the representation (3.5.12), perform the integration and then carry out the process similar to that described in equations (3.5.14) - (3.5.17) rather than attempt a direct integration of equation (3.5.19).

We now determine I_2 in similar fashion as

$$I_2 = \Big[-iG_A/K \sinh K(y+h) \, e^{iK|x-\xi|} + \sum_{n=1}^{\infty} L_n + 2|x-\xi|/h \Big]_{y_j}^{y_{j+1}} - \int_{y_j}^{y_{j+1}} \sum_{j=1}^{2} \frac{1}{2\pi} \log 2\sqrt{M_j} \qquad (3.5.26)$$

with

$$L_n = \frac{P_n}{m_n} \sin m_n(y+h) \, e^{-m_n|x-\xi|} - \frac{1}{h} e^{-\frac{n\pi}{h}|x-\xi|} \sin \frac{n\pi}{h}(y+h) \cos \frac{n\pi}{h}(\eta+h) \qquad (3.5.27)$$

and $$M_j = \sin^2 \frac{\pi}{2h} Y_j \cosh^2 \frac{\pi}{2h} |x-\xi| + \cos^2 \frac{\pi}{2h} Y_j \sinh^2 \frac{\pi}{2h} |x-\xi| \qquad (3.5.28)$$

The integral (I_3) appearing in (3.5.26) is troublesome. In the special case $x = 0$ it may be recognised as Catalan's integral, which may be conveniently calculated after an integration by parts (see Chapter 2). For non-zero X, similar methods may be used. For example, for $j = 1$ we have

$$I_3 = \frac{\pi}{h} |y-\eta| \log 2\sqrt{M_1} - \int_0^{\pi/h |y-\eta|} dp \, \frac{p}{2} \sin \frac{p}{2} \cos \frac{p}{2} S \qquad (3.5.29)$$

where $S = \sin^2 \frac{p}{2} \cosh^2 \frac{\pi}{2h} |x-\xi| + \cos^2 \frac{p}{2} \sinh^2 \frac{\pi}{2h} |x-\xi|$

(3.5.30)

This last integral may be efficiently evaluated by standard methods (e.g. Simpson's rule).

Having determined I_1 and I_2 the matrix elements $A_{ij},\ldots,F_{ij}$ are immediately known for all frequencies ν. As has been said before, the above method is not very efficient for large values of νh. Up to values of $\nu h \sim 10$ it is found that this causes no difficulties. For efficient evaluation of the matrix elements at high frequency, some different method must be used. No such methods were obtained in the present work. It is probable, though, that some kind of analytical asymptotic theory would be more useful than any numerical approach at high frequency.

3.6 Results

The above was coded on the Adelaide University CDC 6400 computer. It was found that satisfactory accuracy was achieved at moderate frequency by the inversion of a 60×60 matrix Z. However, at higher frequency, to maintain the level of accuracy, larger matrix inversions were required, and in fact the accuracy obtainable will decrease as frequency

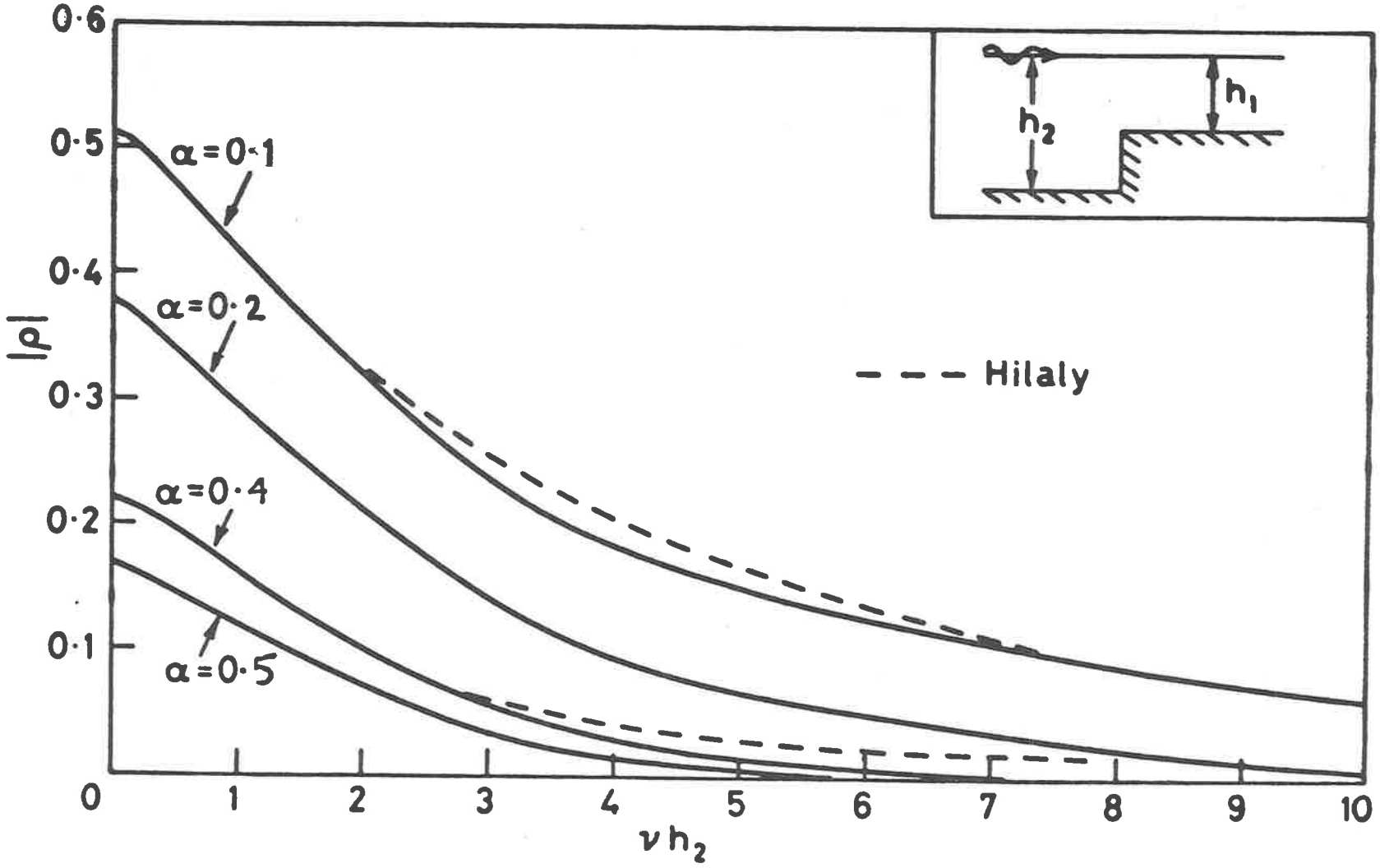

Figure 13 Reflection coefficient for a single step.

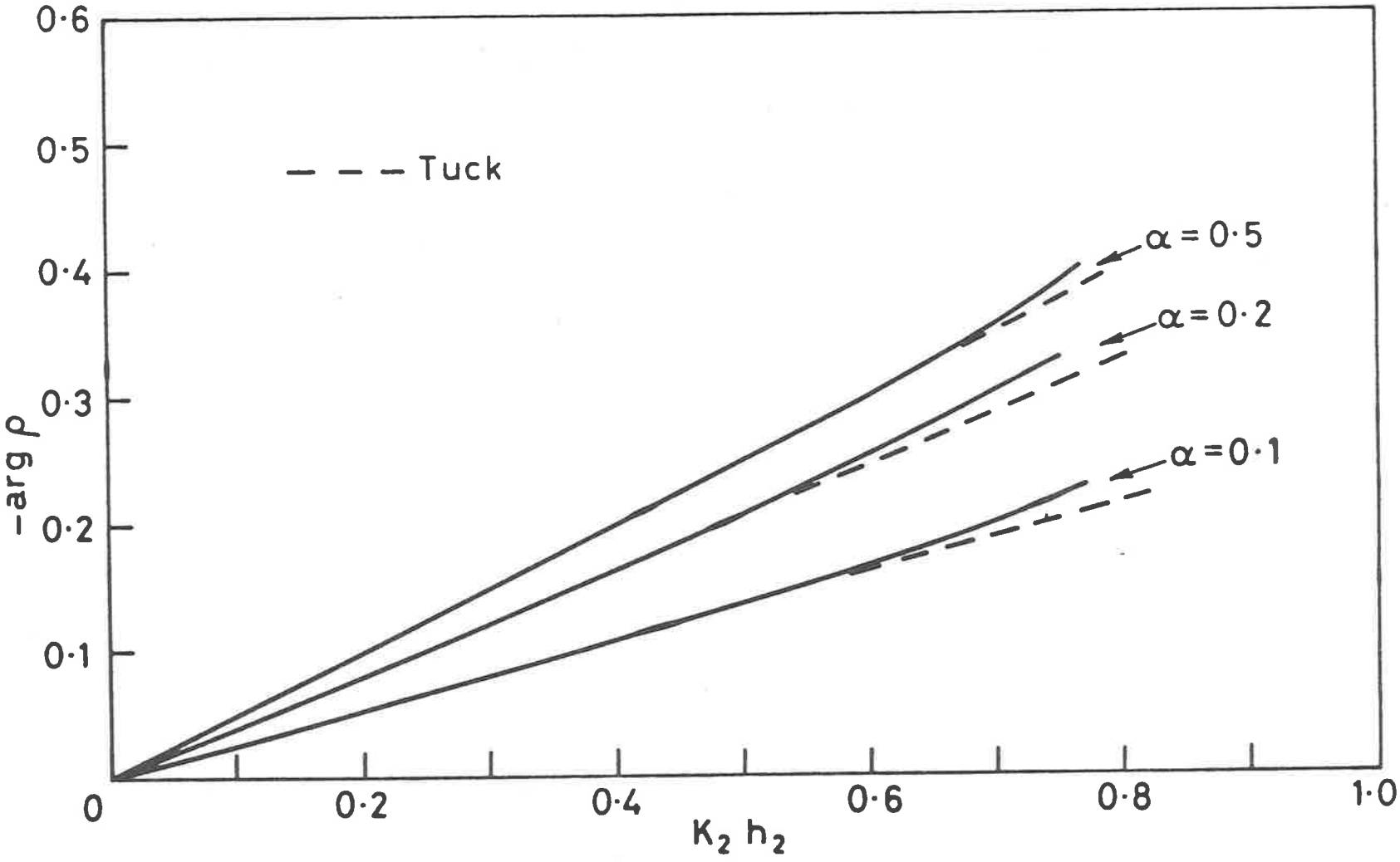

Figure 14 Reflection coefficient for a single step at long wavelength: comparison with asymptotic result of Tuck (1976).

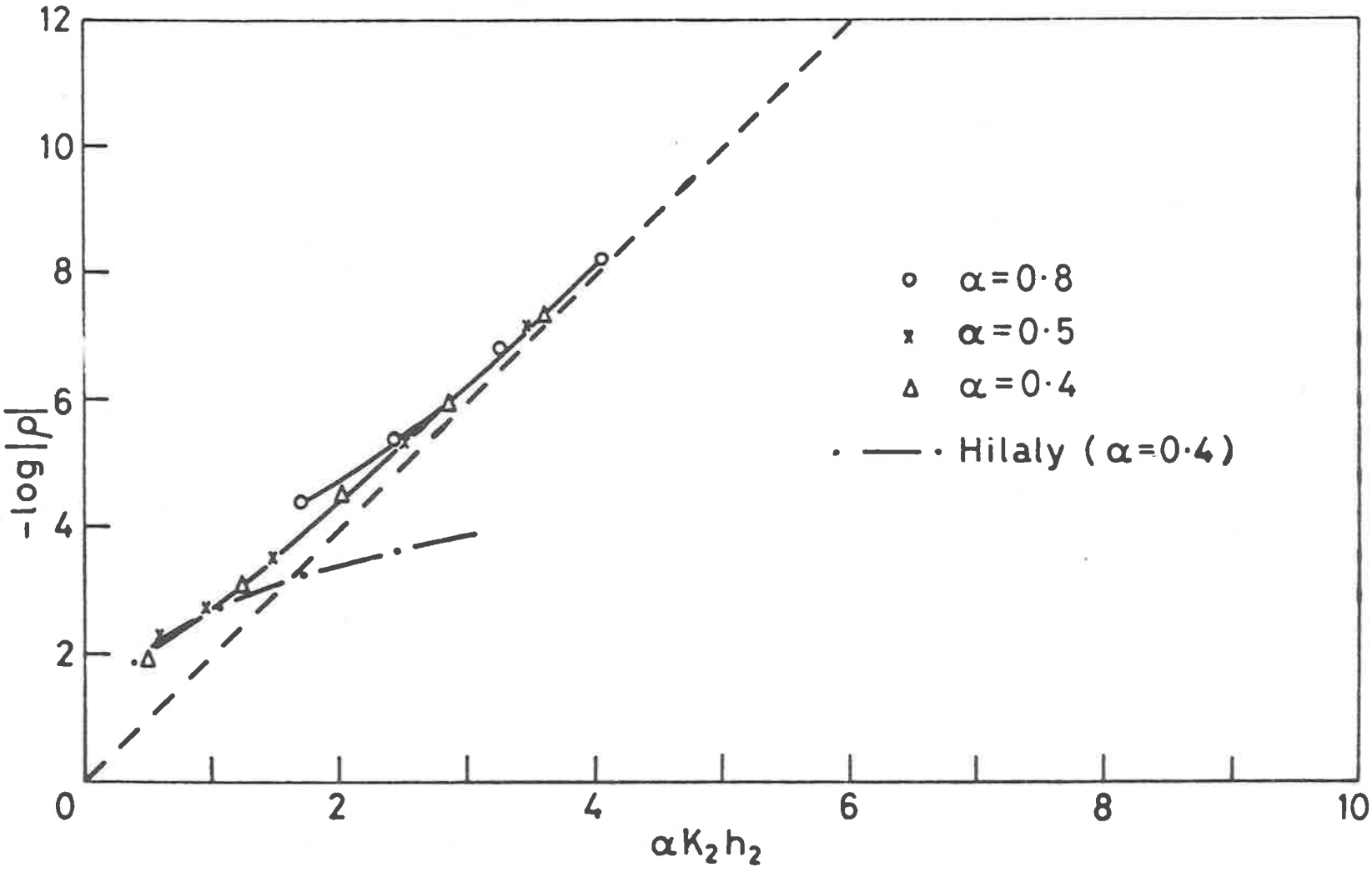

Figure 15 Reflection coefficient for a single step. Predicted asymptotic behaviour for short waves.

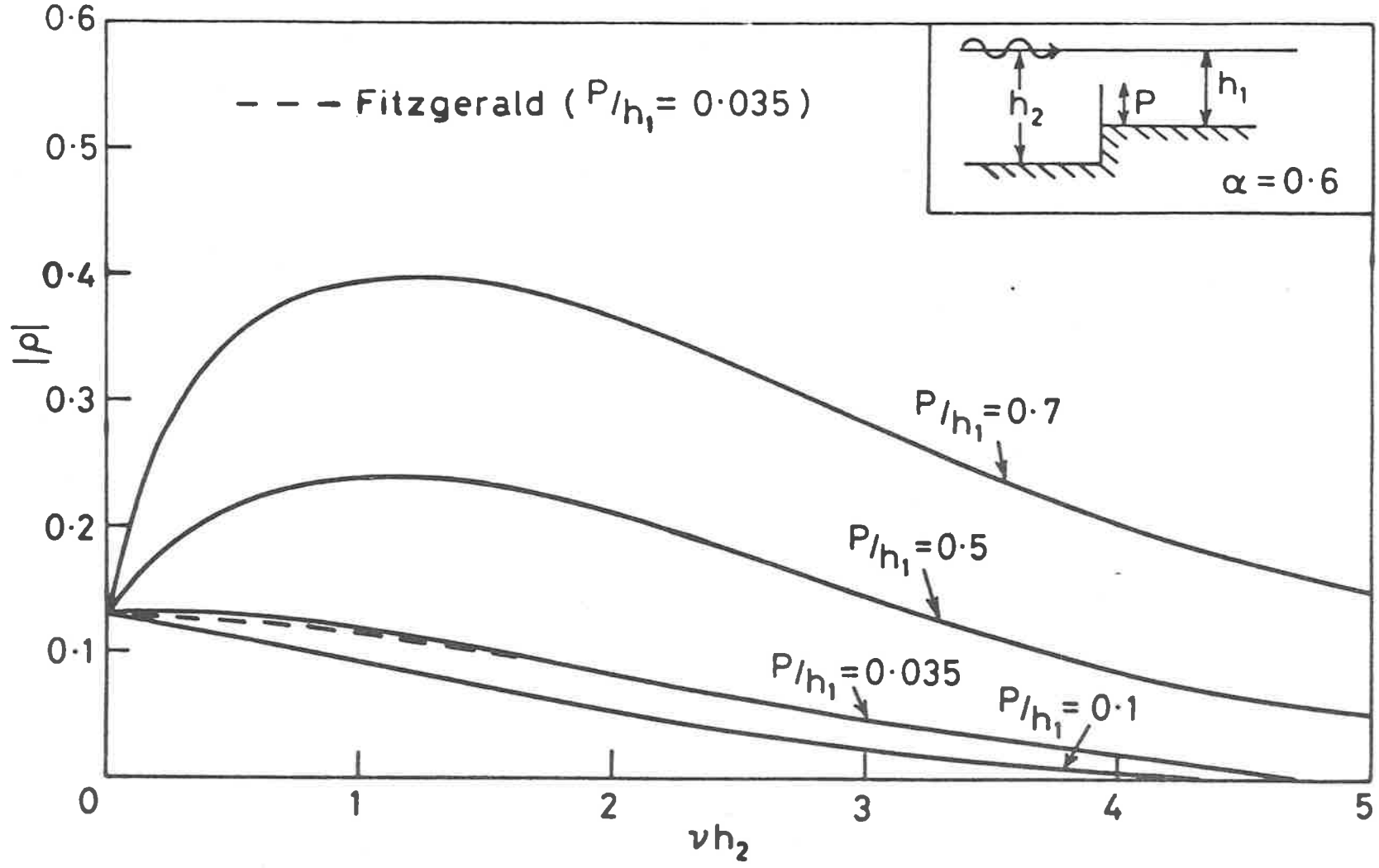

Figure 16 Reflection coefficient for a step with a vertical barrier at x=0 reaching partway to the surface.

increases.

The most obvious problem to test the completed programme on was the simple step, for which results for a wide range of frequency and the depth ratio α have been given by Hilaly (1967). As can be seen in Fig. 13, good agreement is obtained, except at high frequency. For low frequency, Tuck (1976) has extended the shallow water approximation for this type of problem. His first-order correction indicates that the magnitude of the reflection coefficient is constant for all frequencies but also predicts a linear increase with wave number in the phase of the reflection coefficient. Fig. 14 indicates good agreement between this theory and the present work.

At high frequency, the asymptotic form of the reflection coefficient is of interest. Fitzgerald (1976) has developed an analytic theory for some bottom contours (including the simple step), but his final answer is rather obscure. The present programme was used to attempt to find, numerically, the high frequency behaviour for a simple step. As can be seen in Fig. 15, it appears that

$$\rho \to e^{-2k_2 h_2 \alpha} \qquad (3.6.1)$$

No such limit appears in Hilaly's results. Since the result (3.6.1) might have been predicted by purely intuitive arguments, it tends to suggest that the present results may be more accurate than Hilaly's for large frequency.

An extension to the simple problem of the step is that of a step with a vertical barrier at $x = 0$ extending part of the way to the free surface. The results for this problem (Fig. 16) are interesting in that for fixed α, as the flow is closed off more and more (i.e. as the top of the barrier

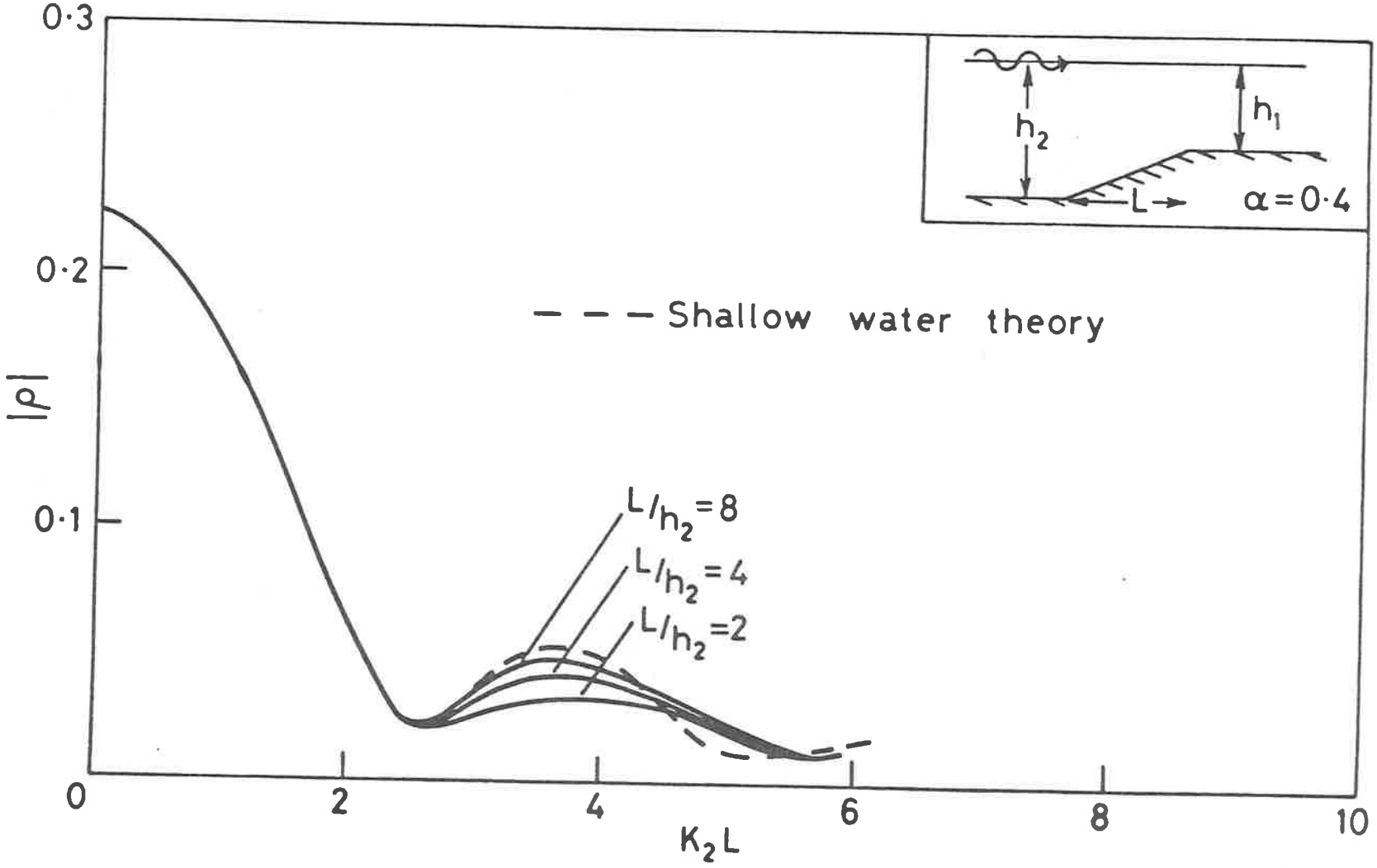

Figure 17 Reflection coefficient due to a linear decrease in depth.

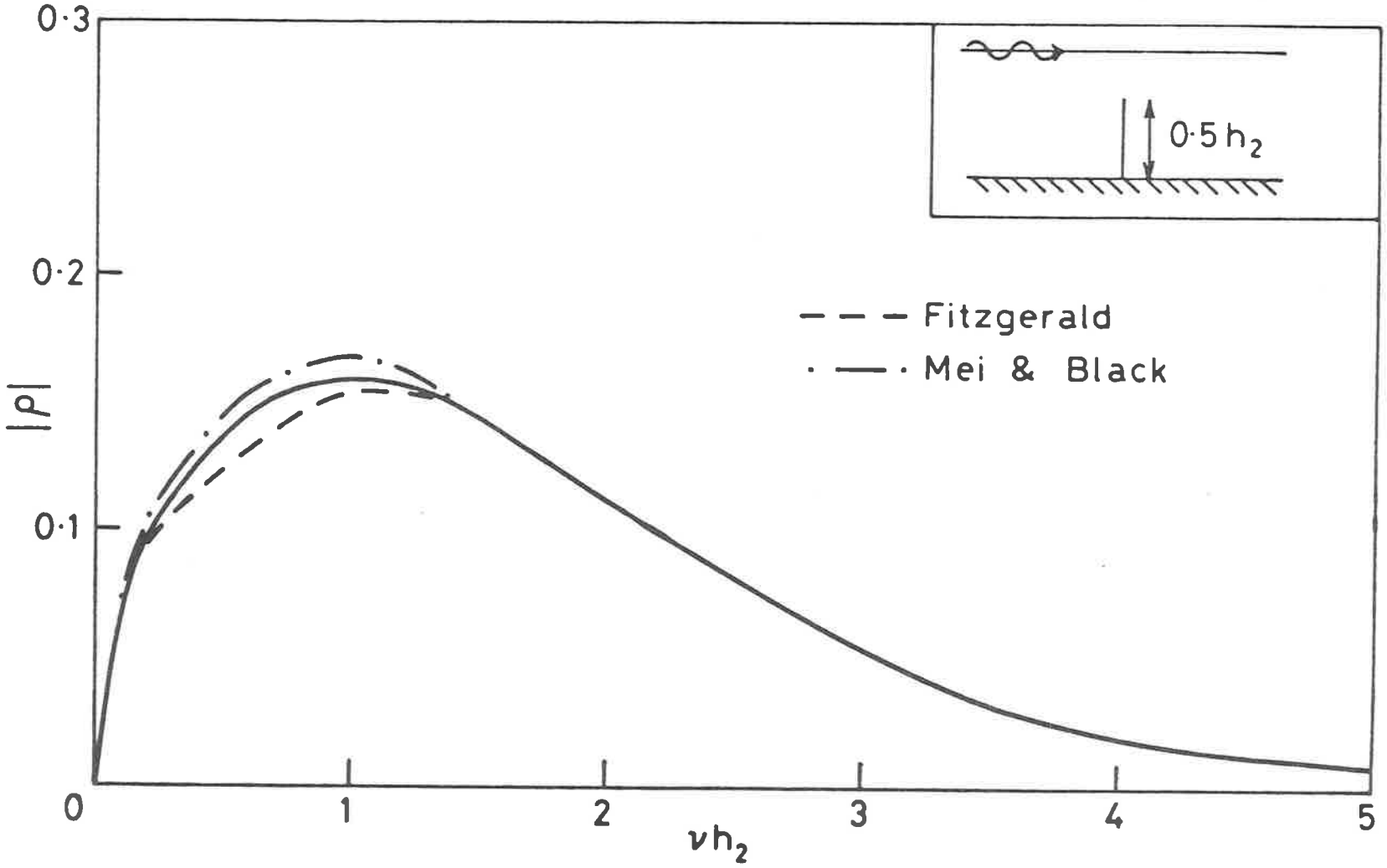

Figure 18 Reflection coefficient for a single barrier reaching partway to the surface in water of constant depth.

gets closer to the free surface), a distinct peak in the reflection coefficient becomes apparent, whereas for the simple step the reflection coefficient decreases monotonically with frequency. Fitzgerald (1976) examined this behaviour, but only for small values of p/h. It may also be noticed that however much the gap above the barrier is closed off, the zero frequency result is always the same, indicating that the transmission of very long waves is independent of barrier geometry.

Another problem of practical interest is that where $y = -h(x)$ is given by a straight line joining the two unequal depths $y = -h_1$ and $y = -h_2$. This bottom topography, in contrast to those treated previously, allows the possibility of multiple maxima and minima in the reflection coefficient, due to the presence of the two corners. It may be seen (Fig. 17) that successive minima are indeed obtained as frequency increases. The locations of these minima are quite accurately predicted by shallow water theory, and as L/h_2 becomes larger, there is agreement in the magnitude of the reflection coefficient. An asymptotic analysis of this problem, for high frequency, would be complicated by the fact that the reflection coefficient does not decay monotonically.

Although the programme was not originally designed for problems where $h_1 = h_2$, these too can be investigated by suitable location of the mesh points. For instance, a single vertical barrier at $x = 0$ extending from $y = -h_2$ partway to the surface may be considered. Results for this problem have been obtained both by Fitzgerald (1976) and by Mei and Black (1969), who used a variational approach. The present work (see Fig. 18) shows better agreement with the theory of

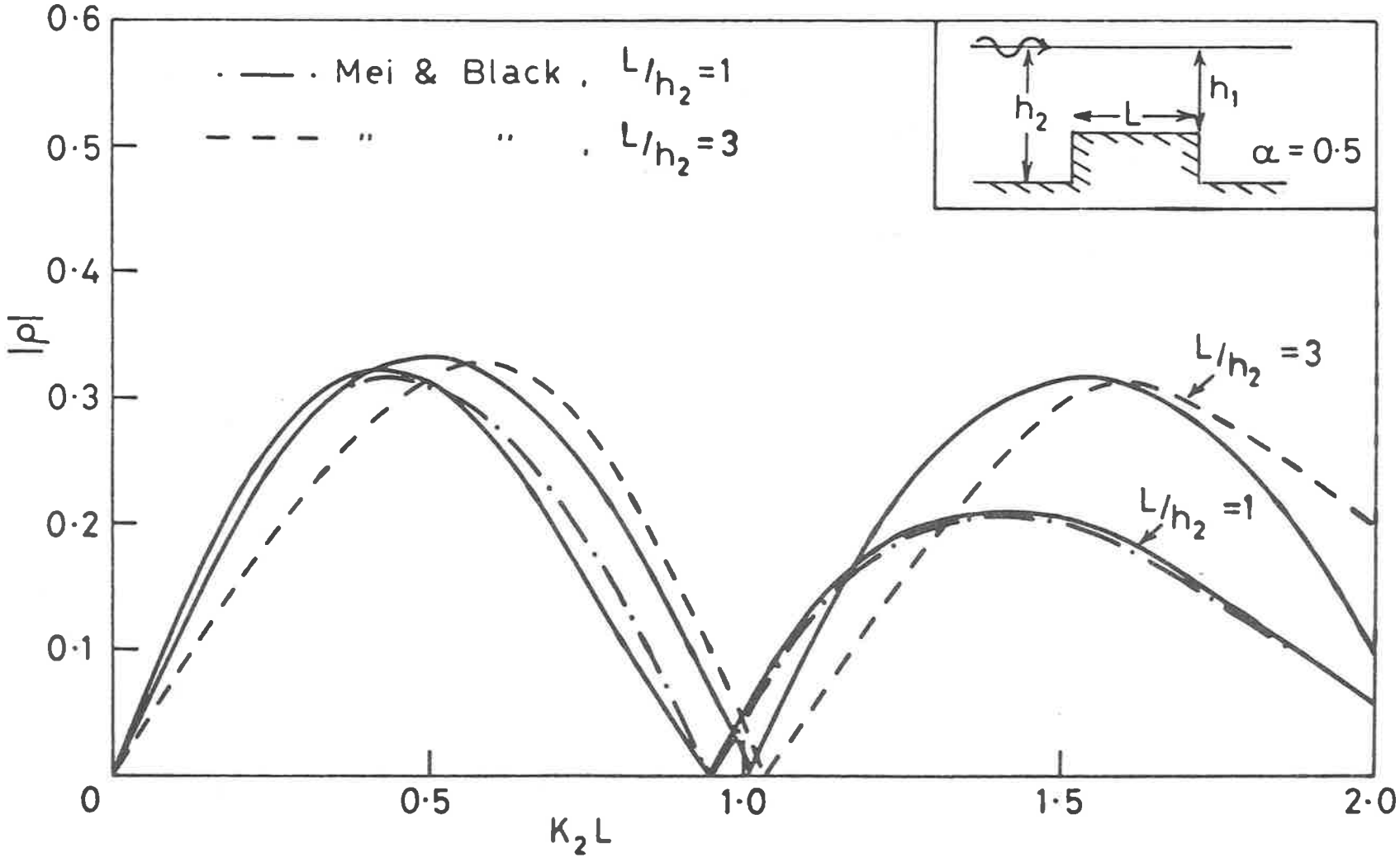

Figure 19 Reflection coefficient for a square hump on the bottom in water of constant depth.

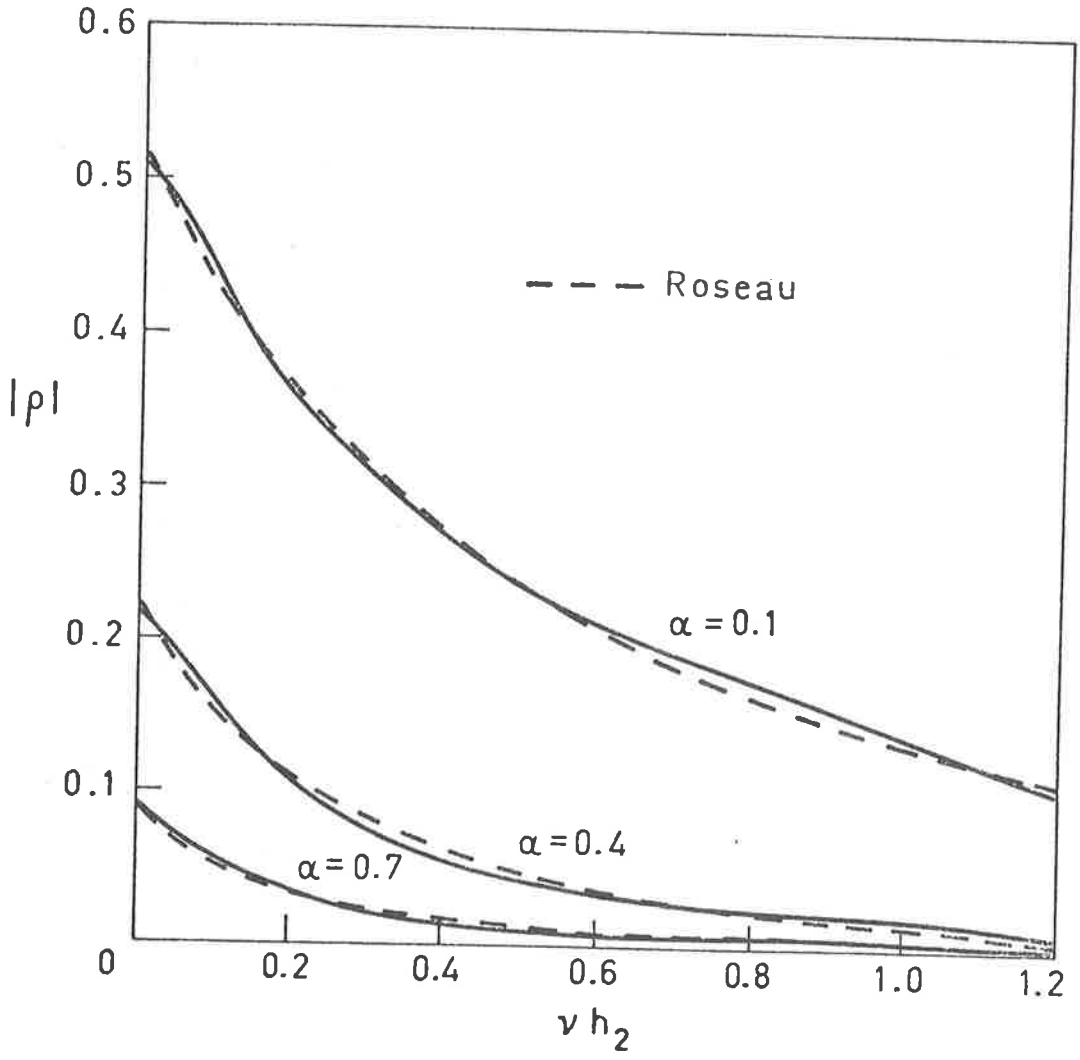

Figure 20 Reflection coefficient for the particular bottom geometry treated analytically by Roseau (1976).

Mei and Black than with that of Fitzgerald, although the differences between all three solutions are marginal and may be considered to be due to numerical error.

Mei and Black also give results for a square hump on a bottom of fixed finite depth (see Fig. 19). Again, good agreement is shown with the present work. Indeed, the curve for $L/h_2 = 3$ is especially encouraging since it shows that the programme is able to deal successfully with situations where the assumption made about ϕ being slowly varying on the arc B might be suspect.

Finally, in Figure 20, we present results for a particular bottom geometry for which Roseau (1976) has given an analytic solution.

The bottom contour is given implicitly as

$$\frac{y}{h_2} = -\alpha + (\alpha-1) \arctan (e^{\xi} \sin 1/(e^{\xi} \cos 1+1)) \qquad (3.6.2)$$

and

$$\frac{x}{h_2} = \alpha\xi + 0.5(1-\alpha) \log(e^{2\xi} + 2e^{\xi} \cos 1+1) \qquad (3.6.3)$$

where ξ ranges from $-\infty$ to ∞.

As can be seen, agreement between the exact theory and the numerical method is reasonably good. There are two reasons why the agreement is not as good as might be hoped. The first is that the depth change takes place over a large distance in comparison with the water depth. This means that a large number of mesh-points must be used to achieve satisfactory accuracy - in other words, to attain very good agreement for a problem of this sort, a prohibitive number of mesh-points must be taken. This indicates that the method is not well-suited to the treatment of such bottom geometries.

The second possible source of error is due to the fact that the curve shown above only asymptotes to the limits $y = -h_1, -h_2$. Thus any finite range of integration, as must be used in a computer programme, will necessarily give some truncation error.

CHAPTER 4

REFLECTION OF WATER WAVES BY A PERMEABLE BREAKWATER

4.1 Introduction

This chapter deals with the transmission and reflection of surface waves incident on an infinitely thin vertical barrier, in water of finite depth. As in the previous chapter, only the two-dimensional problem is considered. The barrier is assumed to have some known permeability, that may vary with depth. This permeability may be identified as $1/C$ where C is a blockage coefficient similar to that defined in Chapter 2. In other words, we may regard the barrier as being perforated by many small pores, with the pores being small when C is large (i.e. low permeability) and large when C is small (high permeability).

In small-amplitude unsteady flows, such as those we are dealing with here, the Bernoulli equation may be linearized. This implies that the acceleration of the fluid across the porous barrier is proportional to the pressure jump across it, specifically

$$a_c = - \frac{1}{2\rho C} \Delta p \qquad (4.1.1)$$

where ρ is the density of the fluid, a_c is the fluid acceleration, Δp is the pressure jump and C is the blockage coefficient referred to above. In time-sinusoidal flows with a (suppressed) time-dependence $e^{-i\sigma t}$, we know that $a_c = i\sigma V$ where V is the streaming velocity through the barrier, so that equation (4.1.1) becomes

$$V = - \frac{\Delta p}{2\rho i\sigma C} \qquad (4.1.2)$$

which is of similar form to the well-known Darcy law for flow in porous media (Morse and Ingard (1968), p.252)

$$V = - k\Delta p \qquad (4.1.3)$$

where k is the Darcy coefficient. This quantity is usually determined experimentally and determines the dissipation due to viscous effects. C will be real in an inviscid fluid, so that inclusion of this quantity measures local inertial effects at the barrier. However, if we use the results of Chapter 2, where both real and imaginary parts for C are obtained for a porous screen, we see that viscous effects may also be included. This means that we have available a quantity akin to a Darcy constant which may be determined theoretically for any viscosity, frequency or ratio of pore size to pore separation. In water wave problems, viscous dissipation is generally of minor importance, but the same is not true for the inertial impedance of the barrier. The method presented in this chapter allows the comparison of the efficiency of, say, a loosely packed submerged breakwater with a completely solid one. The main drawback with the method is that thickness effects cannot be modelled, although it could possibly be modified to allow this.

Using a variable permeability also allows the determination of results for solid obstacles with one or more large gaps. One example of such a problem is that treated by Ursell (1947). This problem was that of reflection of surface waves, in infinite water depth, by a single surface-piercing barrier reaching partway to the bottom. This corresponds to our general variable permeability formulation with $C = \infty$ on the barrier and $C = 0$ everywhere else. In a similar fashion the barrier reaching partway to the surface, treated by Dean

(1945), may also be considered. In finite depth, these two problems have been solved (numerically) by Mei and Black (1969). Again, the method described here may be used for verifying and extending the results.

Problems of flow through one or more gaps have been treated by several authors. All previous work, with one exception, has dealt with infinite water depth. The exception is the solution for flow through a single small gap, in finite depth, due to Packham and Williams (1972). Tuck (1975) gives a slightly different formulation for this problem, but obtains the same results.

In infinite water depth, reflection by a barrier with any number of gaps has been treated by both Lewin (1963) and Mei (1969). The solutions obtained are extremely complicated, however, and in both cases no numerical results are presented. For a single gap, both Guiney (1972) and Porter (1972) have obtained solutions and they both present comprehensive results, but a large amount of numerical integration is involved. More recently, Porter (1974) has presented a simpler method than those of Lewin (1963) and Mei (1969) for the general problem of an arbitrary number of gaps. Again, though, no numerical results are presented.

All the above problems are included in the present formulation. In presenting our results for problems with more than one gap, however, only the problem with two gaps of equal size, in water of infinite depth, is used. This is merely to reduce the number of parameters in the problem (e.g. gap width/gap separation, gap width/mean depth of submersion of two gaps etc.) so that some valid conclusions may be drawn. The method is easily applicable to more than two gaps (at the

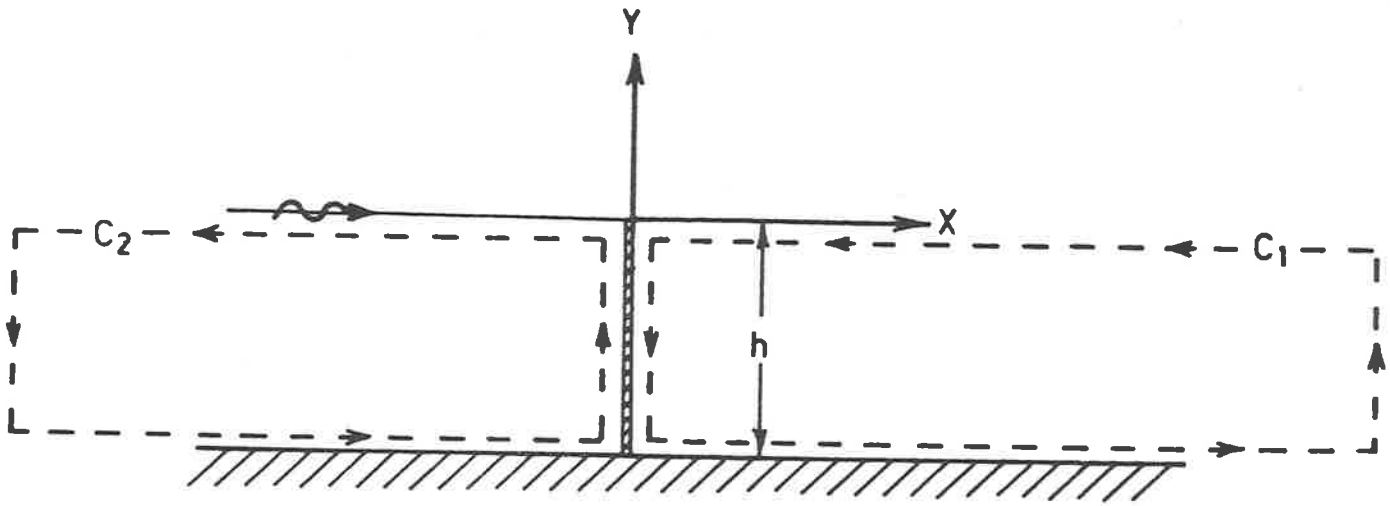

Figure 21 Schematic diagram of the permeable barrier.

expense of a small increase in computing time) but to give a proper coverage of results would be extremely laborious and would convey very little extra information.

4.2 Mathematical Formulation

A similar formulation to the following was outlined briefly by Tuck (1975) for the breakwater problem in water of infinite depth. In this section it is assumed that the depth is finite, but is everywhere constant. In the limit as the depth approaches infinity, it is shown that Tuck's result is regained.

Cartesian co-ordinates x and y are used (see Fig. 21). The fluid is assumed non-viscous and the flow irrotational, so that a velocity potential $\Phi(x,y,t)$ exists which satisfies Laplace's equation

$$\nabla^2 \Phi = 0 \qquad (4.2.1)$$

everywhere in the fluid.

Sinusoidal time-dependence is assumed so that a complex-valued potential function $\phi(x,y)$ may be introduced, where

$$\Phi(x,y,t) = \mathcal{R}e[\phi(x,y)\, e^{-i\sigma t}] \qquad (4.2.2)$$

and σ is the wave frequency.

Since the waves are assumed to be of small amplitude, the linearized free surface condition may be used, that is

$$\frac{\partial \phi}{\partial y} - \nu\phi = 0, \quad y = 0 \qquad (4.2.3)$$

where $\nu = \sigma^2/g$ and g is the acceleration due to gravity. There must also be no normal fluid velocity on the bottom $y = -h$, so that

$$\frac{\partial \phi}{\partial y} = 0 \quad -\infty < x < \infty \qquad (4.2.4)$$

Plane progressive waves of unit amplitude are incident from $x = -\infty$, so that ϕ takes the form

$$\phi \to (e^{iKx} + \rho e^{-iKx}) \frac{\cosh K(y+h)}{\cosh Kh} \tag{4.2.5}$$

and

$$\phi \sim \tau e^{iKx} \frac{\cosh K(y+h)}{\cosh Kh} \tag{4.2.6}$$

where ρ and τ are the complex-valued reflection and transmission coefficients. K is the characteristic wave number for waves of frequency σ in water of depth h, given by

$$\nu = K \tanh Kh. \tag{4.2.7}$$

It is also necessary to define a Green's function $G(x,y;\xi,\eta)$ satisfying the boundary conditions (4.2.3) and (4.2.4), and the equation

$$\nabla^2 G = \delta(x-\xi)\ \delta(y-\eta) \tag{4.2.8}$$

G must also satisfy suitable radiation conditions at $x = \pm \infty$; specifically, it should behave like an outgoing wave. A suitable Green's function is that discussed in Chapter 3 (p.65).

If Green's theorem is now applied to the circuit C_1, on the right-hand side of the barrier in Figure 21, then

$$\phi(\xi,\eta) = \oint_{C_1} \phi(x,y) \frac{\partial G}{\partial n}(x,y;\xi,\eta) - G(x,y;\xi,\eta) \frac{\partial \phi}{\partial n}(x,y)\, d\ell \tag{4.2.9}$$

The only contribution to the integral in (4.2.9) comes from the arc $-h < y < 0$, $x = 0_+$. There is no contribution from the free surface or the bottom, since both ϕ and G satisfy equations (4.2.3) and (4.2.4). At $x = \infty$, since both ϕ and G behave like outgoing waves, there is again no contribution to the integral. Thus (4.2.9) becomes

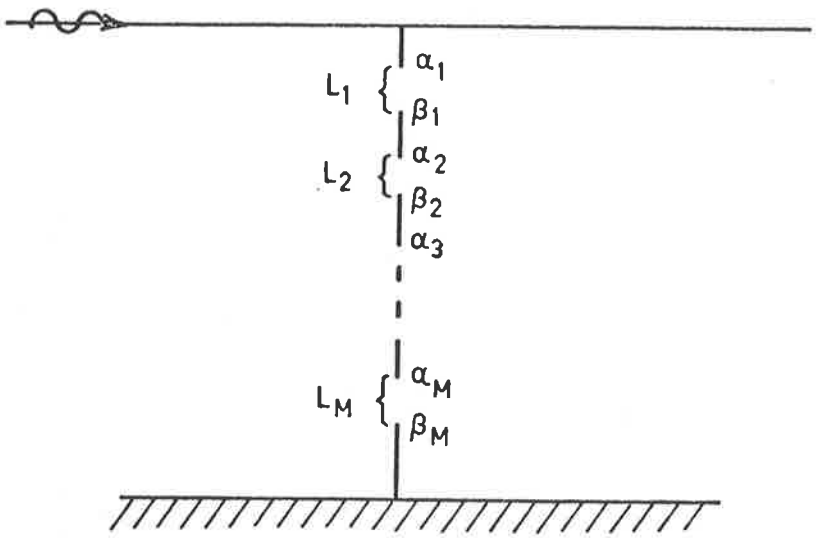

Figure 22 Schematic diagram of a many-gap barrier.

$$\phi(\xi,\eta) = \int_{-h}^{0} \frac{\partial\phi}{\partial x}(0_+,y)\ G(0_+,y;\xi,\eta) - \phi(0_+,y)\ \frac{\partial G}{\partial x}(0_+,y;\xi,\eta)dy \tag{4.2.10}$$

If we apply Green's theorem over the circuit C_2 we obtain in a similar manner

$$\phi(\xi,\eta) = \phi_0(\xi,\eta) - \int_{-h}^{0} \frac{\partial\phi}{\partial x}(0_-,y)\ G(0_-,y;\xi,\eta)dy + \int_{-h}^{0} \phi(0_-,y)\ \frac{\partial G}{\partial x}(0_-,y;\xi,\eta)dy \tag{4.2.11}$$

In this case there is a contribution from the part of the circuit at $x = -\infty$ since ϕ has an incoming component. Specifically, this contribution is

$$\phi_0 = \frac{\cosh K(\eta+h)\ e^{iK\xi}}{\cosh Kh} \tag{4.2.12}$$

In equations (4.2.10) and (4.2.11), we have available solutions for $x \geqslant 0$ and $x \leqslant 0$ separately. To complete this formulation we need to match the two equations across $x = 0$. Since $\partial G/\partial x$ behaves like a delta function as $\xi \to x$, (4.2.10) becomes, with $\xi \to 0_+$

$$\phi(0_+,\eta) = 2\int_{-h}^{0} \frac{\partial\phi}{\partial x}(0_+,y)\ G(0_+,y;0_+,\eta)dy \tag{4.2.13}$$

while (4.2.11) reduces to

$$\frac{1}{2}\ \phi(0_-,\eta) = \phi_0(0_-,\eta) - \int_{-h}^{0} \frac{\partial\phi}{\partial x}(0_-,y)\ G(0_-,y;0_-,\eta)dy \tag{4.2.14}$$

as $\xi \to 0$. To obtain a final integral equation from (4.2.12) and (4.2.13) requires some form of matching condition across $x = 0$, $-h < y < 0$. Problems where the barrier is made up of impermeable material perforated by large totally-permeable gaps are easily treated. We refer to Figure 22.

Across all open sections $y \in L_m$, $m = 1,\ldots M$, there is no flow restriction across $x = 0$, so that

$$\frac{\partial \phi}{\partial x}(0_-,y) = \frac{\partial \phi}{\partial x}(0_+,y) = \frac{\partial \phi}{\partial x}(0,y) \qquad (4.2.15)$$

and $$\phi(0_-,y) = \phi(0_+,y) = \phi(0,y) \quad y \in L_m,\ x = 0 \qquad (4.2.16)$$

For all other points on $x = 0$, there is no flow at all, since the barrier is totally impermeable. This means that the normal velocity across the barrier must be zero at these points, although there may be a discontinuity in the potential function. This condition we write as

$$\frac{\partial \phi}{\partial x}(0_+,y) = \frac{\partial \phi}{\partial x}(0_-,y) = 0,\ y \notin L_m,\ x = 0. \qquad (4.2.17)$$

On using these conditions, and observing that the Green's function G is continuous across $x = 0$, we may reduce (4.2.13) and (4.2.14) to the single integral equation

$$\sum_{m=1}^{M} 2\int_{L_m} \frac{\partial \phi}{\partial x}(0,y)\ G(0,y,0,\eta)dy = \frac{\cosh K(\eta+h)}{\cosh Kh} \qquad (4.2.18)$$

This equation may be discretized and solved numerically for any barrier configuration that may be described as a series of disconnected arcs L_m. The problems treated by Porter (1972), Dean (1945) and Ursell (1947), for example, may all be treated in this way.

The problem becomes more involved if the permeability is no longer either zero or infinite as in the above examples. There is now the possibility of an effective potential jump across $x = 0$ at points where the velocity is non-zero. Subtracting (4.2.14) from (4.2.13) gives

$$\Delta\phi = \phi(0_+,\eta) - \phi(0_-,\eta)$$

$$= 2\int_{-h}^{0} G(0,y,0,\eta)\left[\frac{\partial \phi}{\partial x}(0_+,y) + \frac{\partial \phi}{\partial x}(0_-,y)\right]dy - 2\,\phi_0(0,\eta) \qquad (4.2.19)$$

In this equation we have implicitly assumed the continuity of G and ϕ_0 across $x = 0$. It now is necessary to use the concept of a blockage coefficient C, as defined in Chapter 2. For non-zero finite permeability, the barrier at $x = 0$ may be considered to be perforated by some (assume given) array of small pores. The local flow at any point on $x = 0$ may then be regarded as unsteady streaming flow through a screen. At each point y on $x = 0$ the screen will have some local permeability or blockage coefficient C(y). At a distance from the barrier that is large compared with the average pore size, but still is small when compared with all other dimensions in the problem, the flow will tend to

$$\phi(x,y) \to U(y)\ x + U(y)\ C(y)\ \text{sgn}\ x \qquad (4.2.20)$$

where U(y) is the streaming velocity appropriate for any point (0,y). Since the distance from the barrier is still small, in terms of the outer flow, U may be recognised as

$$U = \phi_x(0_+,y) = \phi_x(0_-,y) = \phi_x(0,y). \qquad (4.2.21)$$

This means that there is no jump in velocity across the barrier as far as the outer flow pattern is concerned. By (4.2.20), however, there is a jump in the velocity potential, given by

$$\Delta\phi = 2\phi_x(0,y)\ C(y) \qquad (4.2.22)$$

so that (4.2.19) becomes

$$\phi_x(0,\eta)\ C(\eta) + \phi_0(0,\eta) = 2\int_{-h}^{0} G(0,y;0,\eta)\ \frac{\partial\phi}{\partial x}(0,y)\,dy \qquad (4.2.23)$$

It must be noted that for validity of the above reasoning, the length scale for variation in C(y) must be much larger than the length scale for the pores in the breakwater. It should be noted, too, that viscous dissipative effects may be

included by introducing an imaginary component in the blockage coefficient.

Since $C(y)$ is assumed known (determined theoretically from Chapter 2, or obtained experimentally), equation (4.2.23) constitutes an integral equation of the second kind in the normal velocity across $x=0$.

This equation has a unique solution under certain integrability and boundedness conditions on the kernel function G. This means that any numerical method we use to solve this equation has a good chance of success. The same is not necessarily true, however, for equation (4.2.18) which is an equation of the first kind. It is found in practice, however, that the method used to solve (4.2.23) also deals successfully with equation (4.2.18).

Equation (4.2.18) may also be regarded as a special case of (4.2.23). For $y \in L_m$, $m=1,\ldots,M$, the blockage coefficient is zero. For all other points the normal velocity is zero. Using these two facts, we may immediately recover (4.2.18) from (4.2.23).

Finally, Tuck's (1975) infinite depth formulation may be recovered by allowing $h \to \infty$ in (4.2.23) so that

$$C(\eta)\ \phi_x(0,\eta) + e^{K\eta} = 2\int_{-\infty}^{0} G_\infty(0,y;0,\eta)\ \frac{\partial\phi}{\partial x}(0,y)\,dy \qquad (4.2.24)$$

where G_∞ is the limiting form of G as $h \to \infty$. This limiting form is well-known, and is indeed a great deal simpler than G for finite depth. Thus, for problems where the depth is very large, the infinite depth Green's function will be used (see Wehausen and Laitone, (1960)).

4.3 Numerical Analysis

There are now two forms of the integral equation that may be used, depending on the nature of the breakwater, namely (4.2.18) and (4.2.23).

First we consider the numerical solution of equation (4.2.23). We may use a similar approach to that adopted in Chapter 3. The present problem is much simpler in some respects. In the first place, we have only the normal velocity across $x=0$ as the unknown, in contrast to the shelf problem where the velocity potential itself also had to be found. Secondly, we have only a single equation to solve, in contrast to the set of coupled integral equations we had to deal with in Chapter 3. This means that, for the problem we are dealing with here, much smaller matrices will have to be inverted, with attendant decrease in computer time and storage, to obtain a given accuracy.

In (4.2.23) we assume that ϕ_x is slowly varying at $x=0$. We divide the arc $x=0$, $0 \geqslant y \geqslant -h$ into N segments (y_j, y_{j+1}) with $y_j > y > y_{j+1}$, $j=1,\ldots,N$. Then, as usual, the approximation $\phi_x(0,y) = \phi_{xj}$ = constant is made. We must now make a choice of meshpoints. So long as the blockage coefficient $C(y)$ is slowly-varying, the obvious choice is a uniform distribution of points. For the special case described by equation (4.2.18), where we have introduced sharp corners at the end of each arc L_m, we may make a better choice. We know that in the near vicinity of these corners the velocity potential has a square-root singularity, so on $L_m = (\alpha_m, \beta_m)$, for example, we take

$$y_{j,m} = \alpha_m + \left[\sin \frac{\pi}{2}\left(\frac{j-1}{N}\right)\right](\beta_m - \alpha_m), \quad j=1,2,\ldots,N+1 \qquad (4.3.1)$$

It should be noted that a separate set of meshpoints y_{mj}, $j=1,\ldots,N$ is required for each arc L_m.

We satisfy the integral equation at the N points

$$\eta_i = \left(\frac{y_i + y_{i+1}}{2}\right) \quad i=1,\ldots,N \tag{4.3.2}$$

for problems with slowly-varying C(y). For problems involving one or more large gaps, as described by equation (4.2.18), we choose

$$\eta_{i,m} = \alpha_m + \left[\sin \frac{\pi}{2}\left(\frac{i-\frac{1}{2}}{N}\right)\right](\beta_m - \alpha_m) \quad i=1,\ldots,N \tag{4.3.3}$$

which is consistent with the choice of meshpoints y_j in equation (4.3.1).

With these assumptions, (4.2.23) may be written in discrete form as

$$\phi_{xi} C_i + \phi_{0i} = 2 \sum_{j=1}^{N} \phi_{xj} \int_{y_j}^{y_{j+1}} G(0,y_j;0,\eta_i)\,dy \quad i=1,\ldots,N \tag{4.3.4}$$

where ϕ_{0i} represents the obvious discretization $\phi_0(0,\eta_i)$. In a similar way we may write (4.2.18) as

$$\phi_{0i,m} = 2 \sum_{j=1}^{N} \phi_{xj,m} \int_{y_{j,m}}^{y_{j+1,m}} G(0,y_{j,m};0,\eta_{i,m})\,dy \tag{4.3.5}$$

for $i=1,\ldots,N$, $m=1,\ldots,M$.

Thus (4.3.4) becomes

$$A\underset{\sim}{\Phi} = \underset{\sim}{\Phi}_0 \tag{4.3.6}$$

where $$A = [A_{ij}] \tag{4.3.7},$$

and $$A_{ij} = \int_{y_j}^{y_{j+1}} G(0,y_j;0,\eta_i)\,dy \tag{4.3.8},$$

$$\underset{\sim}{\Phi} = (\phi_{x1},\ldots,\phi_{xN})^t \tag{4.3.9},$$

and $$\underset{\sim}{\Phi}_0 = (\phi_{0\,1}, \ldots, \phi_{0\,N})^t \qquad (4.3.10)$$

Equation (4.3.5) may be represented in similar fashion. It should be noted in (4.3.5) that increasing the number of gaps generally increases the amount of computing time required to solve the problem, since introducing extra singularities (by way of more corners) will increase the number of points required to obtain satisfactory accuracy.

Once we have the problem in the form (4.3.6), with $[A_{i\,j}]$ known, we can find the normal velocity through the gap by inverting the matrix equations. Once the normal velocity has been obtained, the transmission and reflection coefficients follow by use of the original integral equations, in a similar fashion to that described in Chapter 3.

The only remaining problem is the actual evaluation of the elements $A_{i\,j}$. These follow immediately from equation (3.5.22), where the integral is obtained explicitly. In the special case when the depth is infinite, or very large, it is more desirable to use the infinite-depth Green's function. For these problems we truncate the range of integration from the interval $(0,-\infty)$ to say $(0,-h^*)$. Our choice of mesh points is now the same as for finite depth problems with h^* replacing h. This means that we are actually assuming a solid barrier for $y < -h^*$. In practice this should not affect the transmission, so long as h^* is chosen large enough, as there is exponential decay in the wave motion of the form e^{Ky}. The only other change we make is in the evaluation of the elements $A_{i\,j}$, which now become

$$A_{i\,j} = \int_{y_j}^{y_{j+1}} G_\infty(0,y_j\,;0,\eta_i)\,dy \qquad (4.3.11)$$

where G_∞ is the infinite depth Green's function referred to in Section 4.2. A convenient form of this function is

$$G_\infty = \frac{1}{2\pi}(\log|y-\eta| - \log|y+\eta|) - \frac{1}{\pi}\int_0^\infty \frac{e^{p(y+\eta)}}{p-K}dp - ie^{K(y+\eta)} \tag{4.3.12}$$

We may immediately write A_{ij} as

$$A_{ij} = \left[\frac{y-\eta}{2\pi}\log|y-\eta| - \frac{(y+\eta)}{2\pi}\log|y+\eta| - \frac{ie^{K(y+\eta)}}{K}\right]_{y_j}^{y_{j+1}} - \frac{1}{\pi}\int_{y_j}^{y_{j+1}}\int_0^\infty \frac{e^{p(y+\eta)}}{p-K}dpd\eta \tag{4.3.13}$$

On interchanging the order of integration in the integral in (4.3.12) we may finally determine A_{ij} as

$$A_{ij} = \left[\frac{y-\eta}{2\pi}\log|y-\eta| - \frac{y+\eta}{2\pi}\log|y+\eta| - \frac{ie^{K(y+\eta)}}{K} - \frac{1}{K\pi}\log|y+\eta| + \frac{1}{K\pi}e^{K(y+\eta)}\,\overline{Ei}(-K(y+\eta))\right]_{y_j}^{y_{j+1}} \tag{4.3.14}$$

Here $\overline{Ei}(x)$ is the exponential integral (see Abramowitz and Stegun (1964)). This function may be quickly and easily computed for all values of its argument with the use of polynomial approximations.

4.4 Results

We consider first problems of the type described by equation (4.2.18). Any results given for infinite depth were computed using the infinite depth Green's function, as given in equation (4.3.12), in preference to using the finite depth Green's function with a large depth parameter.

The first set of curves is for flow past a surface-piercing barrier of height ℓ, in water depth h. This is the problem first treated by Ursell (1947), for water of

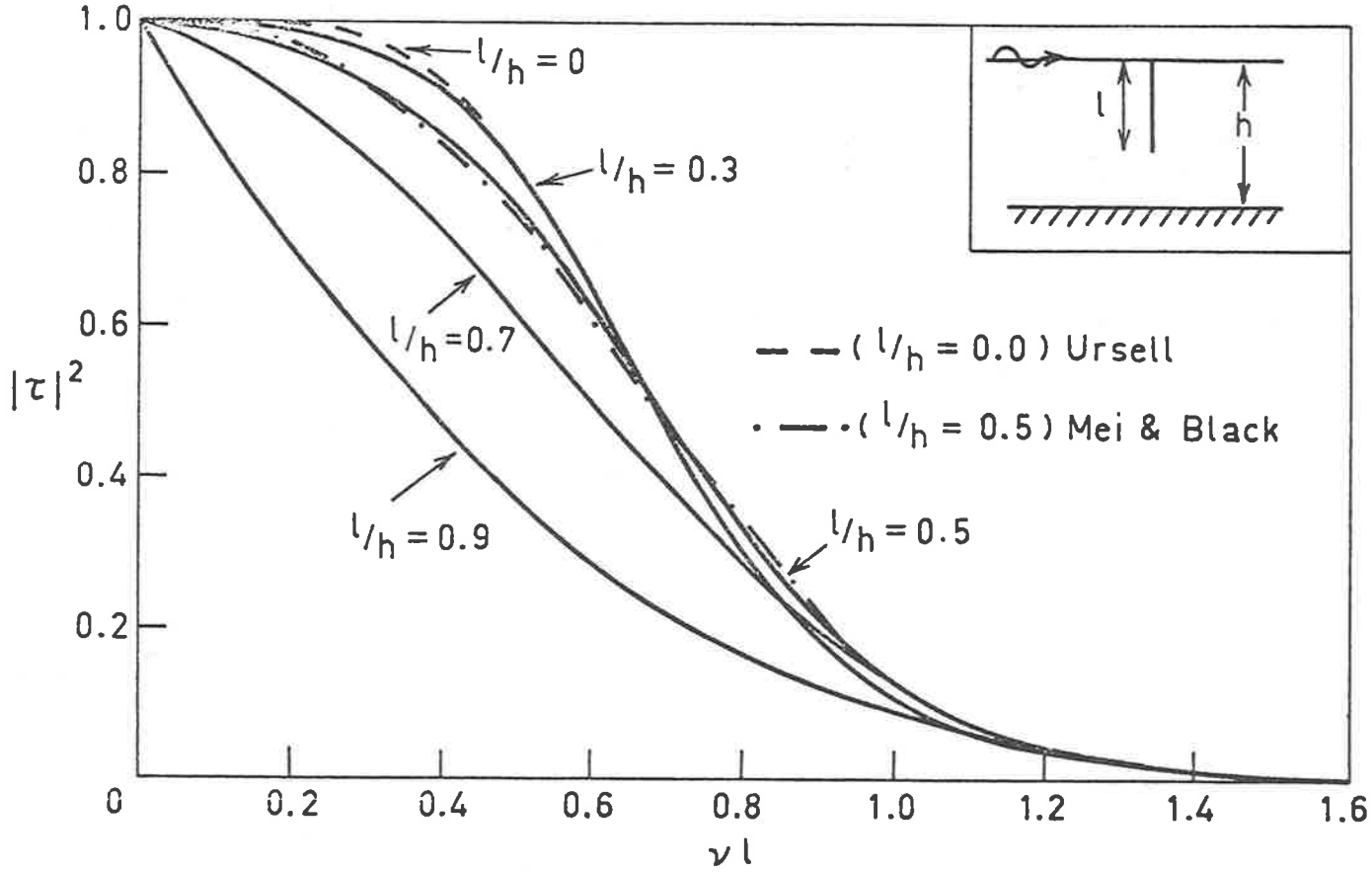

Figure 23 Transmission coefficient for a surface-piercing barrier in water of finite depth.

infinite depth. In Figure 23 the transmission coefficient is plotted against $\nu\ell$. The present work agrees very well with Ursell's results - the two results are indistinguishable on the scale shown. When the depth is finite, certain interesting trends become apparent.

As ℓ/h becomes larger, the opening closes off more and more - this is indicated by a general reduction in the transmission coefficient. For values of ℓ/h in the range 0.5 - 0.7 it can be seen, by contrast, that the transmission coefficient is actually higher than Ursell's result for waves of moderate frequency. At high frequency, however, all curves collapse on to the infinite depth result.

For $\ell/h = 0.5$ a result due to Mei and Black (1969) is shown. At low frequency, there is some small disparity with the present work. At high frequency, however, the two curves both collapse on to the infinite-depth result. At this stage, it should be noted that Ursell's results appear to have been misleadingly graphed in Mei and Black, so that agreement between their theory and Ursell's appears to be less good than it actually is. Plotting the curves against $\nu\ell$, rather than $K\ell$, as was done in Mei and Black, shows much better agreement. In the infinite-depth case $\nu=K$, so that only one curve may be drawn, whatever the choice of axis. In finite-depth problems, however, ν is not equal to K, so that two different graphs may be drawn for the purpose of comparison. It appears in this case that plotting against $\nu\ell$ is preferable.

In fact, although it is not shown in Figure 23, the result of Mei and Black for $\ell/h = 0$ shows good agreement

with both the present results and with the theory of Ursell.

In Figure 24 results are displayed for the situation where there is a single vertical barrier extending from the bottom partway to the surface. This is in a sense complementary to the surface-piercing barrier problem. Indeed, the analytic solution by Dean (1945), for the case of infinite-depth, appeared only a few years before Ursell's paper. For convenience, we show the magnitude of the reflection coefficient rather than that of the transmission coefficient. The present work again shows excellent agreement with Dean's result and the answers obtained are essentially the same. For finite-depth, extensive results have been given by Mei and Black (1969). As can be seen, the agreement between the two theories is very good over the whole range of frequency for all values of the parameter h/H. It should be noted that the variational method used by Mei and Black becomes less accurate as h/H increases. This is because the method involves approximating an infinite series by taking the first few terms. The fact that the disparities between the two methods become more marked as h/H increases is probably a consequence of this, since the present method gives equally good accuracy for all h/H, at least at low frequency. That the variational method overestimates the reflection coefficient seems to be borne out by the comparison with Dean (1945) for infinite-depth. All in all, though, agreement is very good, much more so than for the surface piercing barrier considered above.

We now turn to the problem of transmission through a single gap in a vertical wall. For infinite depth, this

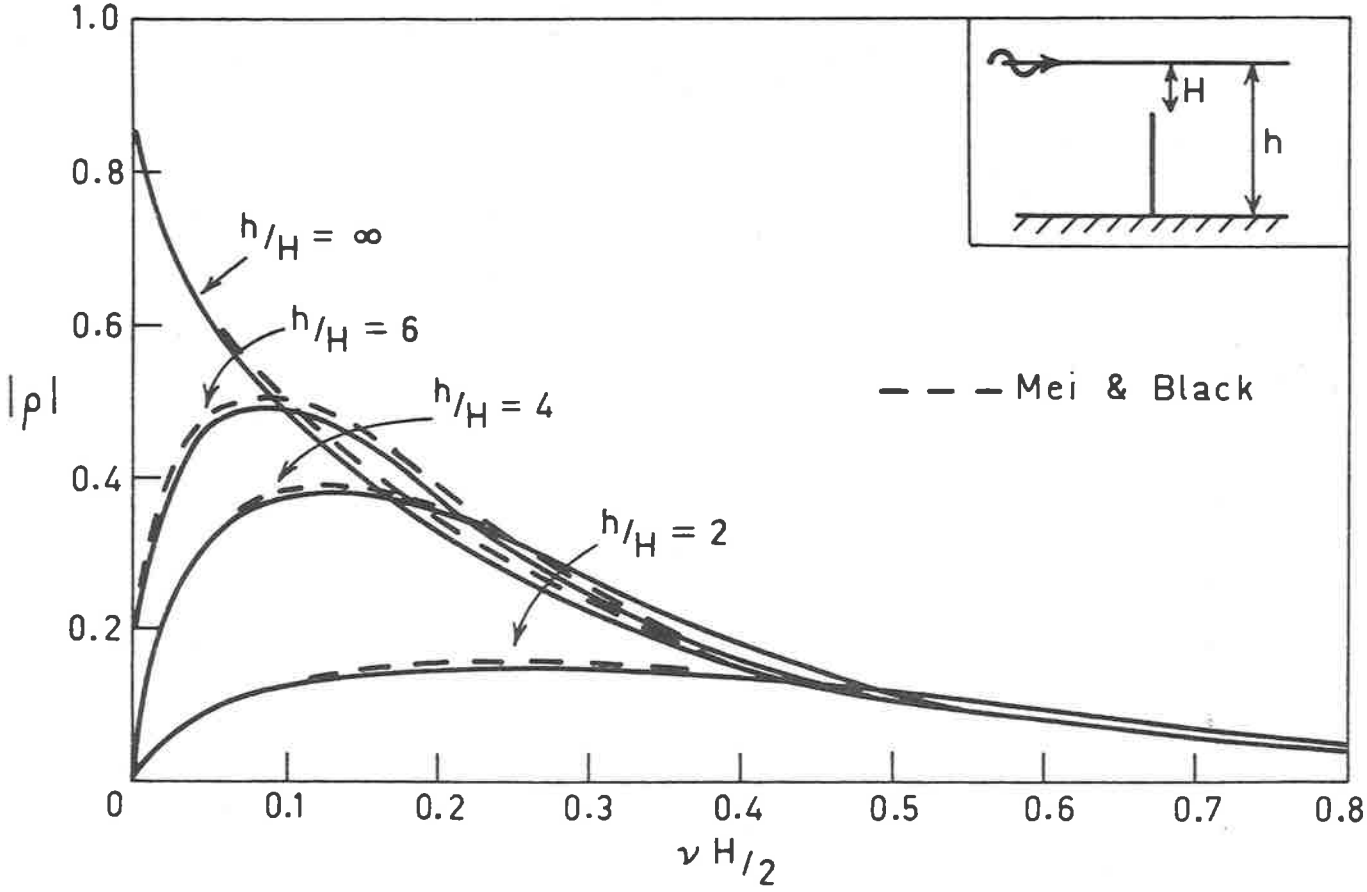

Figure 24 Reflection coefficient for a single barrier reaching partway to the surface in water of finite depth. Note that this geometry is also treated in Chapter 3 (Figure 18).

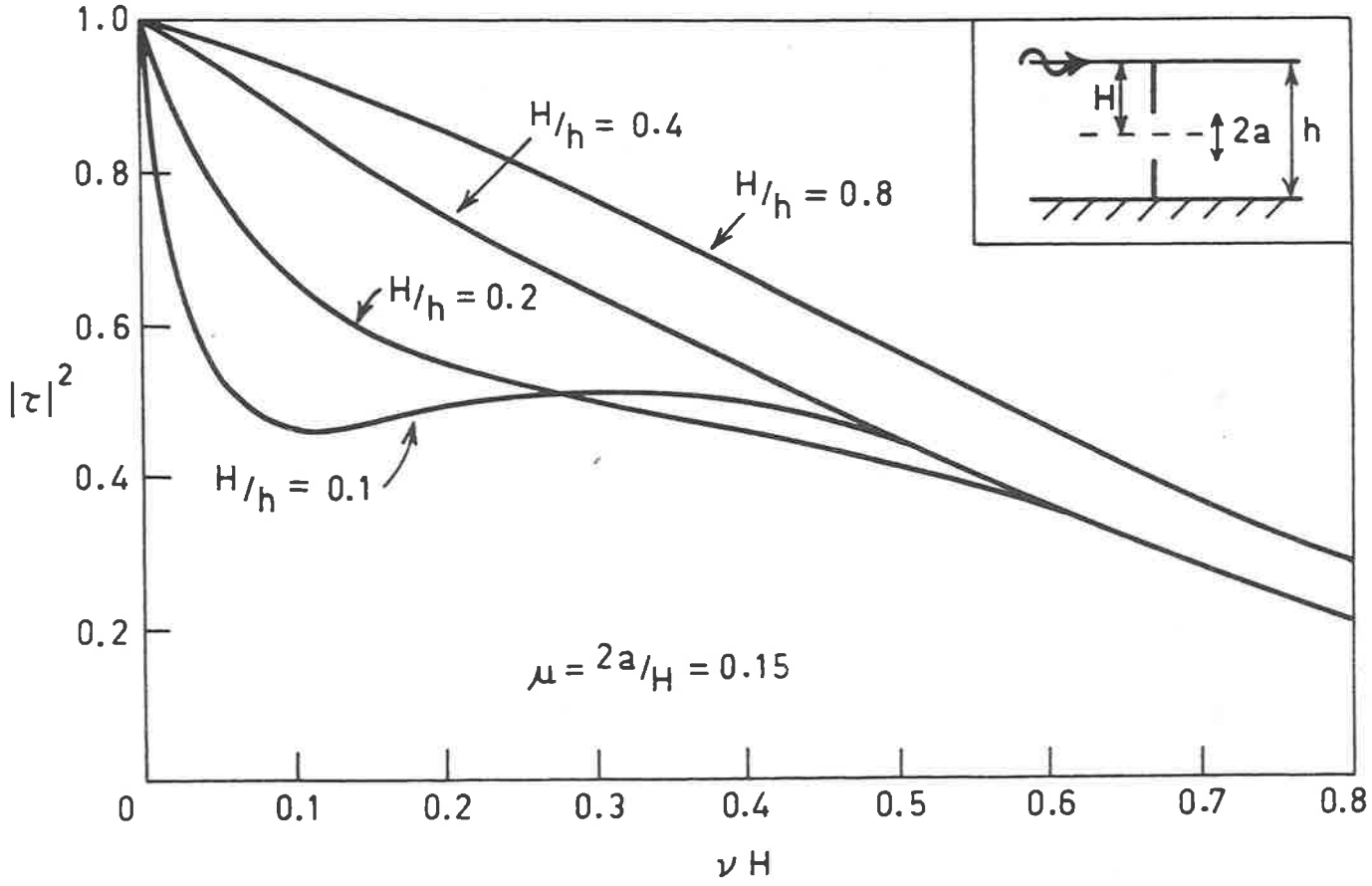

Figure 25 Water wave transmission through a single gap barrier in water of finite depth (μ = 0.15).

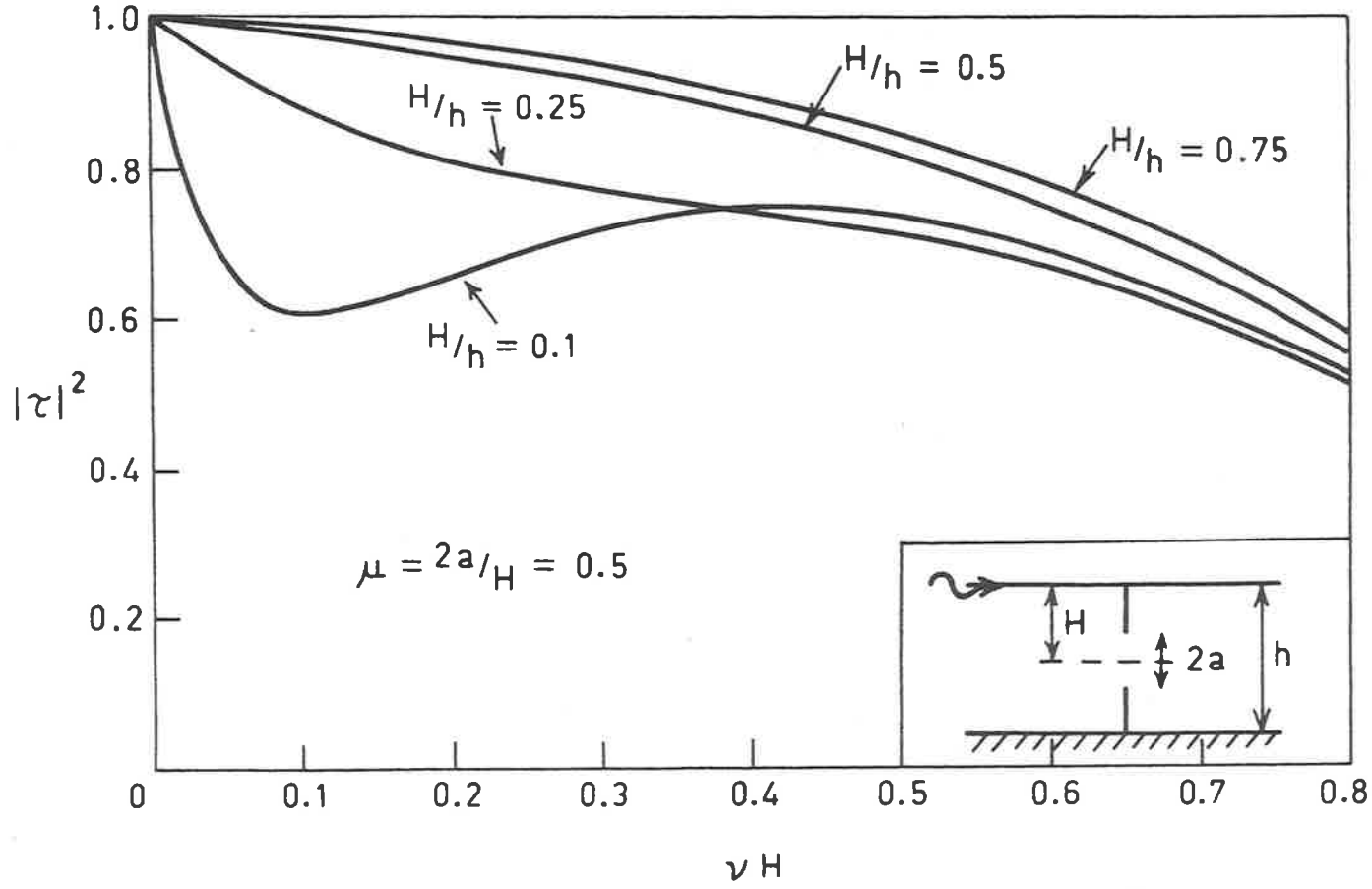

Figure 26 Water wave transmission through a single gap barrier in water of finite depth ($\mu = 0.5$).

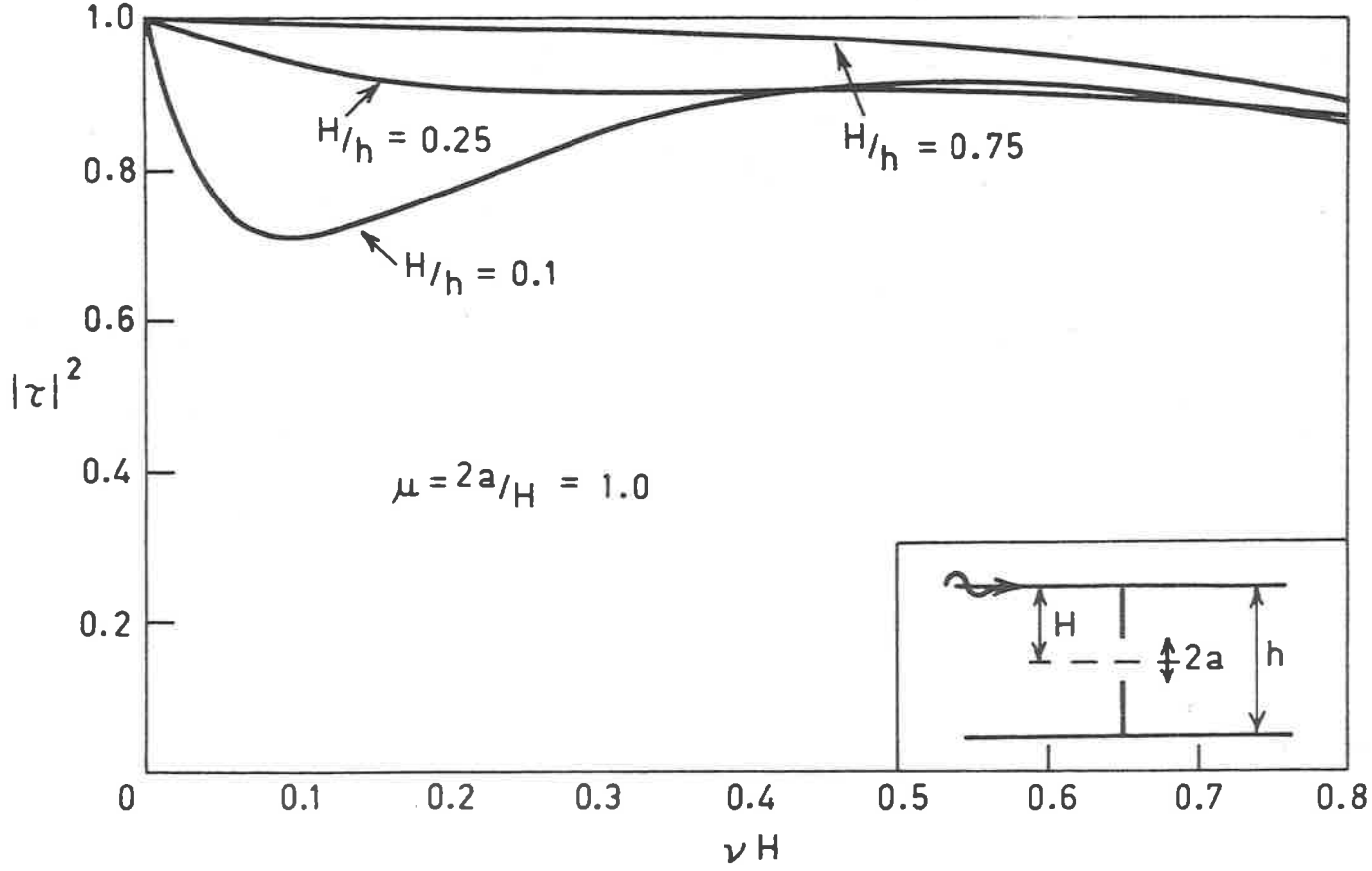

Figure 27 Water wave transmission through a single gap barrier in water of finite depth (μ = 1.0).

problem has been solved exactly by Porter (1972) and Guiney (1972), while an earlier theory by Tuck (1971) solves the problem when the gap is small. In this case, it is convenient to define a parameter $\mu = 2a/H$ where $2a$ is the gap width and H the mean depth of the gap. It was found that over the full frequency range, at any value of μ, excellent agreement was obtained with the exact theory of Guiney. The results of Porter appear to be the same. Since both exact methods require a large amount of numerical integration to obtain final answers, it is possible that the present method is preferable for these problems, since good accuracy can be obtained rapidly and easily, and the present method is more flexible.

For flow through a single gap in finite depth, there are no published results for arbitrary μ. However, for small gaps, both Tuck (1975) and Packham and Williams (1972) have obtained solutions that agree very well. Comparison of Tuck's result with the present work, at $\mu = 0.15$, showed almost exact agreement, even at high frequency. This indicates that the small-gap theory is very good for μ of this order. For completeness, results obtained by the present method are displayed in Figure 25 for $\mu = 0.15$. As has been said, however, the results are for all practical purposes identical with those published elsewhere. Unfortunately, no small-gap results are available for larger μ. It is quite likely that the small-gap approach would be successful for quite large μ, especially at low frequency. (Surprisingly good agreement has been demonstrated for infinite-depth (see, e.g. Tuck (1975)).

In Figures 26 and 27 the magnitude of the transmission coefficient is plotted for various values of H/h with

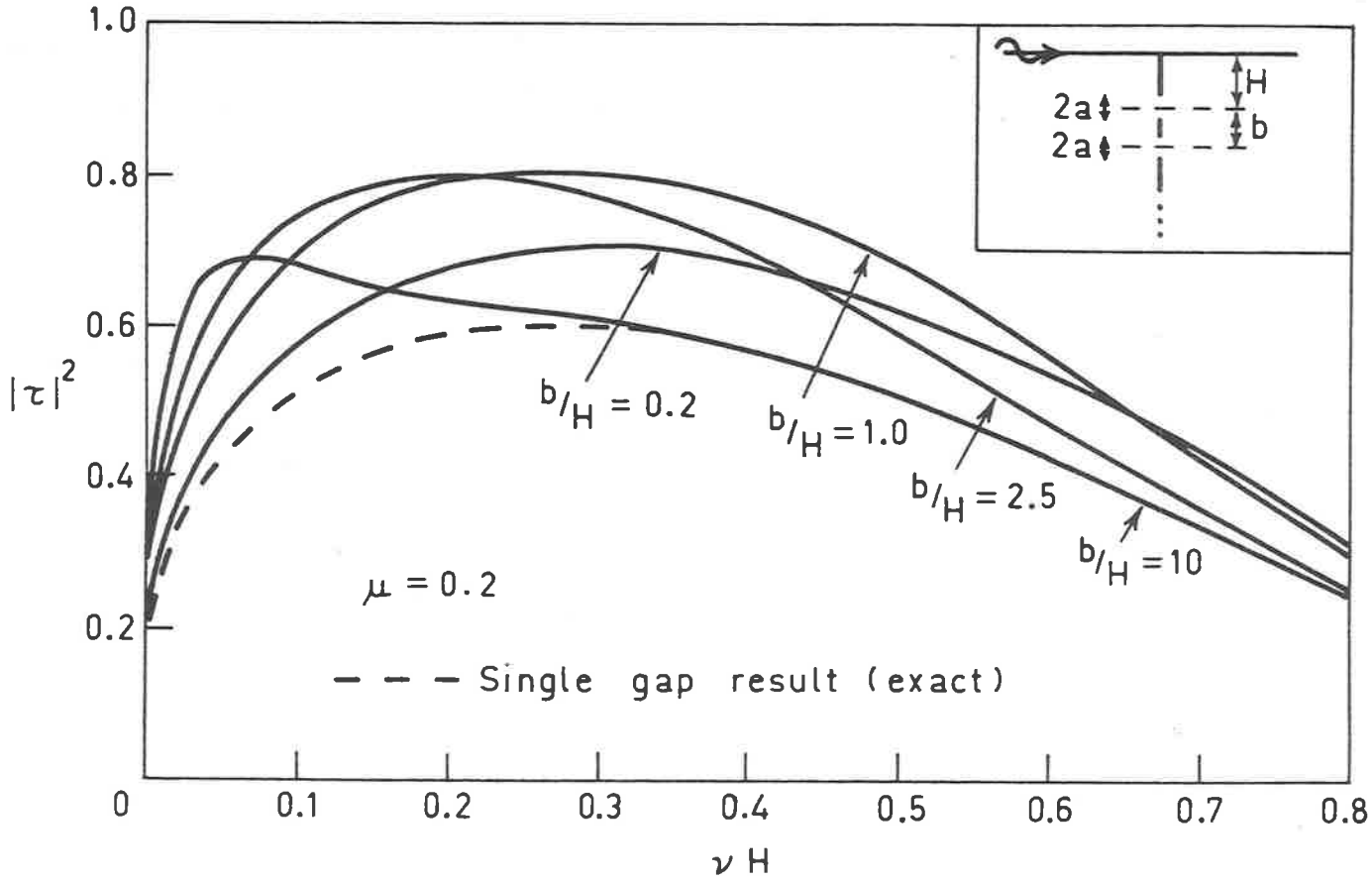

Figure 28 Water wave transmission through a two gap barrier in water of infinite depth ($\mu = 0.2$).

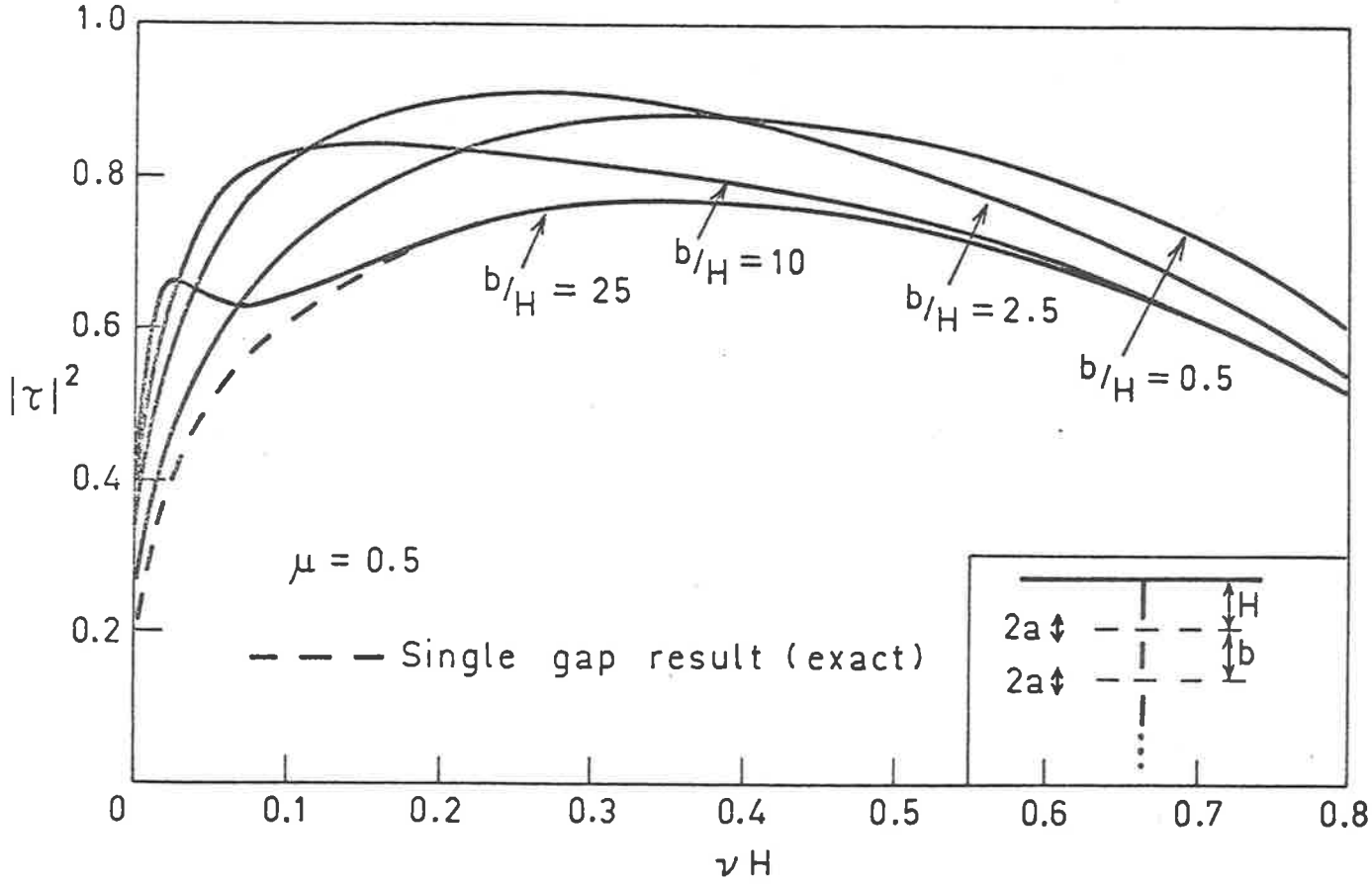

Figure 29 Water wave transmission through a two gap barrier in water of infinite depth ($\mu = 0.5$).

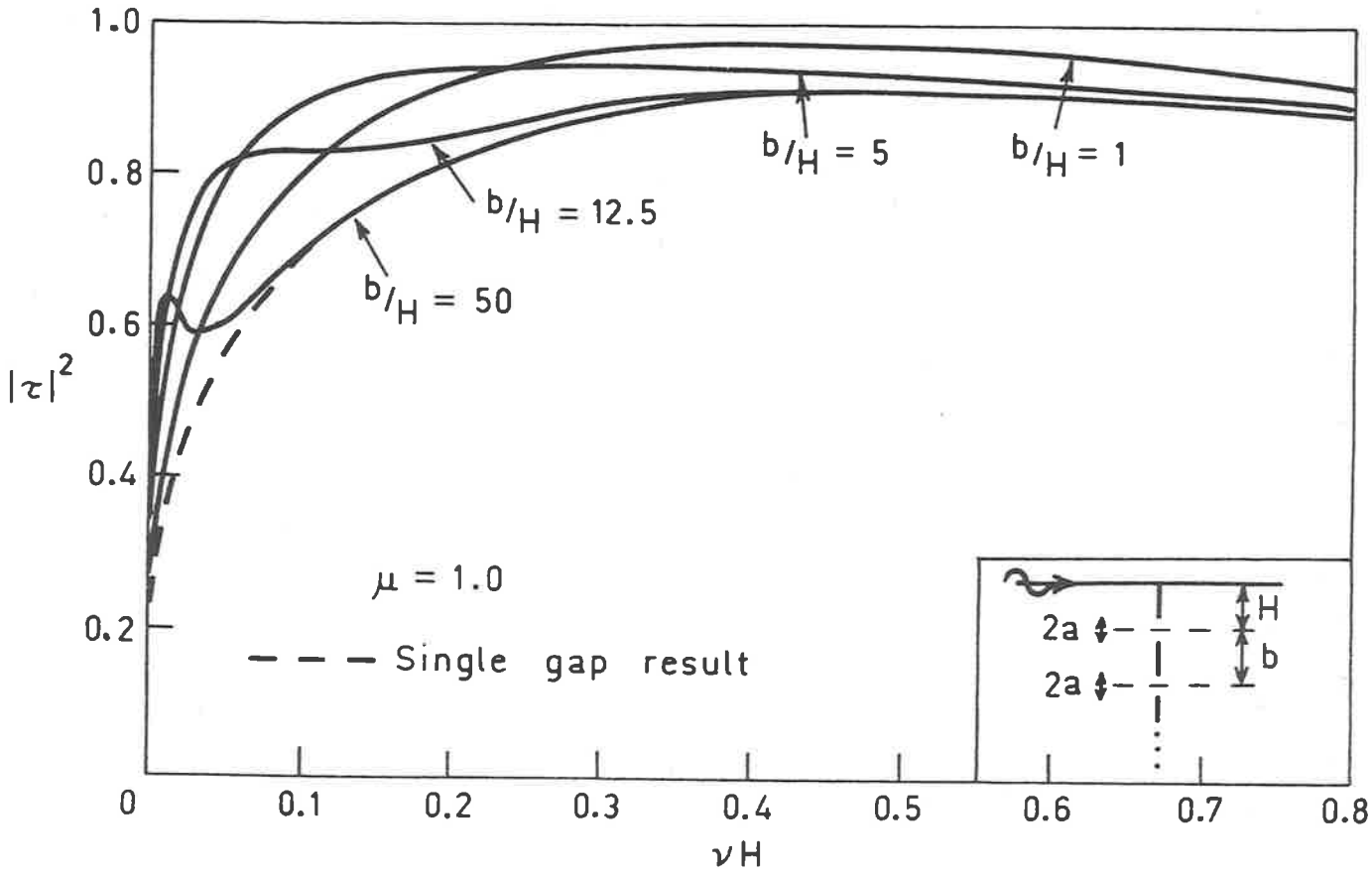

Figure 30 Water wave transmission through a two gap barrier in water of infinite depth ($\mu = 1.0$).

$\mu = 0.5$ and 1.0 respectively. As can be seen, no qualitative change from the small gap problem is apparent. In a quantitative sense, transmission increases as the gap becomes bigger, as might be expected.

We now turn to flow problems with more than one gap. For simplicity, only infinite depth results are presented, although the method works just as well for finite depth. Both gaps are assumed to be of width $2a$, with their centres separated by a distance b. In Figures 28,29 and 30 the transmission coefficient is plotted for various values of b/H, where H is the mean depth of submersion of the upper gap. We will discuss Figure 30 in detail - the same arguments apply to Figures 28 and 29. The limiting curve $b/H = 1$ corresponds to the two gaps being side by side, so forming a single gap of width $4a$. Thus the results obtained should be the same as for a single gap with $\mu = 4/3$. This in fact turns out to be the case, with the results agreeing exactly with those obtained for the single gap problem. We now increase the value of b/H. This corresponds to holding the top gap in place while moving the bottom one down. At low frequency, the incoming wave appears to see less impedance than would be the case if there were no interaction effects. Thus the transmission coefficient is larger than for the $b/H = 1$ curve. At higher frequency this is no longer true and in fact the transmission coefficient is smaller than the $b/H = 1$ value. This is probably due to the fact that short waves are confined to a thin surface layer and so cannot "feel" the deeply-submerged bottom gap. As b/H becomes larger it is interesting to note that a definite peak becomes apparent in the transmission coefficient, at reasonably low

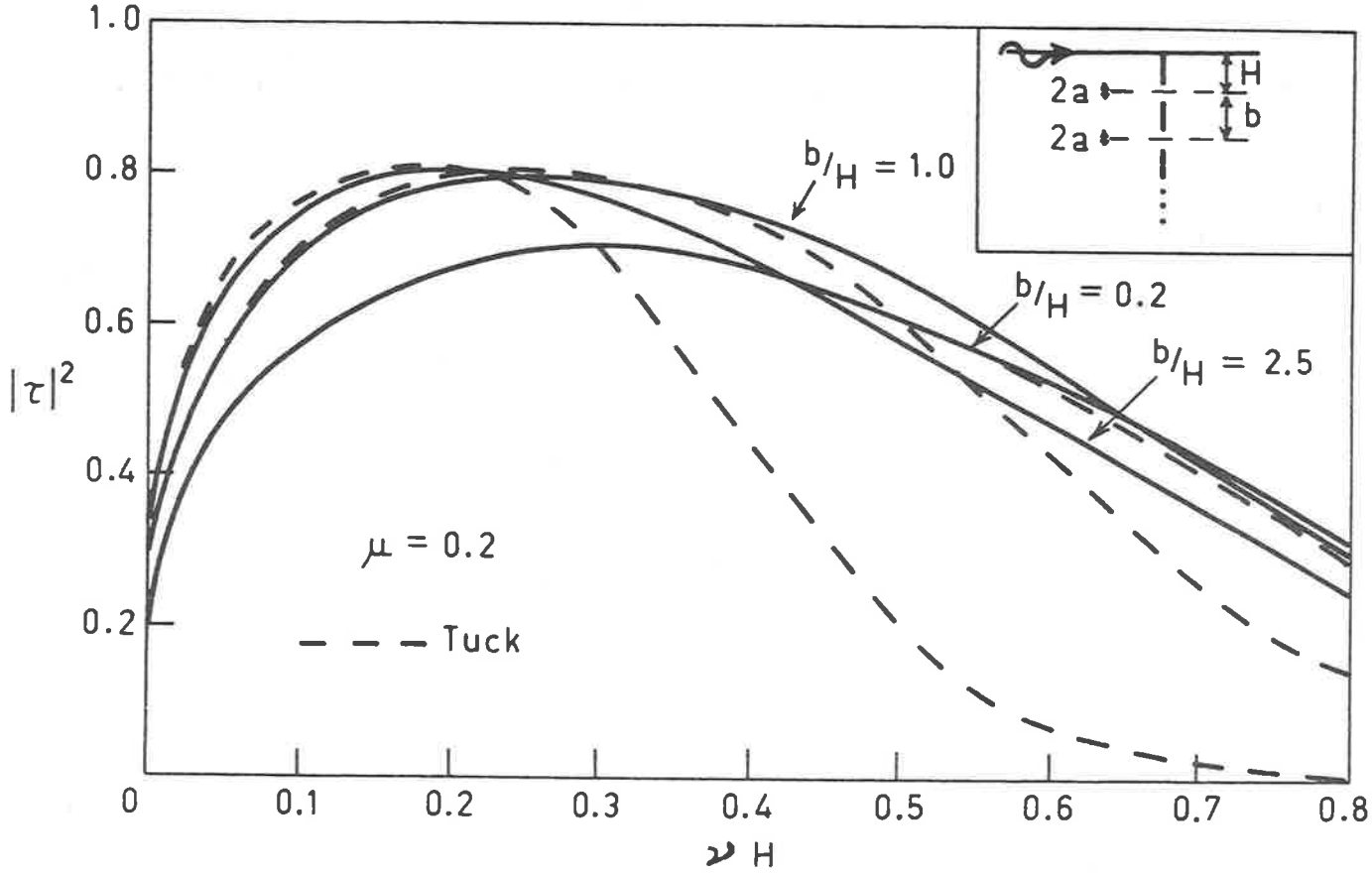

Figure 31 Water wave transmission through a two gap barrier in water of infinite depth ($\mu = 0.2$). Comparison with small gap theory of Tuck (1976).

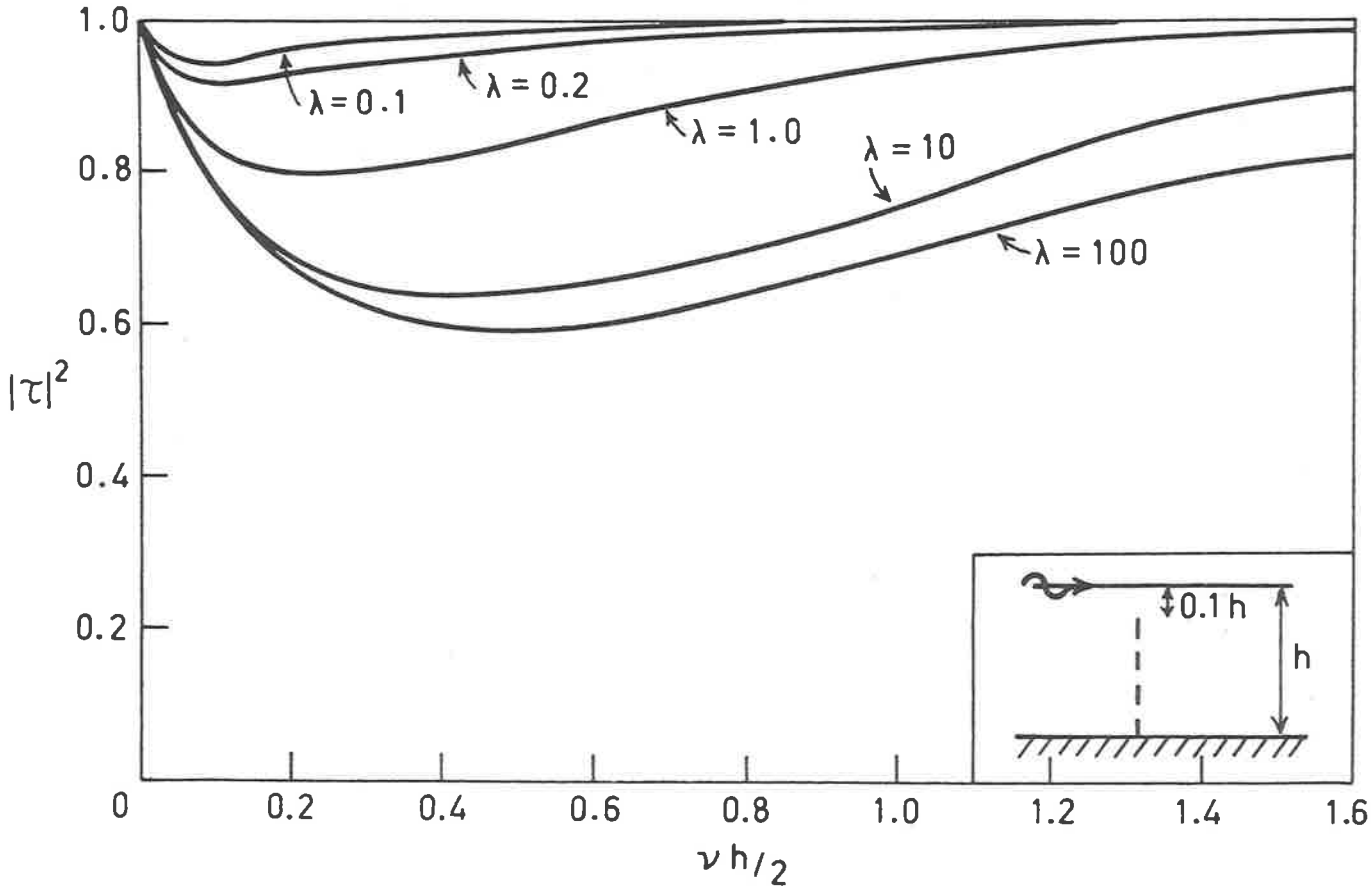

Figure 32 Transmission coefficient for a semi-permeable barrier. Large λ corresponds to low porosity.

frequency. This indicates that some sort of resonance effect is taking place due to the interaction of the flow with the two gaps. It is possible that in many-gap problems we might obtain a large number of peaks of this form, although this has not been checked.

As b/H becomes very large, we expect the transmission coefficient curve to collapse down to that for a single gap of width $2a$, since the waves on the surface are not affected by the deeply submerged lower gap. Indeed this is so and we see that for values of νH greater than 0.1, the $b/H = 50$ curve agrees with that for a single gap with $\mu = 1.0$.

For small gaps, Tuck (1975) has postulated that an array of gaps may be regarded in the far-field as a single-gap, of suitable width, if the gap separation and gap width are small compared to the mean depth of submersion of the array. This theory was tested in Figure 31 for two gaps of equal width with $\mu = 0.2$. Tuck (1975) predicts that the effective gap width of the two gaps is $\sqrt{b^2-a^2}$. Using this result in his single-gap theory for small gaps we obtain the dotted line solution shown in Figure 31. As can be seen, for small-gap separation, the agreement is very good, even at reasonably high frequency.

For larger gap separation, however, the assumptions behind Tuck's (1975) theory break down and the agreement with the present work is less good. At low frequency, however, good agreement is still obtained, even at large separation.

Finally, in Figure 32, we consider a semi-permeable barrier which extends from the bottom partway to the surface (in the example shown, the breakwater has a height equal to $0.9h$ where h is the water depth). For this problem, the

blockage coefficient $C(y)$ is no longer infinite or zero. We take

$$C(y) = \lambda\left(\frac{1}{(h-y)} - \frac{1}{0.9h}\right) \qquad (4.4.1)$$

so that the blockage coefficient is infinite at $y = -h$ and decreases linearly to zero for $|y| \leq 0.1h$. It should be noted that $C(y)$ is assumed real here, so that no viscous dissipative effects are included. Such effects can be modelled by allowing $C(y)$ to have a non-zero imaginary part.

An increase in the parameter λ corresponds to a decrease in the permeability of the barrier, i.e. the barrier will present a greater obstruction to the flow. This problem, therefore, may be regarded as a first approximation to reflection of water waves by a rock-fill breakwater. Since thickness effects are not included one would generally expect greater wave reflection in a real breakwater.

For very small λ, one would expect only very low wave reflection. This is borne out by the computer results. As λ becomes larger, the transmission would be expected to decrease. This is indeed the situation. For large wave frequency, the transmission coefficient approaches unity. Again, this is to be expected, since very short waves are confined to a thin surface layer and so do not "feel" the barrier.

CONCLUSION

It has been shown that the boundary integral equation method can deal successfully with a variety of fluid flow problems, both in viscous and non-viscous fluids. In the present work, only one particular numerical method of solution has been used - it is probable that improvements may be made to the method, although this might be at the expense of its essential ease of application.

Extensions to the work on viscous flow are certainly possible - the most useful would be the calculation of the impedance of an array of holes, of arbitrary shape. In Chapter 2, only a two-dimensional array of slits was considered, while in Chapter 1, flow through a single circular gap was treated. If the method detailed here was used without modification, the resulting integral equation for an array would have an extremely complicated kernel which would almost certainly require an excessive amount of computer time for numerical evaluation. In future work, it might be more suitable to modify the original method of formulation so that a simpler integral relation could be derived. Alternatively, it should be possible to work with the numerical results presented here for single gaps and then attempt to derive laws of combination for many-hole problems. (Tuck (1975) has treated sparse combinations of small holes in an inviscid fluid in this way.) It would also be useful to match the results of Chapter 2 with an exterior acoustic field, thus giving a complete solution for acoustic streaming through a screen.

The immediate extension to the work of Chapters 3 and 4 on water waves is to consider a complete three-dimensional

formulation so that the effects of oblique incidence of waves and of depth changes in two dimensions may be included. Obviously, there will be numerical difficulties involved, but it seems that these could be overcome. A related problem that has yet to be overcome is the question of uniqueness of solution and the possibility of the existence of "trapped waves" along a submerged shelf, at least in the three-dimensional situation. (See Evans (1972) for a discussion of these problems.)

A more straightforward modification of the present work is the treatment of the problem of reflection of waves by a porous vertical barrier in water of changing depth. This may easily be treated using the methods of Chapters 3 and 4, with very little increase in complexity.

Finally, analytic work remains to be done in the asymptotic short-wave problems of water-wave reflection by a submerged shelf. These results are not only of theoretical interest but would also greatly increase the usefulness of the numerical results given here, since once exact solutions have been obtained in the short-wave region, bounds can be put on the frequency range in which the numerical method is accurate.

APPENDIX A

NUMERICAL TREATMENT OF THE DOUBLE-POLE SINGULARITY

In this section we give a rigorous justification for the treatment of the double-pole singularity appearing in the kernels of the integral equations in Chapters 1 and 2 (see equations (1.3.14) and (2.3.13)). The difficulty arises because the kernel contains terms like $\frac{\partial}{\partial\xi}\left(\frac{\xi-x}{(x-\xi)^2+y^2}\right)$ which are singular in the limit as $y \to 0$. Specifically, we have to deal with integrals of the type

$$I = \lim_{y\to 0} \int_{-a}^{a} m(\xi)\ \frac{\partial}{\partial\xi}\left(\frac{\xi-x}{(x-\xi)^2+y^2}\right)d\xi \qquad \text{(A1)}$$

where $m(\xi)$ is an unknown function that is well behaved except perhaps at $\xi = \pm a$.

First we perform an integration by parts on (A1). This gives us

$$I = \lim_{y\to 0}\left[\frac{m(\xi)(\xi-x)}{(x-\xi)^2+y^2}\right]_{-a}^{a} - \lim_{y\to 0}\int_{-a}^{a} \frac{m'(\xi)(\xi-x)}{(x-\xi)^2+y^2}\ d\xi \qquad \text{(A2)}$$

We know that $-a \leqslant x \leqslant a$, so that we may break the integral in (A2) into three parts. The first integral is taken over the range $[-a, x-\in]$, the second over $[x-\in, x+\in]$ and the third over $[x+\in, a]$. $\in$ is some small positive quantity. In the first and third integrals, we may immediately take the limit $y \to 0$, since x may never be equal to ξ. Thus we may write

$$I = \lim_{y\to 0}\left[\frac{m(\xi)(\xi-x)}{(x-\xi)^2+y^2}\right]_{-a}^{a} + \left(\int_{-a}^{x-\in} + \int_{x+\in}^{a}\right) \frac{m'(\xi)}{(x-\xi)}\ d\xi - \lim_{y\to 0}\int_{x-\in}^{x+\in} \frac{m'(\xi)(\xi-x)}{(x-\xi)^2+y^2}\ d\xi \qquad \text{(A3)}$$

We rewrite the last integral in (A3) as

$$I_1 = \lim_{y \to 0} \int_{-\epsilon}^{\epsilon} \frac{m'(u+x)}{u^2 + y^2} \, u \, du \tag{A4}$$

We expand $m'(u+x)$ using a Taylor series so that (A4) becomes

$$I_1 = \lim_{y \to 0} \left(m'(x) \int_{-\epsilon}^{\epsilon} \frac{u}{u^2 + y^2} \, du + m''(x) \int_{-\epsilon}^{\epsilon} \frac{u^2}{u^2 + y^2} \, du \right.$$

$$\left. + \frac{m'''(x)}{2!} \int_{-\epsilon}^{\epsilon} \frac{u^3}{u^2 + y^2} \, du + \ldots \right) \tag{A5}$$

Thus

$$I_1 = \lim_{y \to 0} \left[\frac{m'(x) \, \log(u^2+y^2)}{2} \right]_{-\epsilon}^{\epsilon} + \lim_{y \to 0} m''(x) \left(2\epsilon - 2y \, \operatorname{atan} \frac{\epsilon}{y} \right) + \ldots \tag{A6}$$

The first term vanishes by symmetry (as do the third, fifth and seventh terms etc.), while the second term, which is the dominant term in the series, vanishes as $\epsilon \to 0$. The other even terms in the series also go to zero, but more rapidly, as $\epsilon \to 0$.

Thus we may rewrite (A3) as

$$I = \lim_{y \to 0} \left[\frac{m(\xi)(\xi - x)}{(x-\xi)^2 + y^2} \right]_{-a}^{a} + \lim_{\epsilon \to 0} \left(\int_{-a}^{x-\epsilon} + \int_{x+\epsilon}^{a} \right) \frac{m'(\xi)}{(x-\xi)} \, d\xi \tag{A7}$$

Since we require, from physical considerations, $m(\pm a) = 0$, we rewrite (A7) as

$$I = \lim_{\epsilon \to 0} \left(\int_{-a}^{x-\epsilon} + \int_{x+\epsilon}^{a} \right) \frac{m'(\xi)}{(x-\xi)} \, d\xi \tag{A8}$$

which is precisely the Cauchy principal value interpretation. Expressions like (A8) may be treated numerically immediately. In our case, however, it is more convenient to use the original unknown $m(\xi)$ rather than its derivative $m'(\xi)$. We

therefore return to the original variables by a reverse integration by parts. Thus

$$I = \lim_{\epsilon \to 0} \left[\left[\frac{m(\xi)}{(x-\xi)} \right]_{-a}^{x-\epsilon} + \left[\frac{m(\xi)}{(x-\xi)} \right]_{x+\epsilon}^{a} + \left(\int_{-a}^{x-\epsilon} + \int_{x+\epsilon}^{a} \right) \frac{m(\xi)}{(x-\xi)^2} \, d\xi \right] \tag{A9}$$

$$= \lim_{\epsilon \to 0} \left(-\frac{2}{\epsilon} m(x) + \left(\int_{0}^{x-\epsilon} + \int_{x+\epsilon}^{a} \right) \frac{m(\xi)}{(x-\xi)^2} \, d\xi \right) \tag{A10}$$

using $m(\pm a) = 0$ and the fact that $m(x-\epsilon) \sim m(x) \sim m(x+\epsilon)$ to evaluate the integrated parts in (A9) in the limit as $\epsilon \to 0$. Equation (A10) is precisely the Hadamard interpretation (see Mangler (1951)) of the double pole divergent integral.

We are now in a position to determine why the numerical method used in Chapters 1 and 2, which apparently ignores the divergent character of the integral, nevertheless gives the correct result according to the interpretation (A10). We consider a general kernel function $P(x,y,\xi)$ which has the limiting behaviour, as $\xi \to x$, $y \to 0$,

$$P(x,0,\xi) \to \frac{C}{(x-\xi)^2} \tag{A11},$$

where C is some constant. All the integral equations we are concerned with here have kernels of this type. In our matrix representation (e.g. equation (1.7.2)), the only potential difficulty is with the diagonal elements of the matrix, that is, with contributions from an interval (ξ_i, ξ_{i+1}) containing the singular point $\xi = x$ (and the interval $|\xi - x| < \epsilon$) on which we assume that $m(\xi)$ takes the constant value $m_i = m(x)$. Now we write

$$\lim_{y \to 0} \int_{\xi_i}^{\xi_{i+1}} m(\xi) \, P(x,y,\xi) \, d\xi = \lim_{y \to 0} \int_{\xi_i}^{\xi_{i+1}} \frac{m(\xi) C}{(x-\xi)^2} \, d\xi \quad +$$

$$+ \lim_{y \to 0} \int_{\xi_i}^{\xi_{i+1}} m(\xi) \left(P(x,y,\xi) - \frac{C}{(x-\xi)^2} \right) d\xi \qquad \text{(A12)},$$

where we have subtracted the most singular portion of the kernel. In the second integral we may now take the limit $y \to 0$, since the resulting expression is convergent. The first integral may be treated using (A10). Thus we find

$$\lim_{y \to 0} \int_{\xi_i}^{\xi_{i+1}} m(\xi)\ P(x,y,\xi)\,d\xi = m_i \lim_{\epsilon \to 0} \left(-\frac{2C}{\epsilon} + C\left[(x-\xi)^{-1} \right]_{\xi_i}^{x-\epsilon} \right.$$

$$\left. + C\left[(x-\xi)^{-1} \right]_{x+\epsilon}^{\xi_{i+1}} \right) + m_i \int_{\xi_i}^{\xi_{i+1}} \left(P(x,0,\xi) - \frac{C}{(x-\xi)^2} \right) d\xi \qquad \text{(A13)}$$

We now allow $\epsilon \to 0$ in (A13), so that

$$\lim_{y \to 0} \int_{\xi_i}^{\xi_{i+1}} m(\xi)\ P(x,y,\xi)\,d\xi = m_i \left\{ C\left[(x-\xi_i)^{-1} - (x-\xi_{i+1})^{-1} \right] \right.$$

$$\left. + \int_{\xi_i}^{\xi_{i+1}} \left(P(x,0,\xi) - \frac{C}{(x-\xi)^2} \right) d\xi \right\} \qquad \text{(A14)}$$

If we define $Q(x,0,\xi)$ as the indefinite integral of P, then we may express the integral in (A14) in terms of the anti-derivative $Q(x,0,\xi) - C(x-\xi)^{-1}$, the last part of which exactly cancels the integrated part of (A14). Thus, finally

$$\lim_{y \to 0} \int_{\xi_i}^{\xi_{i+1}} m(\xi)\ P(x,y,\xi)\,d\xi = m_i \left[Q(x,0,\xi) \right]_{\xi_i}^{\xi_{i+1}} \qquad \text{(A15)}$$

The coefficient of m_i in (A15) is determined in exactly the manner used naively in Chapters 1 and 2. It should be noted too that this interpretation agrees with that of Mangler (1951) where the "finite part" of a double pole integral is taken.

APPENDIX B

TESTING OF THE NUMERICAL METHOD

This section is an investigation of the numerical method introduced by Tuck (1969) for the solution of singular integral equations. It is the method used throughout the present work. The technique is applicable to a wide range of integral equations, but we shall only consider equations of the form

$$\int_{-1}^{1} m(\xi)\ f(x,\xi)d\xi = 1 \qquad \text{(B1)}$$

where $m(\xi)$ is unknown and $f(x,\xi)$ is the (given) singular kernel. We treat this type of equation since analytic solutions are available for some particular examples of it. This allows us to study the accuracy of the numerical method, in addition to its rate of convergence.

Basically the method proposed by Tuck (1969) is as follows. We assume that $m(\xi)$ is a slowly-varying function, except near the ends $\xi = \pm 1$. It is important to note that the method is much less effective if this assumption is false.

We divide the range of integration $-1 \leqslant \xi \leqslant 1$ into a set of N segments $\xi_j < \xi < \xi_{j+1}$ $j = 1,\ldots,N$ in each of which we approximate $m(\xi) = \text{constant} = m_j$. Thus (B1) becomes

$$\sum_{j=1}^{N} m_j \int_{\xi_j}^{\xi_{j+1}} f(x,\xi)d\xi = 1 \qquad -1 \leqslant x \leqslant 1 \qquad \text{(B2)}$$

We satisfy (B2) at a set of N points $x = x_i$ so that

$$\sum_{j=1}^{N} A_{ij}\ m_j = 1 \qquad \text{(B3)}$$

where

$$A_{ij} = \int_{\xi_j}^{\xi_{j+1}} f(x_i,\xi)d\xi \qquad \text{(B4)}$$

$$= \left[F(x_i, \xi) \right]_{\xi_j}^{\xi_{j+1}} \qquad \text{(B5)}$$

We can use equation (B5) so long as $F(x,\xi)$, the anti-derivative of $f(x,\xi)$, is known. Modifications to the method must be used if this integral cannot be determined. For example, if $f(x,\xi) \to \log(x-\xi)$ as $\xi \to x$, we can write

$$A_{ij} = \int_{\xi_j}^{\xi_{j+1}} f(x_i - \xi) - \log|x_i - \xi| \, d\xi$$
$$+ \left[(\xi - x_i) \log|\xi - x_i| - (\xi - x_i) \right]_{\xi_j}^{\xi_{j+1}} \qquad \text{(B6)}$$

The integral in this expression may now be evaluated by any standard numerical integration technique (Simpson's rule, for example), since it is no longer singular at $\xi = x$. The correct singular behaviour is still modelled in the numerical scheme, however, by virtue of the integrated part of (B6).

The choice of mesh-points must now be considered. The obvious choice is an evenly spaced mesh. This may be criticised, however, on the grounds that the unknown $m(\xi)$ will generally have some singular nature near the end-points $\xi = \pm 1$, usually of the form

$$m(\xi) = \frac{A(\xi)}{(\xi-1)^{\alpha}} \quad \text{near} \quad \xi = 1$$
$$\text{and} \qquad m(\xi) = \frac{B(\xi)}{(\xi+1)^{\beta}} \quad \text{near} \quad \xi = -1 \qquad \text{(B7)}$$

where $A(\xi)$ and $B(\xi)$ are regular functions of ξ and α and β are in general not integers. At this stage, we will assume either symmetry or anti-symmetry in $m(\xi)$ so that $\alpha = \beta$ and $A(\xi) = \pm B(\xi)$. Because of this behaviour, if

evenly spaced mesh-points were used, then the assumption m_j = constant on $\xi_j < \xi < \xi_{j+1}$ would break down near the end-points.

If α is equal to 0.5 as it is in many physical problems, then the choice

$$\xi_j = -\cos\frac{\pi}{2}\left(\frac{j-1}{N}\right), \quad j = 1,\ldots,N+1 \tag{B8}$$

accommodates the singularities exactly. For α other than 0.5, as occurs in the water-wave problems treated in Chapters 3 and 4, similar formulae may be derived. Once the points ξ_j have been determined, there are two possible choices for the collocation points x_i, $i = 1,\ldots,N$. First we may put

$$x_i = 0.5(\xi_i + \xi_{i+1}), \quad i = 1,\ldots,N \tag{B9}$$

Alternatively, we may make the choice

$$x_i = -\cos\frac{\pi}{2}\left(\frac{i-\frac{1}{2}}{N}\right), \quad i = 1,\ldots,N \tag{B10}$$

Neither of these choices has any obvious advantage over the other at first sight. It will be seen, however, that the choice (B10) gives better results.

Having determined the mesh-points, a solution to the integral equation in question may be obtained by inverting the matrix equation

$$\underset{\sim}{A}\underset{\sim}{m} = \underset{\sim}{1} \tag{B11}$$

where

$$A = [A_{ij}] \tag{B12},$$

$$\underset{\sim}{m} = [m_j] \tag{B13}$$

and all elements of the vector $\underset{\sim}{1}$ are of unit value.

We now consider the forms of $f(x,\xi)$ for which the above method may be used. The singular character of (B1) is

reflected in the behaviour of the kernel function $f(x,\xi)$ as $\xi \to x$. We are interested in kernels with the properties

$$f(x,\xi) \to \begin{cases} \log|x-\xi|, & n = 0 \\ \dfrac{1}{(x-\xi)^n}, & n = 1,2,\ldots,\ \xi \to x. \end{cases} \tag{B14}$$

In practical applications $n = 0,1,2$ are the values of n most commonly found. In this appendix we consider the case where f is given everywhere by (B14) or some combination for various values of n. Problems where the kernel is more complicated appear to behave in a fashion which is mainly dependent on the type of singularity present so that simple test cases allow reasonably general conclusions to be drawn. The other advantage in using these simple test functions is that analytic solutions are available to integral equations with these kernels.

Problems where $f(x,\xi) = \dfrac{1}{(x-\xi)^n}$ with $n \geq 1$ are not defined in the ordinary sense, and we must be careful about the interpretation of integral equations with such kernels. Usually, these kernel functions are encountered in equations like

$$\int_{-1}^{1} \frac{m(\xi)\,(x-\xi)}{(x-\xi)^{n+1} + y^2}\, d\xi = 1 \tag{B15}$$

in the limit as $y \to 0$. Equation (B15) has meaning so long as $y \neq 0$. In the limit $y = 0$, however, we can interpret the integral in the Hadamard sense, so that we have

$$\oint_{-1}^{1} \frac{m(\xi)}{(x-\xi)^n}\, d\xi = 1 \tag{B16}$$

where $$\int^{1}_{-1} \frac{m(\xi)}{(x-\xi)^n}\, d\xi = G(x,1) - G(x,-1) \qquad (B17)$$

with $$\frac{\partial}{\partial \xi} G(x,\xi) = \frac{m(\xi)}{(x-\xi)^n} \qquad (B18)$$

In Appendix A this type of interpretation is justified rigorously for the special case $n = 2$. For general n Manger (1951) derives the results (B17) and (B18). The interpretation (B17) is exactly analogous to the procedure used in the numerical method (B5). Thus integral equations of this type are, in principle at least, amenable to solution by this method.

The numerical procedure was applied to several different test equations. The program was run with $N = 10, 20$ and 30 and the three possible choices for the mesh-points, namely ξ_j given by (B8) and x_i by (B9) or (B10) or with both ξ_j and x_i evenly spaced. (In the latter case the x_i were taken as mid-points.)

If was found that the method did not work at all with $f(x,\xi) = \frac{1}{(x-\xi)}$ $(n=1)$ - wildly oscillating solutions were obtained. This is not surprising, however. Since a solution exists to the homogeneous equation $\int^{1}_{-1} \frac{m(\xi)}{(x-\xi)}\, d\xi = 0$ this may be added to any solution we obtained for the non-homogeneous equation. This means that end-point conditions must be included to ensure a unique solution to the problem (see Mangler (1951) §4.6). Since these are not included in our numerical formulation, there is no reason to suppose that the method will in fact be successful. Indeed, from a numerical point of view, since the elements $A_{ii} = \log|x_i - \xi_i| - \log|x_i - \xi_{i+1}|$ are very close to zero, we see that the matrix

A will not be diagonally dominant and hence will not be easily inverted, if indeed an inverse exists. For test functions of the form $\frac{1}{(x-\xi)^n}$ with $n > 2$, it was found that for n odd, no sensible answers were obtained. For even $n > 2$ the answers obtained were surprising. For example, with $n = 4$ at $N = 10$ $m(\xi)$ was a smooth function as expected. For $N = 20$, the output $m(\xi)$ was of the same shape but its magnitude had decreased by a factor approximately equal to two. Similar surprising results were obtained as N was increased further. As yet, no explanation has been found for this behaviour.

For all other functions tested, convergence was obtained in all cases, although it was soon found that mesh-points given by the combination (B8) and (B10) gave far superior results.

In Table 2 results are given for the three test functions $f(x,\xi) = \log|x-\xi|$, $\frac{1}{(x-\xi)^2}$ and $0.01 \log|x-\xi| + \frac{1}{(x-\xi)^2}$. These functions were chosen since an analytic solution was available in each case. The table actually shows $\int m(\xi)d\xi$ rather than $m(\xi)$ itself and in the case of $f(\xi) = \log|x-\xi|$ the exponential of the integral has been taken for display purposes.

To obtain some idea of the rate of convergence of the method, it was assumed that the computed results followed a law like

$$m_N = m_\infty + \frac{B}{N^a} \qquad \text{(B19)}$$

where N is the number of mesh-points, B is a constant, m_N is the program output for given N and m_∞ is the limiting solution obtainable from the method at very large N. In principle, m_∞ should be the same as the exact solution,

Kernel Functions	Mesh Points	N = 10	N = 20	N = 30	α	Limit Solution	Analytic Solution
$\frac{\pi^2}{2}\frac{1}{(x-\xi)^2}$	Even Mesh x pts. mid pts. x pts. cosine pts.	1.90476 1.88402 2.0	1.95121 1.94019 2.0	1.96721 1.95971 2.0	0.94 0.93	2.0015 2.0025 2.0	2.0
$-\frac{\log 2}{2}\log\|x-\xi\|$	Even Mesh x pts. mid pts. x pts. cosine pts.	0.49132 0.49881 0.4999 8590	0.49565 0.49970 0.4999 9824	0.49710 0.49987 0.4999 9948	0.99 1.95 3.0	0.500015 0.500011 0.4999999997	0.5
$\frac{\pi^2}{2}\left(\frac{1}{(x-\xi)^2}+0.01\log\|x-\xi\|\right)$	Even Mesh x pts. mid pts. x pts. cosine pts.	1.91396 1.89336 2.009431126	1.96053 1.94957 2.009430515	1.97662 1.96911 2.00943 0455	0.95 0.93 3.0	2.01096 2.01194 2.00943 0430	2.00943 06
Single slit ($-\mathcal{R}e$ log s/a)	Optimal Mesh	1.743276	1.7431851	1.7431760	3.0	1.7431721	-

Table 2. Test results for numerical method with various test functions and mesh-points.

so long as $\alpha > 0$. This quantity α gives some indication of the rate of convergence of the method.

Using the results shown in Table 2, we can calculate m_∞, B and α for any given test function and choice of mesh-points. This was done and the limiting solution and the convergence exponent (α) are also displayed in the table.

As can be seen, the choice of mesh-points is very important. In the case of the log function, the best error is of the order N^{-3}, whereas with evenly spaced points the error is much larger, of order N^{-1}. In fact, there is an interesting progression in the convergence exponent from one to two to three, as we progressively improve our choice of mesh-points, firstly when we use cosine points for the mesh-points ξ_j in preference to evenly spaced points, and then when we choose the collocation points x_i optimally.

Looking at the results for the double-pole test function we see that the method works exactly, at least to the limit of computer accuracy (approximately fifteen significant figures). This is very surprising, as the quantity displayed in the table, $\int m(\xi)\,d\xi$ is evaluated by a rather crude integration routine (consistent with the approximations made throughout)

$$\int_0^1 m(\xi)\,d\xi = \sum_{j=0}^{N=1} m_j\,(\xi_{j+1} - \xi_j) \qquad \text{(B20)}$$

Now even if we know the <u>exact</u> value of m_j at each mesh-point, the above rule will not give the exact answer. This becomes obvious if we consider numerical integration of the exact solution $m(\xi) = \sqrt{1-\xi^2}$, using the set of mesh-points given by (B8) and (B10). We have

$$\int_0^1 \sqrt{1-\xi^2}\,d\xi \simeq \sum_{j=0}^{N-1} \sqrt{1-x_j^2}\,(\xi_{j+1} - \xi_j) \tag{B21}$$

$$= \sum_{j=0}^{N-1} \sin^2\left(\frac{j-\frac{1}{2}}{2N}\right)\pi \sin\frac{\pi}{4N} \tag{B22}$$

Now let us consider the integral in a different way. We make the immediate substitution $\xi = \cos\theta$. Then

$$\int_0^1 \sqrt{1-\xi^2}\,d\xi = \int_0^{\pi/2} \sin^2\theta\, d\theta \tag{B23}$$

$$= -\frac{1}{4}\int_0^{\pi} \cos\theta\, d\theta + \int_0^{\pi/2} \frac{1}{2}\, d\theta \tag{B24}$$

The second integral in (B24) may be evaluated exactly by using the mid-point rule. This is also true for the first integral since $\cos\theta$ is anti-symmetric about $\theta = \pi/2$. Thus the integral may be evaluated with no error if we take as mesh points $\theta_j = \left(\frac{j-\frac{1}{2}}{2N}\right)\pi$ so that

$$\int_0^1 \sqrt{1-\xi^2}\,d\xi = \sum_{j=1}^{N-1} \frac{\pi}{4N} \sin^2\left(\frac{j-\frac{1}{2}}{2N}\right)\pi \tag{B25}$$

Comparing (B22) and (B25) indicates the error involved in our numerical scheme of integration. (It also tends to show why the choice (B10) for the collocation points x_i is the optimal one).

On returning to our consideration of the double-pole problem, we see that the computer program must be generating

$$m_j = m_{j\,\text{exact}} \frac{\pi/4N}{\sin(\pi/4N)} \tag{B26}$$

Indeed, investigation showed this to be the case.

This behaviour was found to occur only if the kernel function was purely a double-pole. Thus, in the third test function considered, we see that for the optimal choice of

mesh-points, the rate of convergence is the same as that for a simple logarithmic function. For non-optimal choice of mesh-points, however, the double-pole becomes the dominant singularity so that the rate of convergence is approximately the same as that for the double-pole test function with the mesh-points chosen incorrectly.

Finally, we consider a more general function to show that the major singularities do indeed determine the rate of convergence. We consider the case of viscous flow through a single two-dimensional slit, at Reynolds number $\beta = 1$. As can be seen, the rate of convergence is the same as for our third test function when the optimal set of mesh-points is used (both problems have the same type of singularity).

It should also be noted that in all the above we have concentrated on equations of the first kind. Equations of the second kind, such as those considered in Chapters 3 and 4, can also be treated using the numerical method described here. Such equations are actually less sensitive to the choice of mesh-points and indeed it is found that in solving an equation like

$$m(x) + \int_{-1}^{1} m(\xi) \log|x-\xi| d\xi = 1 \qquad \text{(B27)}$$

the convergence exponent (α) is approximately equal to two even with an evenly spaced mesh.

BIBLIOGRAPHY

Abramowitz, M. and Stegun, I.A. (1964). Handbook of Mathematical Functions. Dover, New York.

Bartholomeusz, E.F. (1958). The reflection of long waves at a step. Proc. Camb. Phil. Soc., Vol.54, pp.106-128.

Dean, W.R. (1945). On the reflection of surface waves by a submerged plane barrier. Proc. Camb. Phil. Soc., Vol.41, pp.231-238.

de Mestre, N.J. and Guiney, D.C. (1971). Low Reynolds number oscillatory flow through a hole in a wall. J. Fluid Mech., Vol.47, pp.657-666.

Evans, D.V. (1972). The application of a new source potential to the problem of transmission of water waves over a step. Proc. Camb. Phil. Soc., Vol.71, pp.391-410.

Filon, L.N.G. (1929). On a quadrature formula for trigonometric integrals. Proc. Roy. Soc. Edin., Vol.49, pp.38-47.

Fitzgerald, G.F. (1976). The reflection of plane gravity waves travelling in water of variable depth. Phil. Trans. Roy. Soc. Lond., Vol.284, pp.49-89.

Guiney, D.C. (1972). Some flows through a hole in a wall in viscous and non-viscous fluids. Ph.D. thesis, Univ. of Adelaide.

Hilaly, N. (1967). Diffraction of water waves over bottom discontinuities. Univ. of Calif. Berkeley, Rept. HEL1-7.

Lewin, M. (1963). The effect of vertical barriers on progressing waves. J. Maths. Phys., Vol.42, pp.287-300.

Macaskill, C. and Tuck, E.O. (1977). Evaluation of the acoustic impedance of a screen. J. Aust. Math. Soc., Vol.20 (Series B), pp.46-61.

Mangler, K.W. (1951). Improper integrals in theoretical aerodynamics. R.A.E. Tech. Note 2424.

Morse, R.M. and Ingard, K.V. (1968). Theoretical Acoustics. McGraw-Hill, New York.

Mei, C.C. (1966). Radiation and scattering of transient gravity waves by vertical plates. Quart. Journ. Mech. & Applied Maths., Vol.19(4), pp.417-440.

Mei, C.C. and Black, J.L. (1969). Scattering of surface waves by rectangular obstacles in waters of finite depth. J. Fluid Mech., Vol.38, pp.499-511.

Packham, B.A. and Williams, W.E. (1972). A note on the transmission of water waves through small apertures. J. Inst. Maths. Applics. Vol.10, pp.176-184.

Porter, D. (1972). The transmission of surface waves through a gap in a vertical barrier. Proc. Camb. Phil. Soc., Vol.71, pp. 411-421.

Porter, D. (1974). The radiation and scattering of surface waves by vertical barriers. J. Fluid Mech., Vol.63(4), pp.625-634.

Roseau, M. (1976). Asymptotic wave theory. Series in Applied Mechanics, North-Holland, Oxford. Chap. 8.

Sedov, L.I. (1965). Two-dimensional problems in hydrodynamics and aerodynamics. Wiley, New York.

Sheridan, D.J. (1975). Computation of the velocity potential for a pulsating source in a fluid with free surface and finite depth. David W. Taylor Naval Ship Res. and Devel. Center, Report SPD 625-011.

Thorne, R.C. (1953). Multipole expansions in the theory of surface waves. Proc. Camb. Phil. Soc., Vol.49, pp.707-716.

Tuck, E.O. (1969). Calculation of unsteady flows due to small motions of cylinders in a viscous fluid. J. Eng. Maths., Vol.3, pp.29-44.

Tuck, E.O. (1970). Unsteady flow of a viscous fluid from a source in a wall. J. Fluid Mech., Vol.41, 641-653.

Tuck, E.O. (1971). Transmission of water-waves through small apertures. J. Fluid Mech., Vol.49, 65-74.

Tuck, E.O. (1975). Matching problems involving flow through small holes. In Advances in Applied Mechanics, ed. C.S. Yih, New York: Academic, Vol.15, 89-158.

Tuck, E.O. (1976). Some classical water wave problems in varying depth. Proc. IUTAM Symp. on waves on water of varying depth. Aust. Acad. of Science, Canberra. pp.9-20.

Ursell, F. (1947). The effect of a fixed vertical barrier on surface waves in deep water. Proc. Camb. Phil. Soc., Vol.43, pp.374-382.

Wehausen, J.V. and Laitone, E.V. (1960). Surface waves. In "Handbuch der Physik" (S. Flugge, ed.), Vol.9, pp.446-778.

Yeung, R.W. (1975). A hybrid integral equation method for time harmonic free-surface flow. Proc. First Num. Ship Hydro. Conf. Gaithersburg, Maryland, pp. 581-607.